Preliminary Investigation on Welding and Cutting Methods for First Wall Support Leg in ITER Blanket Module

Kensuke MOHRI, Satoshi SUZUKI, Mikio ENOEDA
Satoshi KAKUDATE, Kiyoshi SHIBANUMA and Masato AKIBA

Tokamak Device Group
Fusion Research and Development Directorate

JAEA-Technology

Preliminary Investigation on Welding and Cutting Methods for First Wall Support Leg in ITER Blanket Module

Kensuke MOHRI[※], Satoshi SUZUKI[+], Mikio ENOEDA[+], Satoshi KAKUDATE, Kiyoshi SHIBANUMA and Masato AKIBA[+]

Division of ITER Project
Fusion Research and Development Directorate
Japan Atomic Energy Agency
Naka-shi, Ibaraki-ken

Concept of a module type of blanket has been applied to ITER shield blanket, of which size is typically 1mW x 1mH x 0.4mB with the weight of 4 ton, in order to enhance its maintainability and fabricability. Each shield blanket module consists of a shield block and four first walls which are separable from the shield block for the purpose of reduction of an electro-magnetic force in disruption events, radio-active waste reduction in the maintenance work and cost reduction in fabrication process. A first wall support leg, a part of the first wall component located between the first wall and the shield block, is required not only to be connected metallurgically to the shield block in order to withstand the electro-magnetic force and coolant pressure, but also to be able to replace the first wall more than 2 times in the hot cell during the life time of the reactor. Therefore, the consistent structure where remote handling equipment can be access to the joint and carry out the welding/cutting works perfectly to replace the first wall in the hot cell is required in the shield blanket design.

This study shows an investigation of the blanket module #10 design with a new type of the first wall support leg structure based on Disc-Cutter technology, which had been developed for the main pipe cutting in the maintenance phase and was selected out of a number of candidate methods, taking its large advantages into account, such as 1) a post-treatment can be eliminated in the hot cell because of no making material chips and of no need of lubricant, 2) the cut surface can be rewelded without any machining. And also, a design for the small type of Disc-Cutter applied to the new blanket module #10 has been investigated.

In conclusion, not only the good performance of Disc-Cutter technology applied to the updated blanket module, but also consistent structure of the simplified shield blanket module including the first wall support leg in order to satisfy the requirements in the design have been proposed.

Keywords: ITER, Blanket Module, First Wall, Separable First Wall, Disc Cutter, YAG Laser Beam, Hot Cell, Welding Equipment, Cutting Equipment

---

+ Division of Fusion Energy Technology
※ Cooperative Staff

ITER 遮蔽ブランケットにおける第一壁支持脚の接続構造および接合方法の予備的検討

日本原子力研究開発機構

核融合研究開発部門　ITER プロジェクトユニット

毛利 憲介※、鈴木 哲[+]、榎枝 幹男[+]、角館 聡、柴沼 清、秋場 真人[+]

ITER の遮蔽ブランケットは、製作性及び保守性の観点から 1mW x 1mH x 0.4mB 規模の重量約4トンのモジュール構造を採用している。また、遮蔽ブランケットを構成する第一壁と遮蔽体部は、ディスラプション時の電磁力の軽減、放射性廃棄物量の削減および製作コストの低減のために、両者が構造的に分離できる構造を採用している。第一壁は第一壁に取り付けられた第一壁支持脚においてのみ遮蔽体部と連結されており、その連結部はプラズマのディスラプション時の電磁力に耐えるために冶金的に接続される。しかし、第一壁には寿命中 2 回以上の交換が必要とされているため、遮蔽ブランケットの構造概念を考える際には、交換時にホットセル内で適用する遠隔保守機器の観点からの構造概念の構築が強く求められている。

本研究では、第一壁支持脚の切断方法として、数多くの切断手法の中から、中径管規模の円管切断に特化し数多くの優位性(切削時に切子の発生がなく冷却材も不要のため清掃等の後処理が容易、また再溶接にそのまま切断面を適用できるため開先加工も不要)を有するDick-Cutter 切断技術を高く評価し、この機器が施工可能となる遮蔽ブランケット構造概念の検討を行った。具体的には、第一壁支持脚の連結部構造およびアクセス性を考慮した遮蔽体部の内部構造の検討を行うと共に、第一壁支持脚切断に適用可能な Dick-Cutter の小型化検討を行った。

本研究により、遠隔保守での円管切断に多大な威力を発揮する Dick-Cutter の実機への高い適用性を明らかにすると共に、ITER において課題となっているホットセル内で交換可能な第一壁の支持脚構造および遮蔽ブランケットの構造等に対してシンプルで整合性のある構造案を提案し、実用化への高い可能性を示すことができた。

那珂核融合研究所(駐在): 〒311-0193　茨城県那珂市向山 801-1
+ 核融合エネルギー工学研究開発ユニット
※技術開発協力員

Contents

目次

1. Introduction

A module type of blanket has been applied to the ITER shield blanket in order to enhance its maintainability and fabricability, typically the size of 1mW x 1mH x 0.4mB with the weight of 4 ton. Moreover, a separable first wall (FW) concept from a shield block is applied with a view to reducing an electro-magnetic force (EMF) in disruption events, a radio-active waste in the maintenance work and fabrication cost. FW, which consists of a panel and a support leg, has to be connected metallurgically, which means a leak tight joint, to the shield block through the support leg in order to withstand the EMF and coolant inner pressure [1][2]. On the other hand, in the other requirement for the connection, it is able to replace FW more than 2 times in the Hot Cell during the life time of the reactor.

At present, it is urgently necessary to design the following consistent structure,

- structure of FW support leg and the shield block taking the requirements from suitable welding/cutting methods and remote handling tools applied in the Hot Cell into account.

In this report, a preliminary investigation of the suitable replacement methods for FW in the Hot Cell at the maintenance stage, mainly for cutting and rewelding FW support leg, has been done. The design of FW support leg and shield block structure reflecting the requirements from the replacement methods has been also investigated.

2. Objectives and Design Conditions

2.1 Objectives

According to the shield blanket module design improvement by the ITER International Team (IT), conceptual design of FW support leg and the relating parts have been performed. The update concept of the FW support leg and the relating parts in the shield block proposed by the IT are shown in Figs. 2.1-1 and 2.1-2. The major features of the structure in the concept are as follows:

- applying Race Track shape to the support leg connection,
- on the replacement methods, applying YAG Laser beam to the support leg connection in both cases,
- applying the removable separation parts such as the Expansion Seal and Field through Pipe fixed by bolts, for the purpose of keeping the boundary of the coolant collectors between the inlet one to FW and the outlet from FW. These have to be removed and reset every replacement stage for FW.

Unfortunately, the following issues are not clear in the IT design.

- The applicability of YAG Laser beam to Race Track shape of the support leg replacement in Hot Cell, especially the cutting.
- The reliability of the use of the separation parts, making the structure in the shield block and the procedure of FW replacement in Hot Cell all the more complicated.

Therefore, going back to the starting point, with the object of confirming the applicable methods in the Hot cell and simplifying the complex structure, the following items have been performed in this study.

- The selection of the suitable methods for welding and cutting used in Hot Cell.
- The improvement of the shield block design taking account of the requirement from the selected methods.

2.2 Design Conditions

Table 2.2-1 shows the premise conditions of design requirements for welding and cutting in this study. On the cutting, since this study is the first trial to investigate the applicable equipment to the FW support structure, it is carried out to be based on the present requirement of no use of lubricant.

Table 2.2-1   Premise Conditions of Design Requirements

|	
The number of FW changes	Two times excluded initial assembly
Thickness of back cover plate for welding/cutting	10 mm t
Thickness of FW support leg structure for w/c.	10 mm t
Welding/cutting position in the module	>170mm
in order to keep He production rate 1appm or less	(Distance from the FW surface)
Design strategy	No making alterations in module outer line
	No use of lubricant at cutting and at machining after cutting
Accessibility	Be accessible to FW welding/cutting point through the narrow access hole.
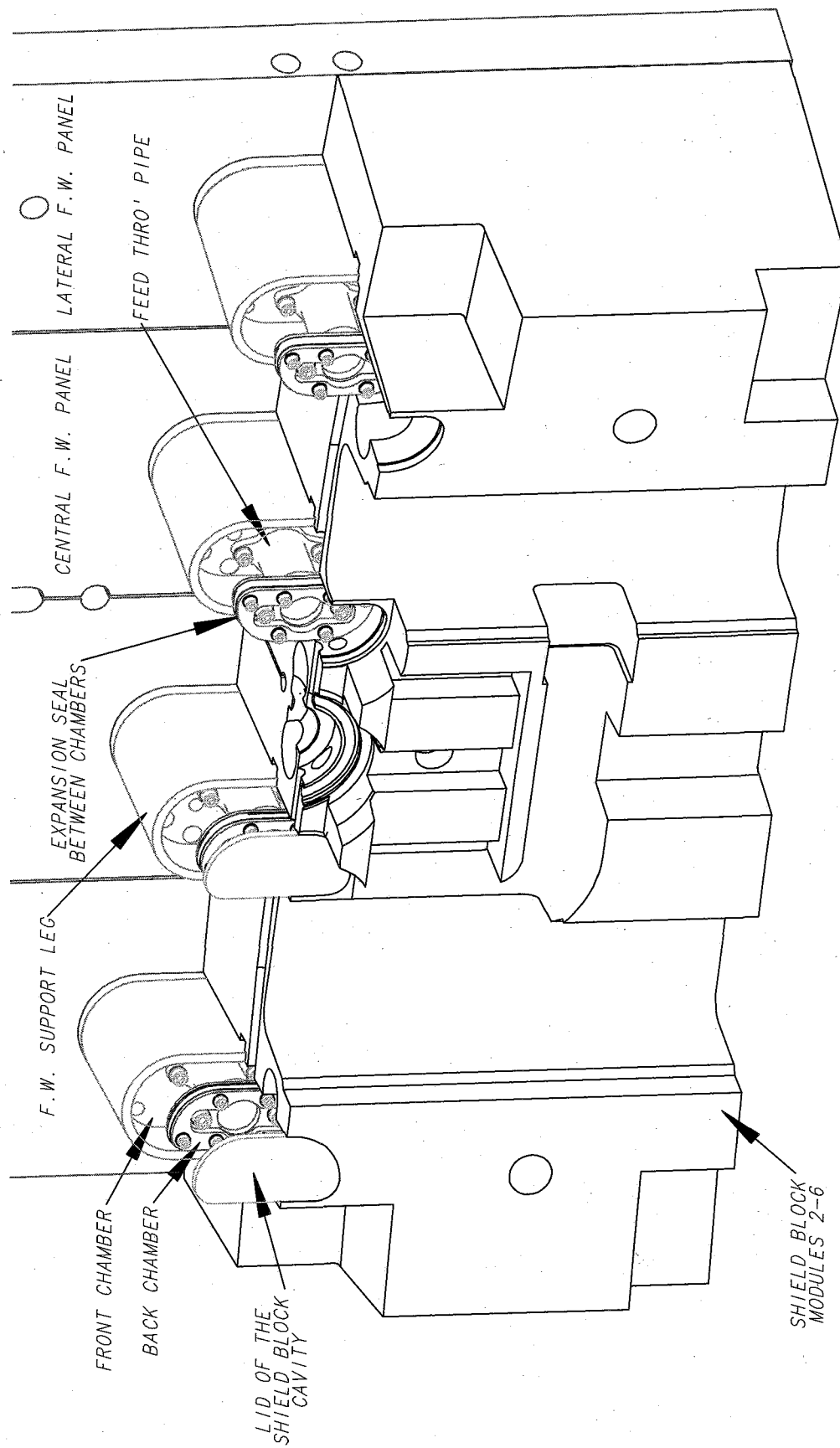
Fig. 2.1-1 Mounting situation of Incidental Parts designed by IT
(Expansion seals , Feed through Pipes and Bolts)

LATERAL F.W. PANEL

CENTRAL F.W. PANEL

FEED THRO' PIPE

EXPANSION SEAL
BETWEEN CHAMBERS

F.W. SUPPORT LEG

FRONT CHAMBER

BACK CHAMBER

LID OF THE
SHIELD BLOCK
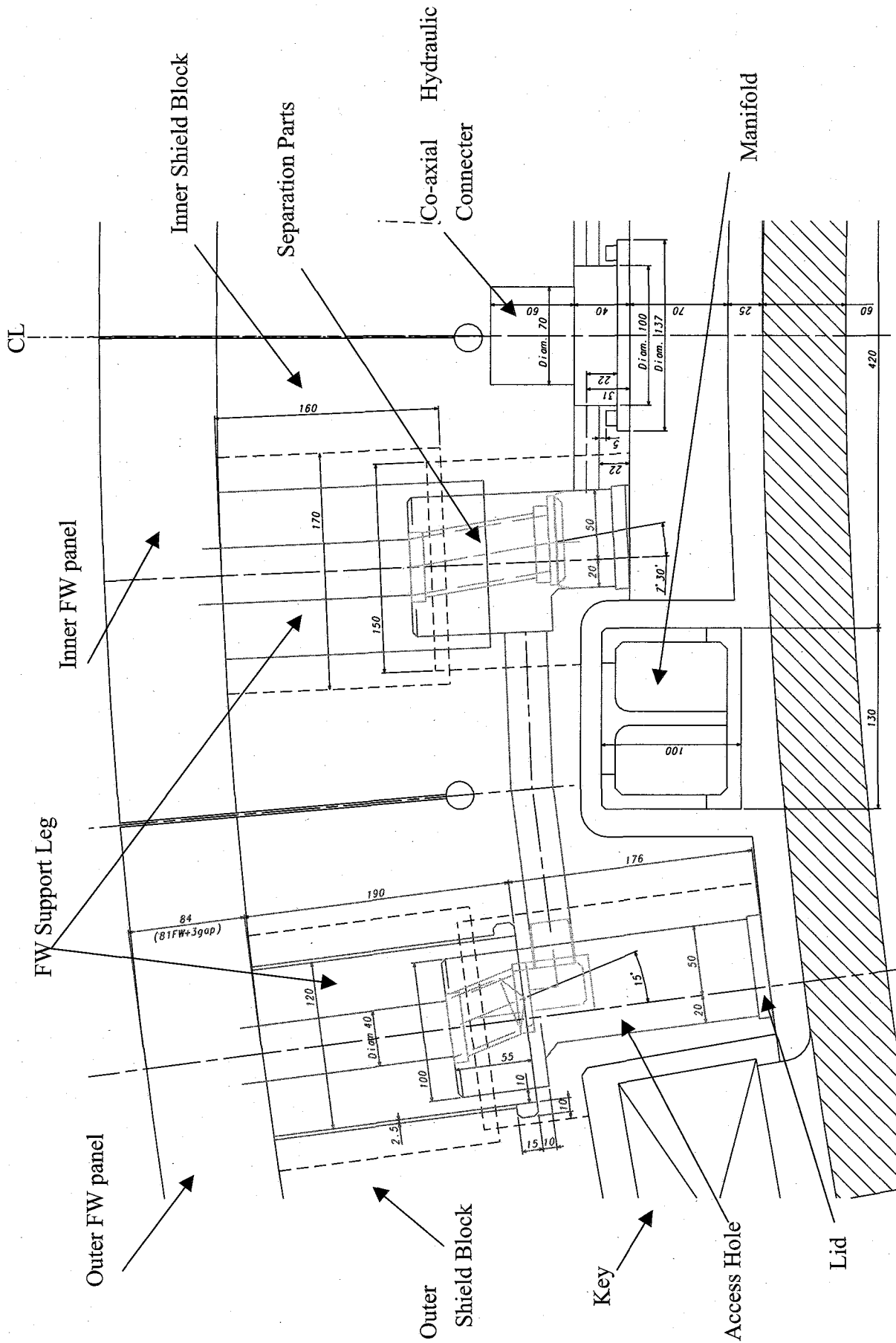CAVITY

SHIELD BLOCK
MODULES 2-6

Fig. 2.1-2 Horizontal cross section of #4 Module (The left half)

3. Investigation of Welding and Cutting Methods

3.1 Welding Equipment

3.1.1 Welding Methods

Five kinds of general welding methods which are possible to weld more than or less 10mm thick austenitic stainless steel are investigated. Main feathers of the five are shown in the followings:

(1) Narrow gap TIG

10mm thick wall :	Possible with multi-layer welding.
Welding position:	In all position
Bead situation:	Stable and high quality bead with penetration bead. Large heat affected zone (HAZ).
Welding efficiency:	A little worse. (It will be improved by using Hot Wire.)
Deformation:	Large

(2) Narrow gap MIG

10mm thick wall :	Possible with multi-layer welding.
Welding position:	In all position except an overhead position.
Bead situation:	A little worse than TIG. Large HAZ.
Welding efficiency:	Good.
Deformation:	Large

(3) CO_2 Laser beam

10mm thick wall :	Possible with a single path welding.
Welding position:	In all position
Bead situation:	Stable and high quality bead.
Welding efficiency:	Good.
Deformation:	Small.
Miniaturization of the head:	Possible.
Key implement:	Mirror system for leading the Laser beam to an object

(4) YAG Laser beam

10mm thick wall :	Possible with a single path welding. (It depends on Laser beam power.)
Welding position:	In all position
Bead situation:	Stable and high quality bead.
Welding efficiency:	Good.
Deformation:	Small.
Miniaturization of the head:	Possible.

Key implement:	Fiberoptics system for leading the Laser beam to an object.

(5) Electron Beam

10mm thick wall :	Possible with a single path welding.
Welding position:	In all position
Bead situation:	Stable and high quality bead.
Welding efficiency:	Good.
Deformation:	Small.
Miniaturization of the head:	Difficult.
Key implement:	Chamber for keeping the weld circumstance vacuum.

3.1.2 Selection of Welding Methods

At an initial assembly stage, while it needs to confirm the weldability through R&D, three kinds of general welding equipments among the above six are proposed for welding of blanket module owing to on workshop fabrication; such as YAG Laser beam welding, and the conventional welding (Narrow gap TIG and MIG).

On the other hand, at the maintenance stage, the YAG Laser beam welding is regarded as the only measure left in consideration of the applicability in Hot Cell and of the accessibility to the weld points passing through the narrow cavity in the module. For giving the actual examples in the reasons, there are issues for the conventional welding to remedy the deformation in the limited narrow space in case of passing over the allowable tolerance.

3.1.3 Welding Conditions of YAG Laser

As the key issues of YAG Laser welding applied to FW support leg are Laser power and root conditions, the welding conditions of YAG Laser in Hot Cell estimated from past R&D results in JAEA are described in the pages that follow. By the way, the root conditions mentioned here indicate a root opening, a slip gap and configuration of grooves.

At first, the Laser beam power to weld the 10mm depth is estimated. The following result was gained in the conditions of SUS304 bead on plate welding by 6kW YAG Laser beam power. Figure 3.1-1 shows the bead cross section by Laser beam, and Fig. 3.1-2 shows the relationship between the welding depth and the velocity.

- Though it was found to be difficult for continuous welding (CW) to weld up to 10mm depth, it could obtain more than 10mm depth weld in the pulse welding conditions while these were not the optimum welding conditions and not the soundness joints. However, it is conceivable that it is possible to obtain the soundness 10mm thick joint with using a level of 6-7kW Laser rated power.

The following results on the root opening condition were gained in conditions of SUS304 plate, 500mm/min velocity, N_2 sealed gas and Φ0.4mm laser focus with using 3kW Laser beam power. Two root opening conditions with 0.4mm and 0.7mm were tested. The example of butt joint x-section, which is 0.4mm case, is shown in Table 3.1-1.

- Soundness weld bead with an about 7mm depth was obtained in the 0.4mm root opening condition, though the underfed was occurred strikingly in the 0.7mm one. From this result, it is found that it needs to keep the gap between weld axis and root face (groove face) within the tolerance of ±0.2mm by machining.

- On a size of the soundness bead obtained from the 0.4mm root opening condition, it was 4.5mmW at the front surface and 1.7mmW at the rear side approximately. From this result, it is found that the maximum allowable deviation among the weld axis and the both root faces is about 0.65mm ([bead width 1.7mm – root gap 0.4mm] ÷ 2). Therefore, it is to be one of the present requirements for welding tool to keep the positioning tolerance.

From an another R&D results, the following results on the slide gap conditions were gained by conditions of SUS316L circular tube (ID54.5mm x 3mmt), 500mm/min, 0.4mm root opening with using 1.1kW Laser beam power. On the slide gap conditions, 4 cases with 0mm, 0.5, 1.0 and 1.5mm were tested. Examples of welded joint x-section in the case of 0.5mm and 1.0mm are shown in Figs. 3.1-3 and 3.1-4, respectively.

- The 0.5mm was the maximum allowable slide gap in order to obtain the soundness joint. It means that it needs to keep the relative slide gap within the tolerance of 0.5mm. Therefore, this is also one of the strong requirements for welding tool to keep the positioning tolerance.

Finally, the configurations of groove for FW support leg and for cover plate are investigated. The proposed joint shapes in comparison with the IT one are shown in Table 3.1-2 and 3.1-3, respectively. For the FW support leg, the angular butt groove is applied which has advantages over than normal butt one in that the damage to the optical instrument in the Laser nozzle by the reflections will be much less, and that it is much easer to set the FW support leg without any slip gap. For the cover plate, the normal butt with square groove is applied which has an advantage to prevent the dross and shavings from scattering.

3.2 Cutting Equipment

3.2.1 Cutting Methods

Five kinds of general cutting methods which are possible to cut more than or less 10mm thick austenitic stainless steel are investigated. Main feathers of the five are shown in the followings:

(1) Powder Gas cutting

10mm thick wall :	Possible to the hundreds mm thickness.
Cutting width:	Wide. (It affects mass of dross)
Cutting accuracy:	Low.
Heat affected zone:	Large.
Discharge:	Iron powder, dross and slag.
Key issues:	Collection of the discharges and protection of the peripheral structure and miniaturization of the head.

(2) Plasma cutting

10mm thick wall :	Possible.
Cutting width:	5-8mm. (It affects mass of dross)
Cutting accuracy:	High and clean.
Heat affected zone:	Small.
Discharge:	Dross and slag
Key issues:	Collection of the discharges, protection of the peripheral structure and miniaturization of the head.

(3) YAG Laser beam

10mm thick wall :	Possible. (It depends to Laser beam power.)
Cutting width:	1-2mm
Cutting accuracy:	High and clean.
Heat affected zone:	Small.
Discharge:	Dross and slag
Key issues:	Collection of the discharges. Protection of the peripheral structure and fiberoptics system for leading the Laser beam to an object.

(4) Abrasive Water Jet

10mm thick wall :	Possible.
Cutting width:	1mm
Cutting accuracy:	High and clean.
Heat affected zone:	Non.

Discharge: Water and polish powder. (Mass of the discharges is great in volume)

Key issues: Protection of the peripheral structure against the cutting penetration power. Collection of the discharges.

(5) Mechanical cutting

  1) General machining (Disc type cutting tool and Hole-Saw)

    10mm thick wall :   Possible.

    Cutting accuracy: High and clean.

    Heat affected zone: Small.

    Discharge: Metal chips and Coolant with lubricant

    Key issues: Collection of the discharges. System of a strong support arm.

  2) Special mechanical cutting (Disc-Cutter)

    10mm thick wall :   Possible, only to pipes. (The possibility depends to an inner diameter of pipe.)

    Cutting accuracy: Very high and clean.

    Heat affected zone: Very small.

    Discharge: Non.

    Key issues: Miniaturization of the head.

3.2.2 Comparison of the applicable Cutting Method

Secondly, in case of the application of the FW support leg and the back cover plate cutting, the other key requirements shown in the followings have to be considered. It should be able to

- reuse the cut cross section for welding without any machining to make the groove,
- make no use of the coolant,
- protect the peripheral structure against the cutting power,
- pass through the narrow access hole from the rear side of FW, in case of the FW support leg cutting.

When these requirements are applied to the above five methods, still Laser Beam and the mechanical cutting methods remain for the candidate cutting method. Therefore, the more detailed feathers and the applicability of both methods have been investigated. The details are described in the pages that follow.

3.2.2-1　Laser Cutting

It is one of the melt cutting methods with using Laser Beam for heat source and also in wide use for thin plate cutting [3]. On the thick plate cutting, since it didn't come into wide use, the cutting condition for YAG Laser investigated on the basis of past experimental results is described in the followings.

The following results were obtained by the conditions of SUS304 6mmt plate inclined at angle of 75° and 90°(normal butt welding), duty 30%, 500mm/min velocity, O_2 assisted gas, with 2kW nominal CO_2 Laser beam power. The cross sections of welded joints as an example are shown in Figs. 3.2-1 and 3.2-2.

1) Soundness joint without defects was obtained in both cases, on the same cutting condition.

2) Cutting gap was about 0.3mm uniformly in both cases.

3) Roughness on the cutting surface was Rmax.52.6μm in the case of angle 75° and 49.9μm in 90° one.

4) Flow mass of shield gas was 115l/min (reaction force at cutting was about 12N), and that of assist gas was 200 l/min (reaction force was about 21N). Therefore, the total mass of gas was 315l/min (reaction force became about 33N). Figure 3.2-3 shows an example of a measuring reaction by Laser beam cutting, for your reference.

5) Dross clung to the rear side of cutting edge was observed. It was easy to remove the dross by metal brush because it had the tendency to be brittle and come off easily.

From the above results, the Laser beam power to cut the 10mm thick SUS316LN is estimated. On the assumption that a mean power of cutting is same as the nominal power 2kW and the duty is 30% - 50%, the peak power is calculated to be 4kW - 6.6kW. Therefore, taking some margin into account, Laser machine which has a nominal 5-7kW power is needed. These power levels of Laser machine have come slowly into use recently, but they still belong to the category of special high power device.

Finally, the Laser Beam cutting method which has the nominal 5-7kW power can be applied to the FW support leg and the back cover plate cutting, though the following issues still remain to be solved.

- Cutability in the narrow space in the shield block.
- The post treatment methods for the cleaning, the dross collection and the machining.

3.2.2-2　General Mechanical Cutting Methods

(1) Disc type cutting tool and Hole-Saw

On the disc type cutting tools, an electro-deposition diamond disc type and a whetstone one are given. These are in general use for cutting and can cut a certain material with a rotating disc at 8000-10000 revolutions per minute without coolant or lubricant. A cutting direction in each method is only in the radial direction on the disc, and their reaction forces for cutting steel are presumed to be 80-200N and 40-120N, respectively. The details which were tested by experiments are shown in Table 3.2-1. In case of the applicability to the FW support leg cutting, though it is able to cut the leg perpendicularly, it needs to make machining to get the prescribed angular groove shape after cutting. And in that to the back cover plate, it is difficult to cut the thick plate along a curved line because it can cut out only in the radial direction of the disc.

On Hole-Saw, it is an excellent cutting machine for making a round hole in the plate, and also has a simple structure with no use of any coolant and has a good portability. Figure 3.2-4 shows an apparatus of the Hole-Saw head and a situation of cutting test which was done in 2004 without any coolant or lubricant. While it can be seen from the figure that it became discolored in some degree at the side surface of the Hole-Saw, an austenitic stainless steel 316L plate with ϕ80mm hole was obtained cutting out a 13mm thick disc without any nicking in the edge. In the applicability, the Hole-Saw machine can be applied to the back cover plate cutting in Hot Cell.

(2) Disc-Cutter

We, JAEA, have developed a Disc-Cutter technology in Fusion Engineering Reactor Design in Japan since 1984, with the view of applying it to main pipe's cutting at the maintenance stage, and have obtained a lot of satisfactory results through the R&D [4]. Schematic drawing of the then Disc-Cutter head and an apparatus of the one manufactured by way of trial are shown in Figs. 3.2-5 and 3.2-6, respectively. On the cutting principle of the Disc-Cutter, it uses a shearing force like a pressed cutting. The Disc-Cutter head shown in the figure mainly consists of a disc knife with a sharp V-shaped tip, of which axis has an own moving system toward the outer direction, and two support rollers which hold the reaction force from the disc knife. The Disc-Cutter head itself has a system of the revolving on the head axis with keeping their relative positions among the disc knife and support rollers. Though the disc knife has only a moving system toward the outer direction mentioned above, it has no system of the revolving itself by force on its axis. Therefore, it is possible to cut a round wall smoothly and spontaneously.

The cutting mechanism process of the Disc-Cutter is as follows:

- The Disc-Cutter head is installed in the correct cutting position of the pipe,

shown in Fig. 3.2-7 (step 1).

- The Disc-Cutter head starts to revolve on the head axis.
- At the same time, the disc knife moves towards the outer direction with keeping pressing force under control, shown in the figure (step 2).
- After the V-shaped tip and the support rollers touched the inner surface of the pipe, the disc knife itself revolves spontaneously along the inner surface of the pipe and cuts into the pipe in proportion as the Disc-Cutter head revolves on the head axis, shown in the figure (step 3).
- The disc knife is housed in place after penetrating the pipe perfectly, shown in the figure (step 4).

Since it has a mechanical tendency in the Disc-Cutter machine that the disc knife keeps to run in a cutting route once made on the inner surface of the pipe, it is no necessary to make a special system to support the Disc-Cutter head except it's own pressing system in cutting.

Large advantages of applying the Disc-Cutter machine to the component in Hot Cell and that in the reactor are as follows:

- It can eliminate post-treatment such as a cleaning after cutting, because the Disc-Cutter machine makes no material chips.
- It is no necessary to use coolant with lubricant, because it causes scarcely generation of heat during the cutting.
- The cut section of the pipe, as it is, can be applied to the rewelding without any machining, because the section is very smooth and has no deformation.

For a disadvantage, it is applicable to only pipe shape with the range of 3-5in Caliber.

Figure 3.2-8 shows an example of pipe cut section obtained from R&D of the Disc-Cutter in 1993. It was applied to the austenitic stainless steel 304 pipe of $\phi 114.3$ $^{ID}/126.3^{OD}$ mm [5]. The condition of the section was very smooth and there was no defect and deformation to be found which interfered with the rewelding by YAG Laser beam. And needless to say it has a reproducibility for cutting.

3.2.3 Selection of the cutting method

From the investigation of the cutting methods mentioned above, we have finally decided on applying the Disc-Cutter to the FW support leg cutting and the How Saw to the back cover plate cutting, for the reference. It is clear from the investigation that the Disc-Cutter has a lot of advantages and is superior to the Laser Beam cutting which is an alternatives.

3.3 Selection of Nondestructive Inspection Method

Though, in general, there are more than four kinds of nondestructive inspection (NDI) methods which are applicable to the normal weld joints, such as a radiographic testing, a liquid penetrant, a magnetic particle and an ultrasonic detection testing (UT), UT is supposed to be the only measure left among the NDI methods on the selection of the NDI method applied to the weld joint of FW support leg and that of cover plate in Hot Cell, taking the preservation of environment and the workability in the narrow space into account.

A schematic UT tool applied to the weld joint of FW support leg is shown in Fig. 3.3-1 and that to the cover plate is shown in Fig. 3.3-2. A 45° injection angle prove is applied and alcohol is used for the vehicle of ultrasonic wave in a gap with 0.5mm between UT prove and an inspection surface. While it has a possibility to use usual water instead of the volatile alcohol, in this case, how to remove it and to keep a circumstance of He leak test after the inspection become one of the key issues.

Table 3.3-1 shows the detectability against typical assumed defects under UT inspection. It can be said that it is possible to detect the defects at the tip on the root in theory. It needs, anyhow, to confirm the applicability and the detectability through R&D.

3.4 Remote Handling Tools for FW replacement in Hot Cell

In this section, investigation of the followings are described, which are based on the remote handling technology cultivated through R&D.

- Components of remote handling tools
- An error range of the FW replacement by remote handling
- A detection error in CCD camera

A conceptual drawing of FW replacement equipment by the remote handling in Hot Cell is shown in Fig. 3.4-1. The equipment for FW replacement consists of a work table, a main machine, replacement unit tolls and a tolls' luck. For the replacement unit tolls, five kinds of unit tools such as for cutting, welding, screwing up, inspection of UT and for back cover gripping are housed in the tolls' luck. The main machine has functional axes which consist of three straight active axes (X, Y and Z axis), two rotating active axes (α, β) and two teaching subordinate axes (a, b). The main function of these axes and the relative accuracy of control are shown in Table 3.4-1. The accuracy of axis Y and Z based on the actual past results are estimated to be about 0.017mm and 0.019mm respectively, and a general mean accuracy that is square root of square sum is to be 0.026mm. Especially,

since the axis of Y, Z and β are main axes to carry out the welding and cutting directly, it is very important to evaluate the accuracy of a control device exactly.

Figure 3.4-2 shows a schematic compliance system on which the remote handling tool is mounted. It can control the a- and b-axis in order to absorb the positioning error of the above mentioned main moving axis.

A flow of optical compliance method and a schematic detection error are shown in Fig. 3.4-3. In order to locate a working point, it is useful to take and evaluate a visual picture through the CCD camera installed on the welding and cutting tools. In the procedure of the revision, after the confirmation of the origin of the coordinate axes by a guide light, the visual picture which detects a boundary of the weld joint (opening root) with moving the guide light to an initial objective point are recorded. After calculating the center line of the boundary from the visual picture, the positioning data is revised to the new. The detection error is equivalent to a diagonal length in one pixel in the visual picture and it depends on the magnification rate in CCD camera. For example, since the radiation resistant CCD camera has 525 x 650 pixels, assuming that an actual 10mm x 10mm area comes within the range of this scope, it is 19μm long in one pixel length and the detection error becomes 27μm.

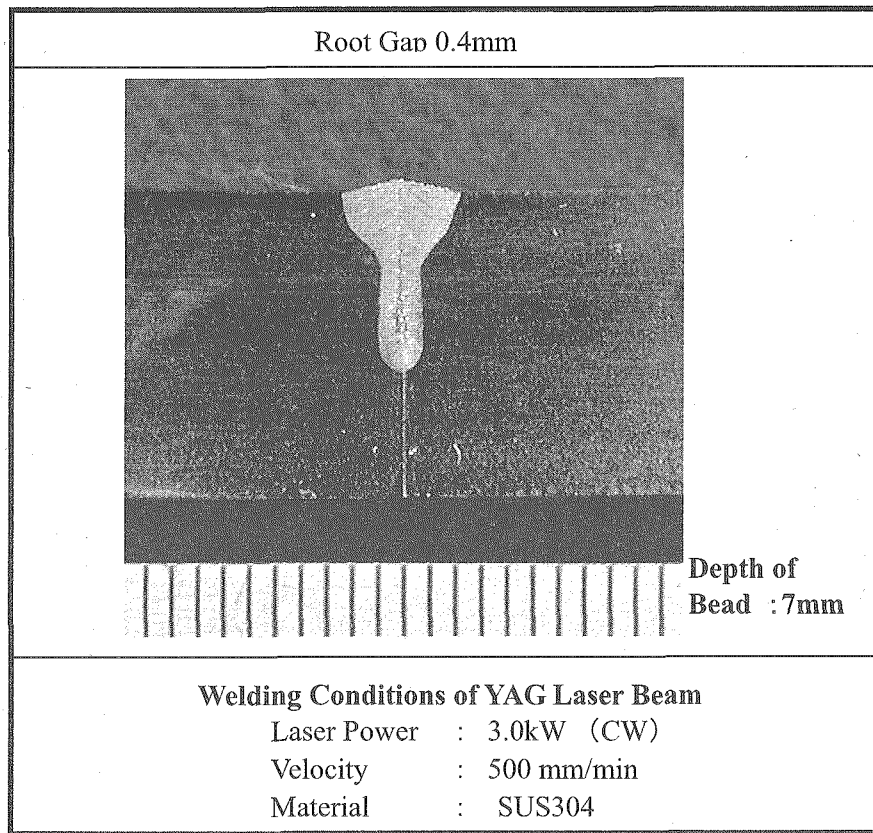Table 3.1-1 Cross-section of Weld Joint under the condition of Root Gap 0.4mm

Root Gap 0.4mm

Depth of Bead : 7mm

Welding Conditions of YAG Laser Beam
Laser Power : 3.0kW （CW）
Velocity : 500 mm/min
Material : SUS304

Table 3.1-2 Comparison of Joints configuration for FW Support Beam
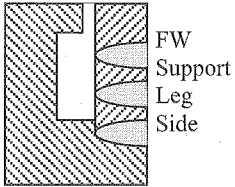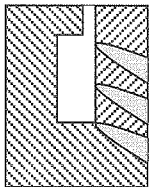
Configuration of Joints	Merit	Demerit
Groove for normal butt welding Shield Block Side · FW Support Leg Side	The structure is simple.	It has a tendency to cause the slide gap. The optical instrument in the nozzle will be damaged by the reflections.
Proposed groove for angular butt welding	The setting is much easer. The damage to the optical instrument in the nozzle by the reflections will be much less.	Actual welding thickness is increased.

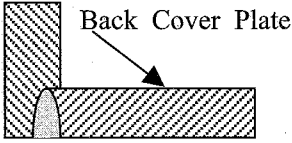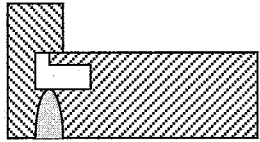Table 3.1-3   Comparison of Joints configuration for Cover Plate

Configuration of Joint	Merit	Demerit
Groove for Socket welding Back Cover Plate	The structure is simple.	It needs to machine the cut section into the Socket shape every Laser cutting. It has a tendency to cause the defects at the tip and at the notch. The rear side damage by Laser cutting is not clear.
Proposed Square Groove	Machining will be unnecessary after Laser Cutting. It can weld the cutting section as it is. It prevents the dross and shavings from scattering.	The structure is complicated, if pressed.

Table 3.2-1   Comparison of Cutting methods for FW Support Beam

Cutting Method		Example of cutting	Reaction force	Lubrications	Demerit
Machining	Cutting	Electrodeposition Diamond disk Disk diameter : 45 mm Thickness : 0.3 mm Number of Rotation :10,000rpm	80-200 N*	No need	-Chipping the disk. -Cleaning the chips. -Machining the inclined root -Frequency in changing disk -Velocity of Cutting.
	Grinding	Cutting whetstone Disk diameter : 45 mm Thickness : 0.7 mm Number of Rotation : 8,000 rpm	40-120 N**	No need	-Chipping the stone. -Cleaning the powder. -Machining the inclined root -Frequency in changing disk -Velocity of Cutting.
Laser Beam Cutting		Pulse Laser Peak Power : 2- 3 kW Cutting Velocity: 300-500mm/min Assist gas : O_2	- 30 N***	No need	-Cleaning the dross -Maintenance of the lens

* Estimated from the power data of supper steel end mil

** Measuring data of Reaction force for SS400 and S45C

*** Estimated from the measuring data on the condition of 115 l/min (Ar velocity).

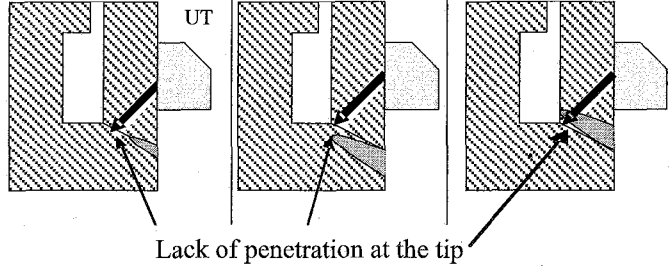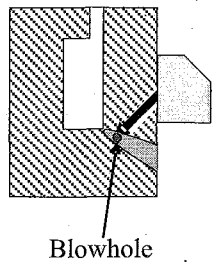Table 3.3-1   Assumed defects under UT inspection and the detectability

Assumed defects	Lack of penetration	Gap of positioning	Gap of positioning	Blowhole
Schematics of Inspection	UT		Lack of penetration at the tip	Blowhole
Detectability	The defects at the tip on the root can be detected in theory.			The minimum limit of detectability for stainless steel within 25mm thickness is 2.4mm diameter.

Table 3.4-1   Error factor and error range in the main axes

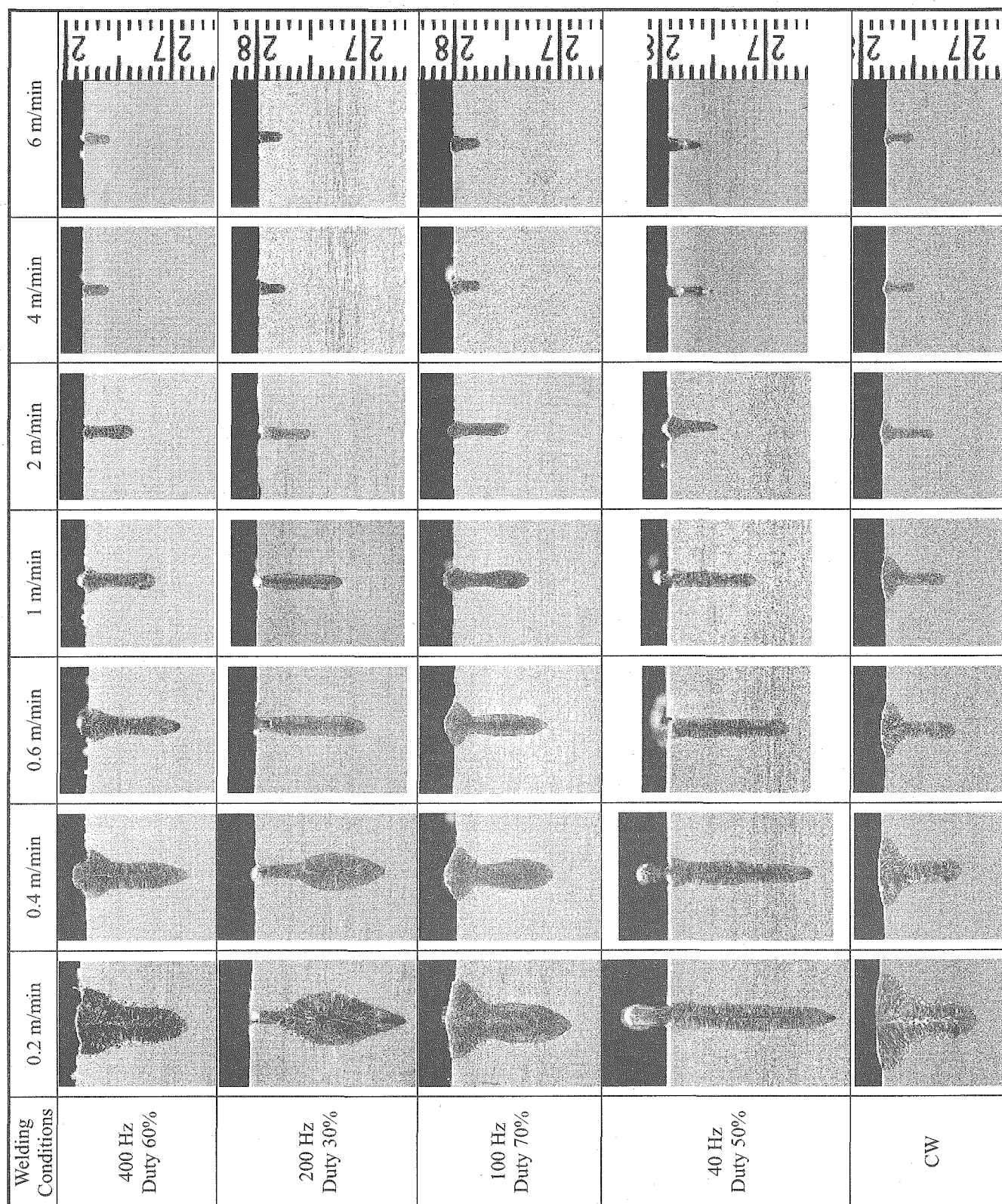| Parts	Primary Factor in Error	Error	
		Y-axis	Z-axis
Resolver	Measurement	1.2μm	1.2μm
Coupling	Backlash	0μm	0μm
	Lost motion	0.7μm	0.7μm
Ball Screw	Leading	3μm	7μm
	D-centering	10μm	8μm
	Gap in Axis	0 (preload)	0 (preload)
Air Check	Repeatability	2μm	2μm
	Total	17μm	19μm

Fig. 3.1-1 Bead cross sections in the case of bead on plate welding by YAG Laser beam (SUS304)
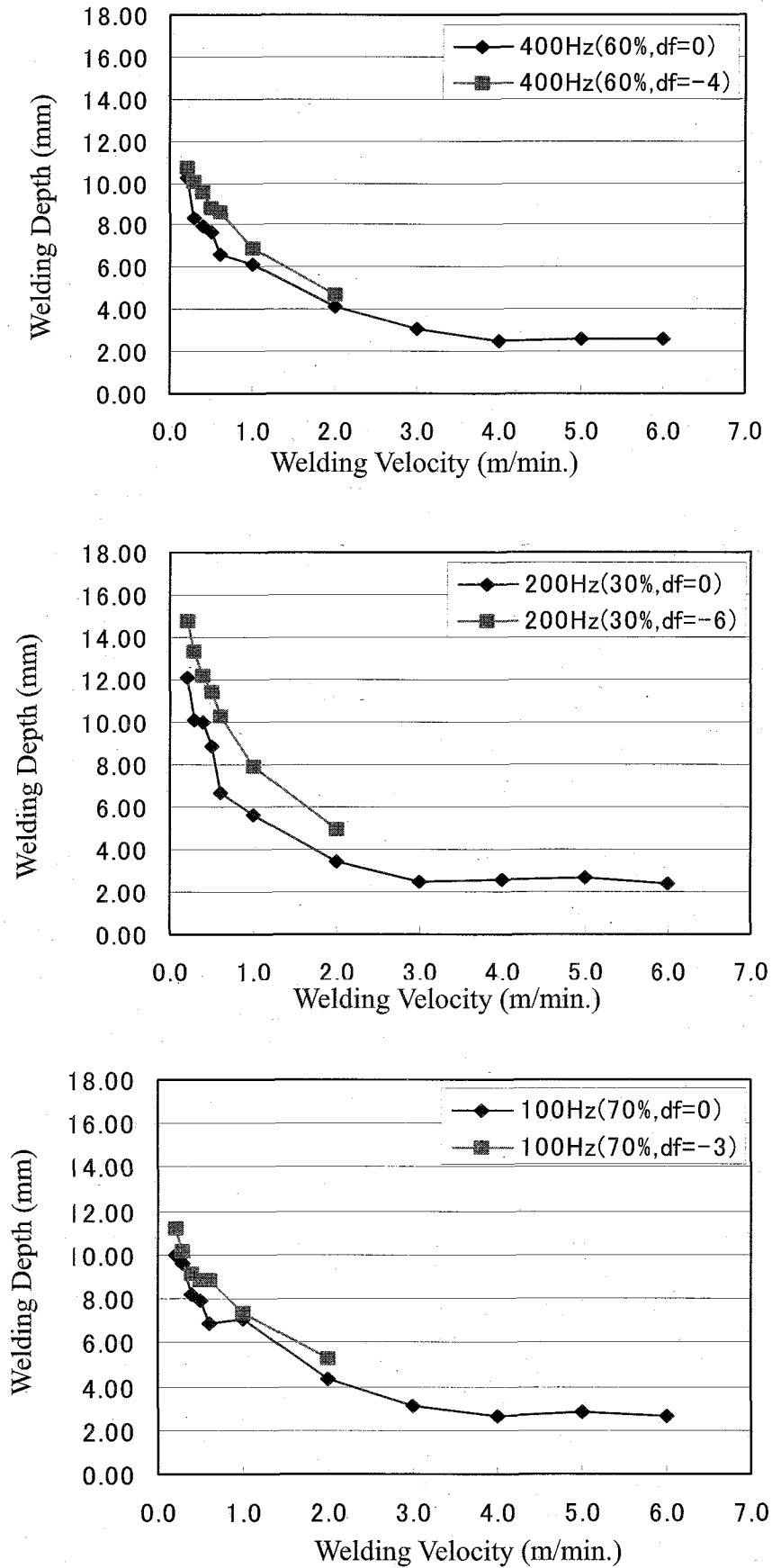
Fig. 3.1-2　Relation between welding velocity and depth (1/2)
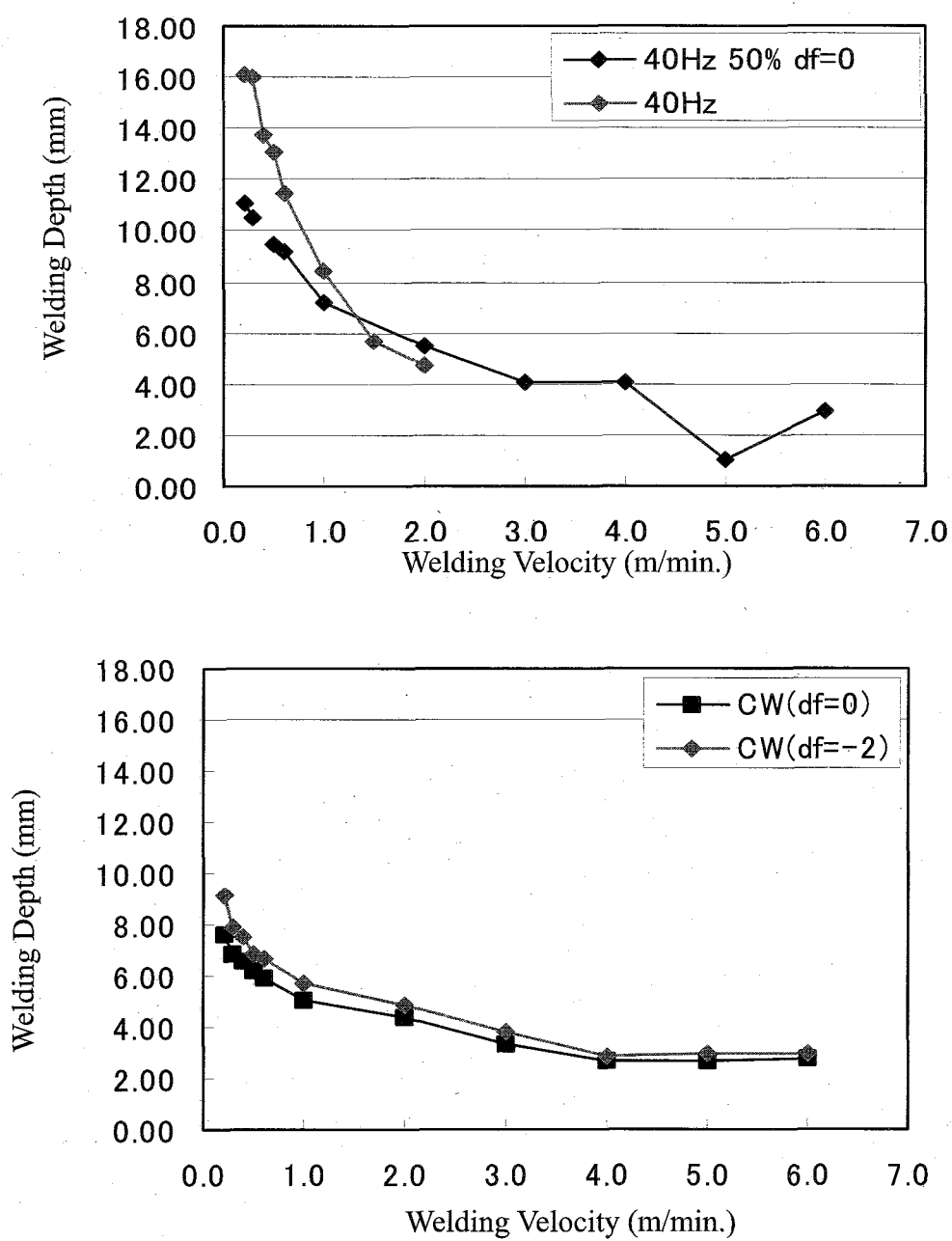
Fig. 3.1-2   Relation between welding velocity and depth (2/2)
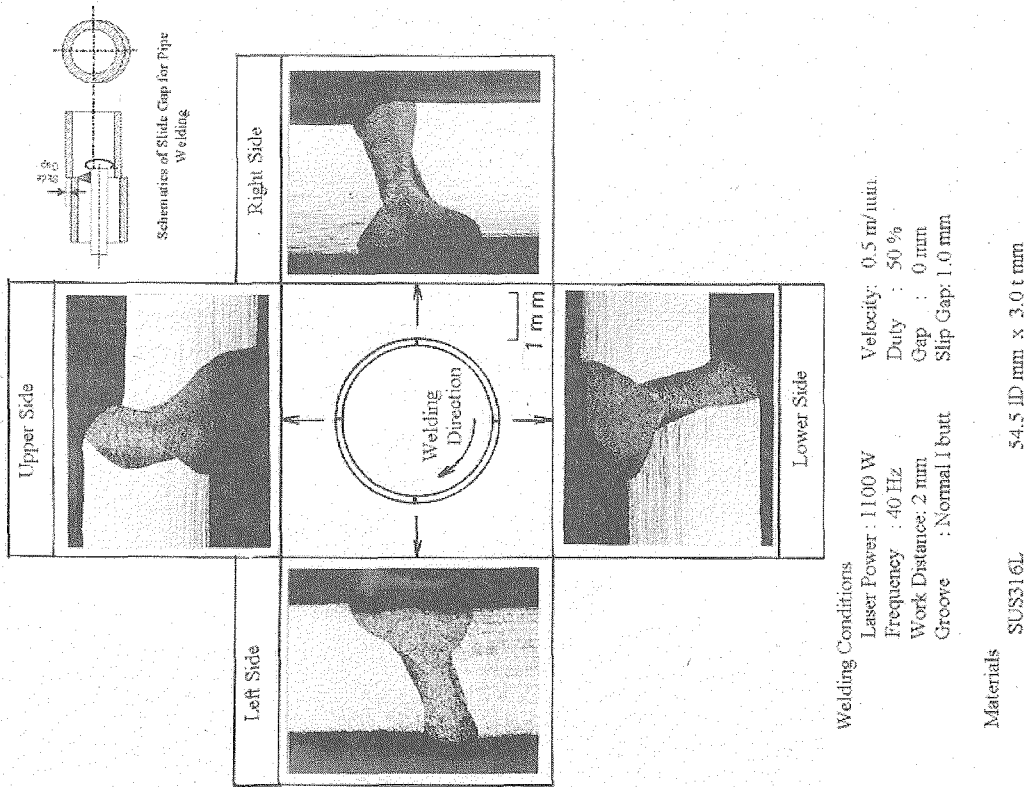
Fig. 3.1-4　Cross section of the weld joint
made by Laser Beam with 1.0mm Slip Gap
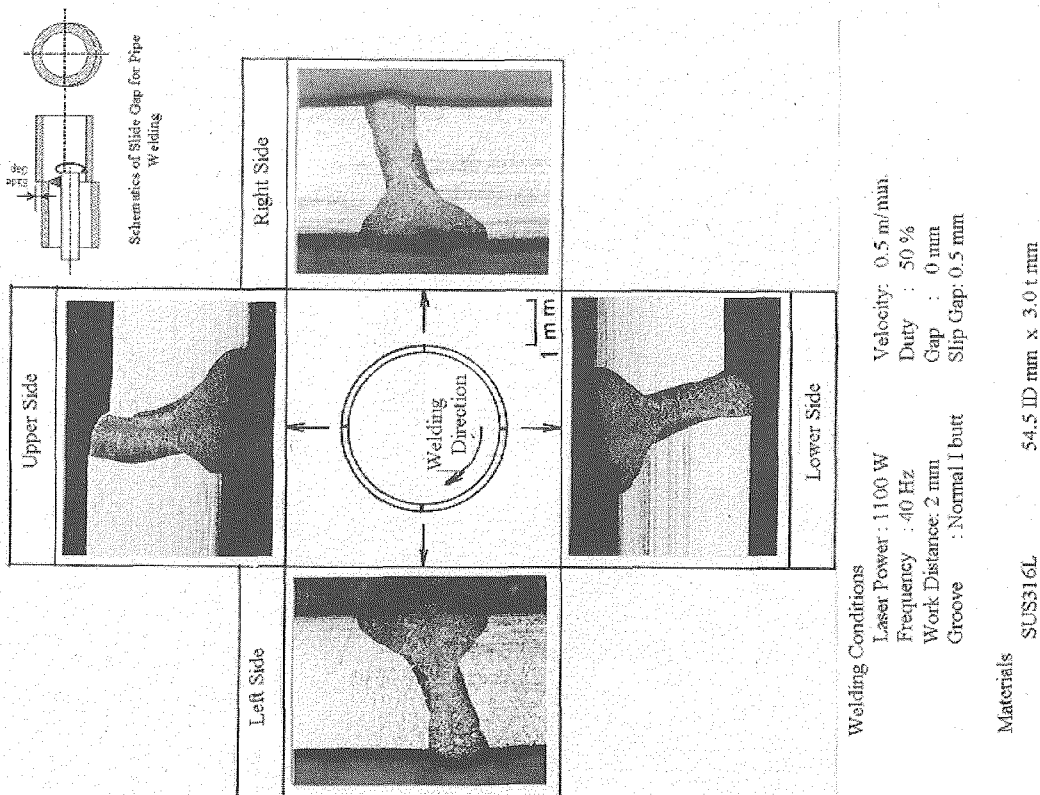
Fig. 3.1-3　Cross section of the weld joint
made by Laser Beam with 0.5mm Slip Gap

Fig. 3.2-2   Results from the Laser Cutting Test
with Angular Groove

Fig. 3.2-1   Results from the Laser Cutting Test
with Normal Angle Groove
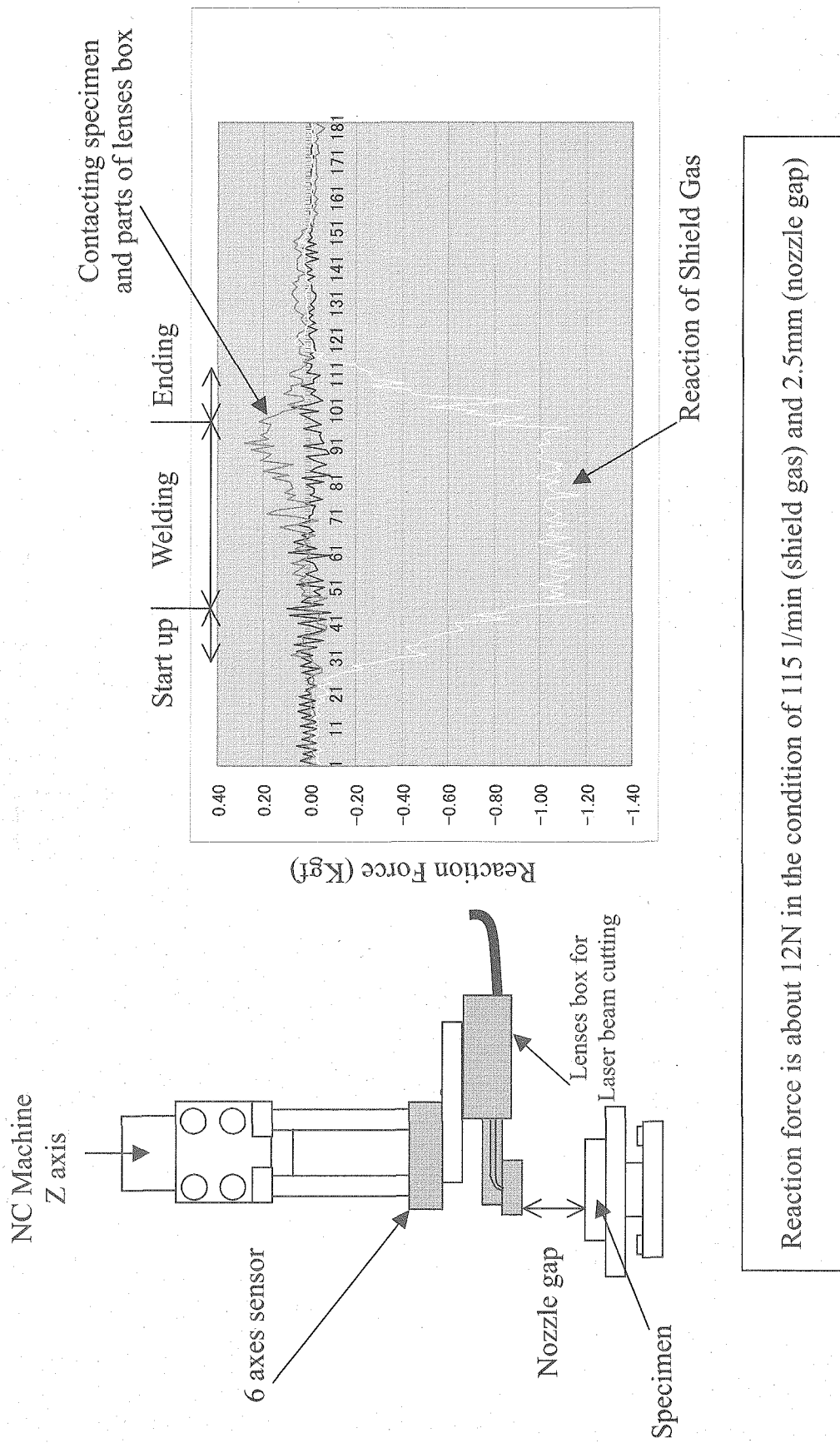
Fig. 3.2-3   Example of a measuring reaction by Laser beam cutting

Reaction force is about 12N in the condition of 115 l/min (shield gas) and 2.5mm (nozzle gap)
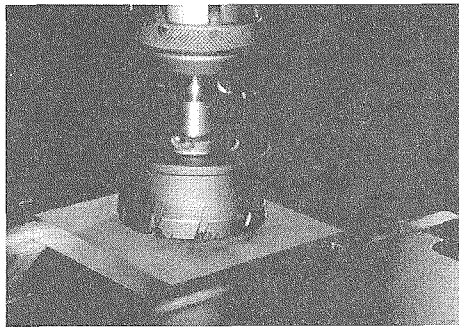
(a) Before Cutting Test
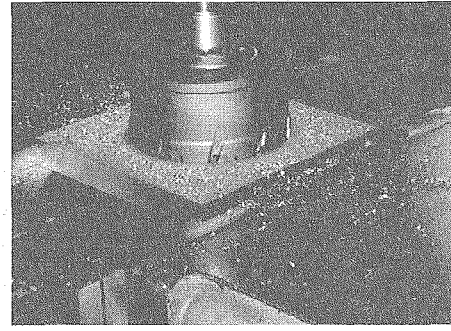
(b) Cutting Test in progress
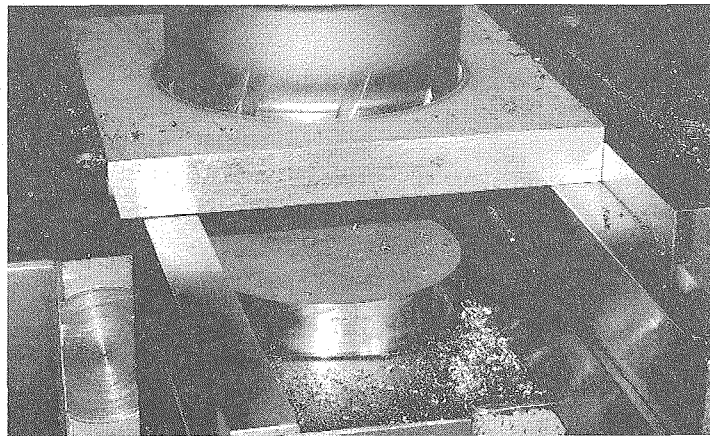
(c) After Cutting Test

Fig. 3.2-4   Appearance of Hole-Saw Head and Situation of Cutting Test
(SUS316L plate with 13mm thickness)

Pipe
($\Phi 102.3^{ID}/\Phi 114.3^{OD}$)

Support rollers

$\Phi 30$

$\Phi 95$

$\Phi 96$

135   43

10   12 12

(87)   Disc knife

Pressing System

400

Before Cutting
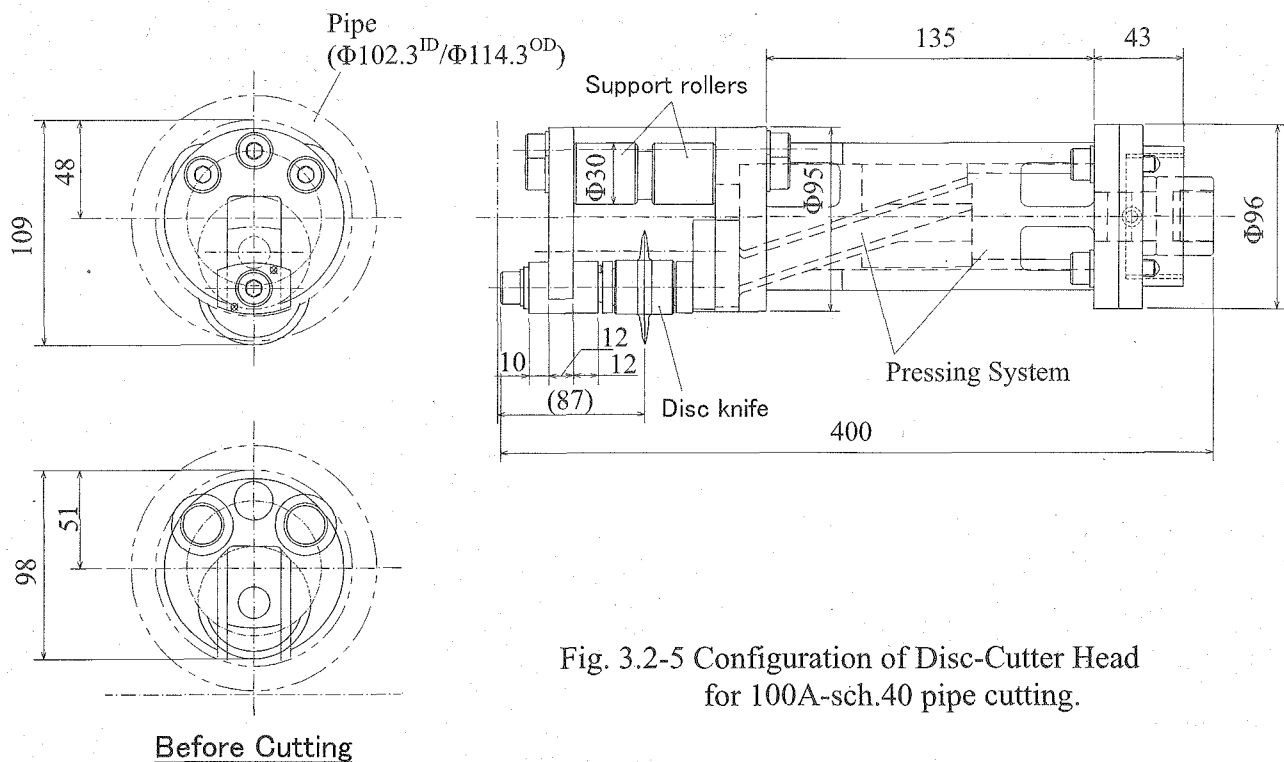
Fig. 3.2-5 Configuration of Disc-Cutter Head
for 100A-sch.40 pipe cutting.
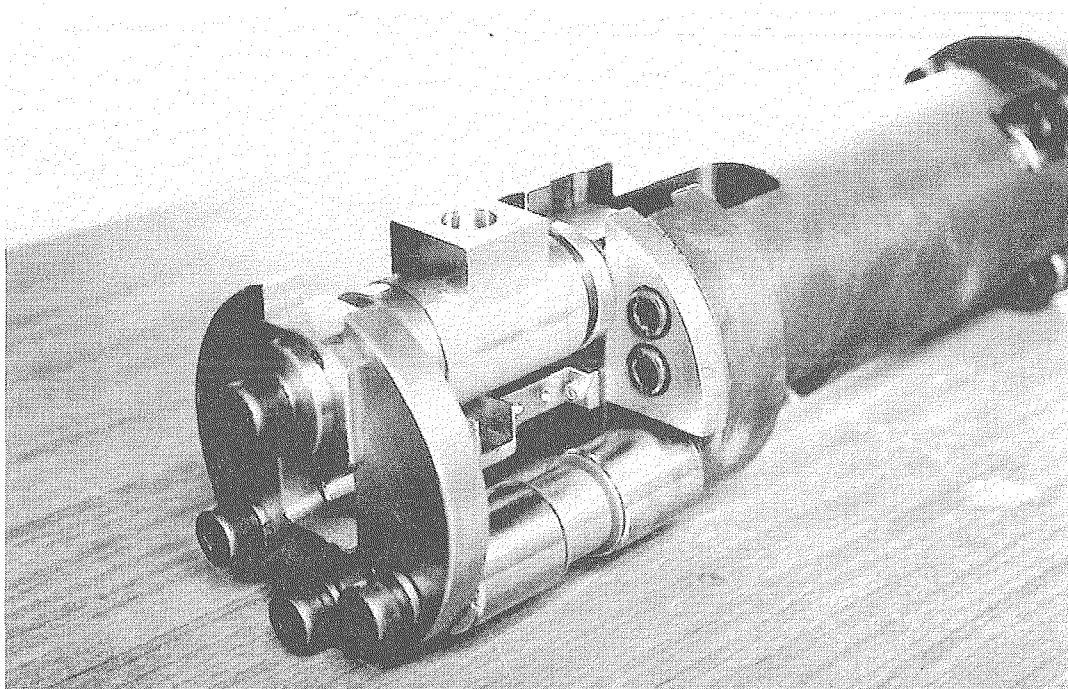
(a) Front View
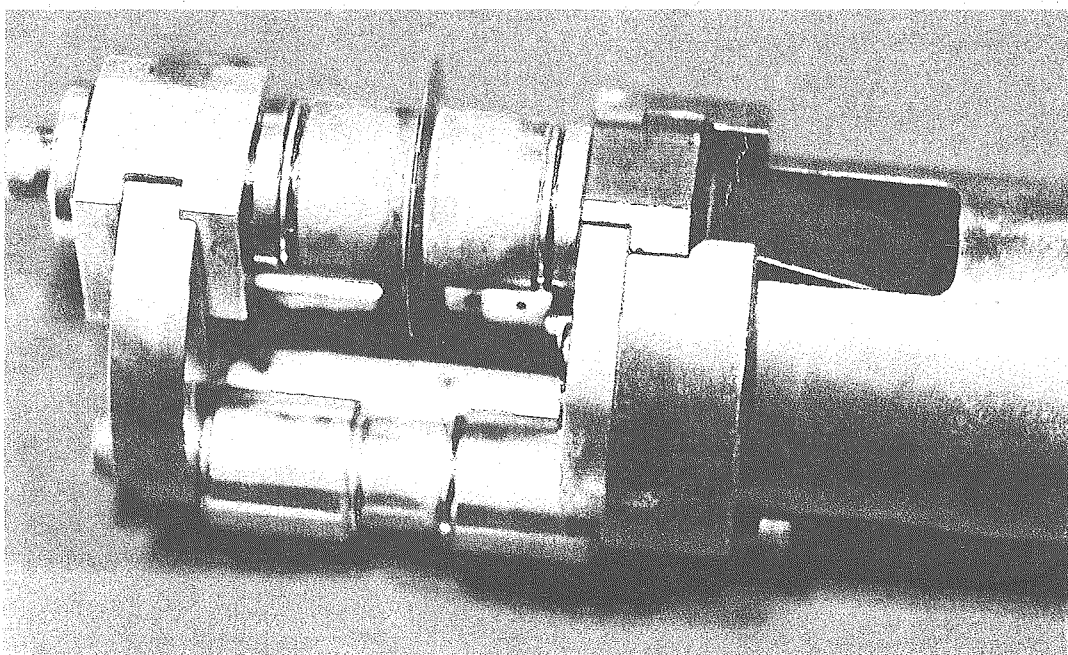
(b) Side View

Fig. 3.2-6　Appearance of Disc-Cutter head manufactured by way of trial.
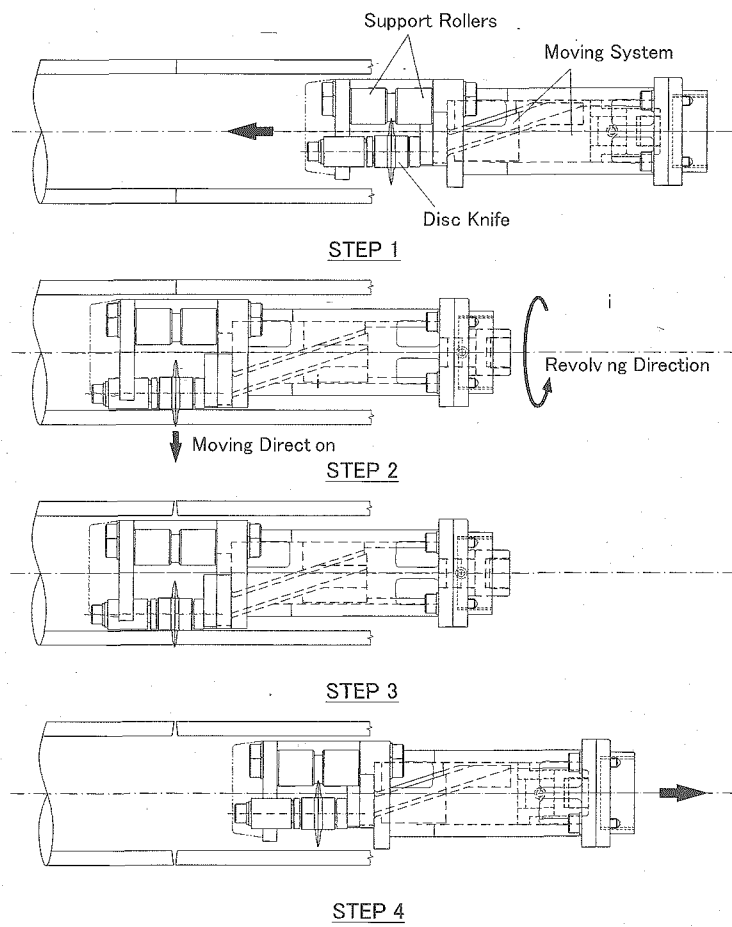
Fig. 3.2-7　Cutting procedure of Disc-Cutter

SUS304
$\Phi114.3^{OD}$mm x 6tmm
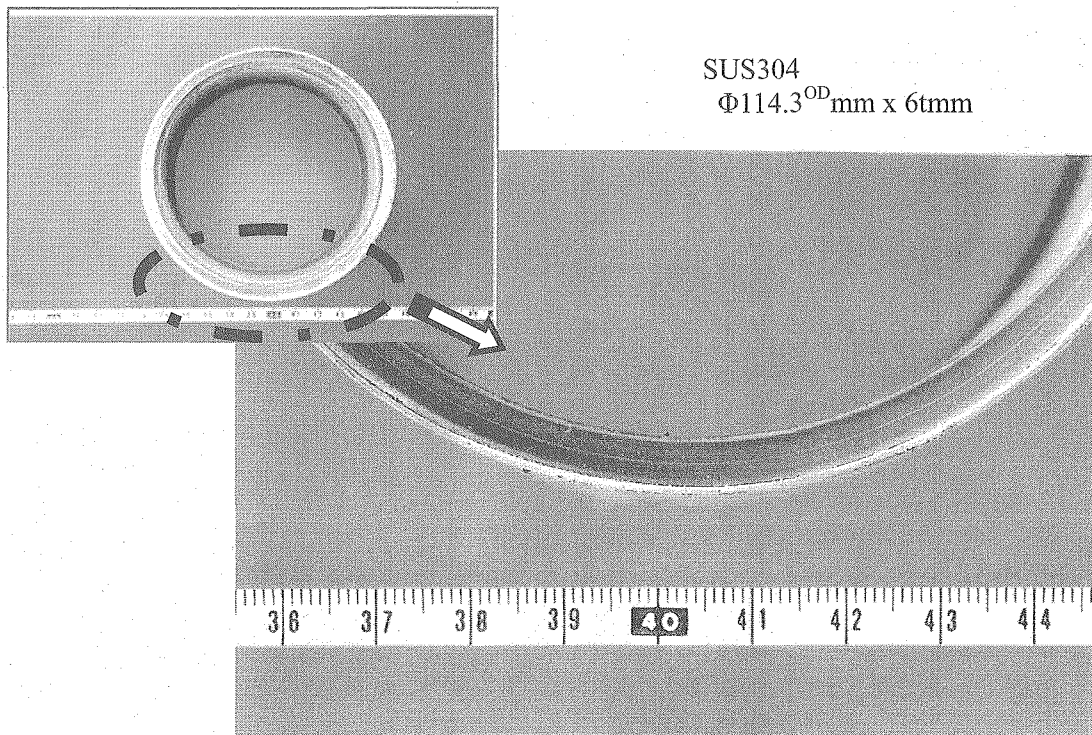
Fig. 3.2-8　Appearance of cutting section by Disc-Cutter

Probe for UT with the angle beam method
(Inclined angle is 45°)

Projection

10

10

Projection

Fitting direction

Spring Plate with the function of the compliance mechanism fitting UT probe onto weld joint surface

Tubes of supply alcohol
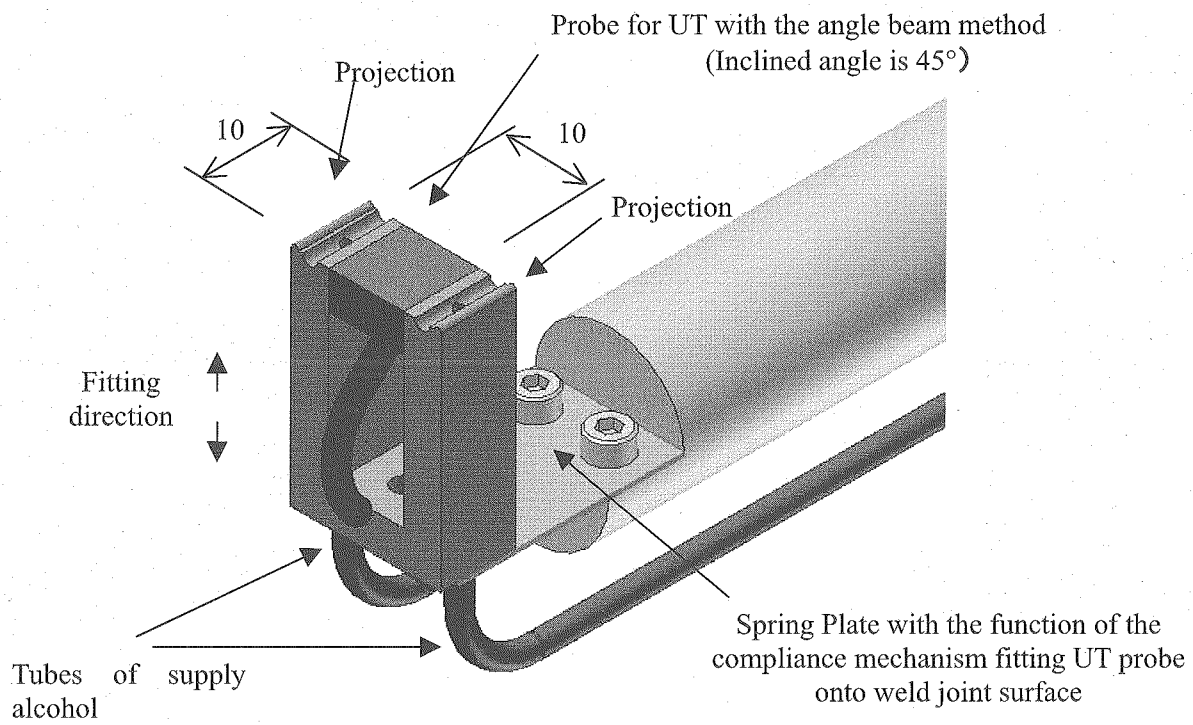
Fig. 3.3-1   UT Tools for Inspection of FW support leg weldment

10

5

Fitting direction

Probe for UT with the normal beam method

Spring Plate with the function of the compliance mechanism fitting UT probe onto weld joint surface

Tube of supply alcohol
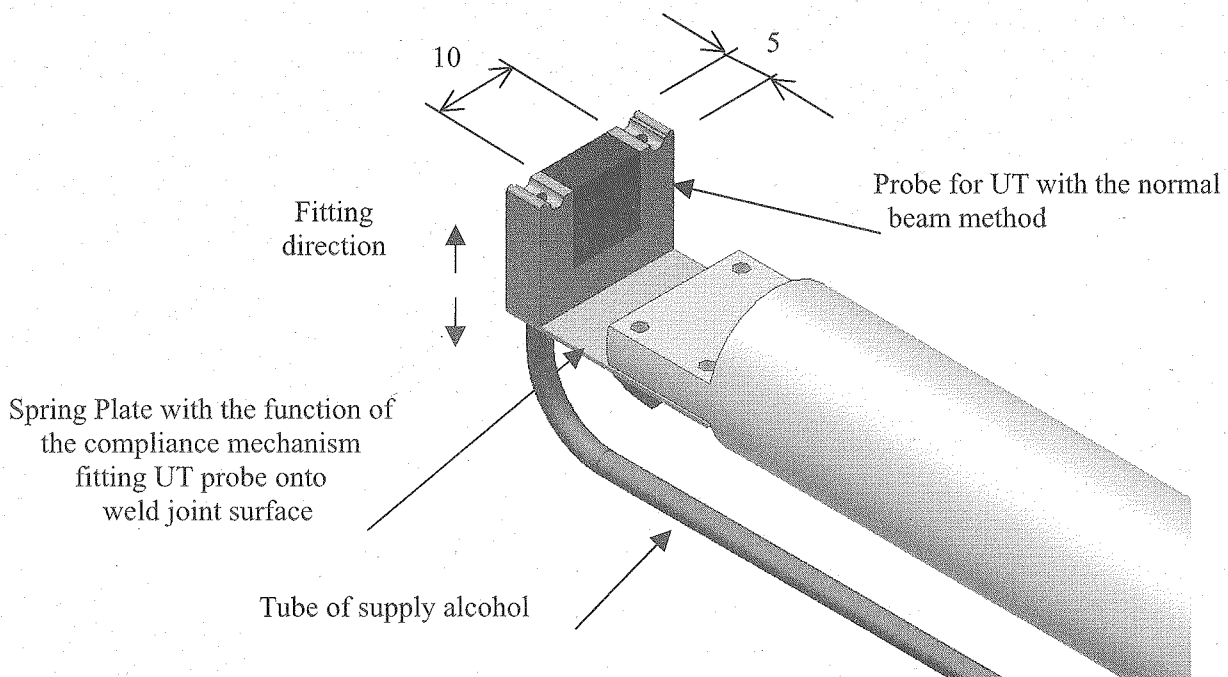
Fig. 3.3-2   UT Tools for Inspection of Cover Plate weldment

Tool for
Screwing up

Blanket Module

Tool for
Welding

Tool for Cutting

Tool for UT

Camera

Tool for
Cover Plate
Gripping

Tool Rack

Z(3)

β(5)

α(4)

a(6)

b(7)

Y(2)

X(1)

Machining Table
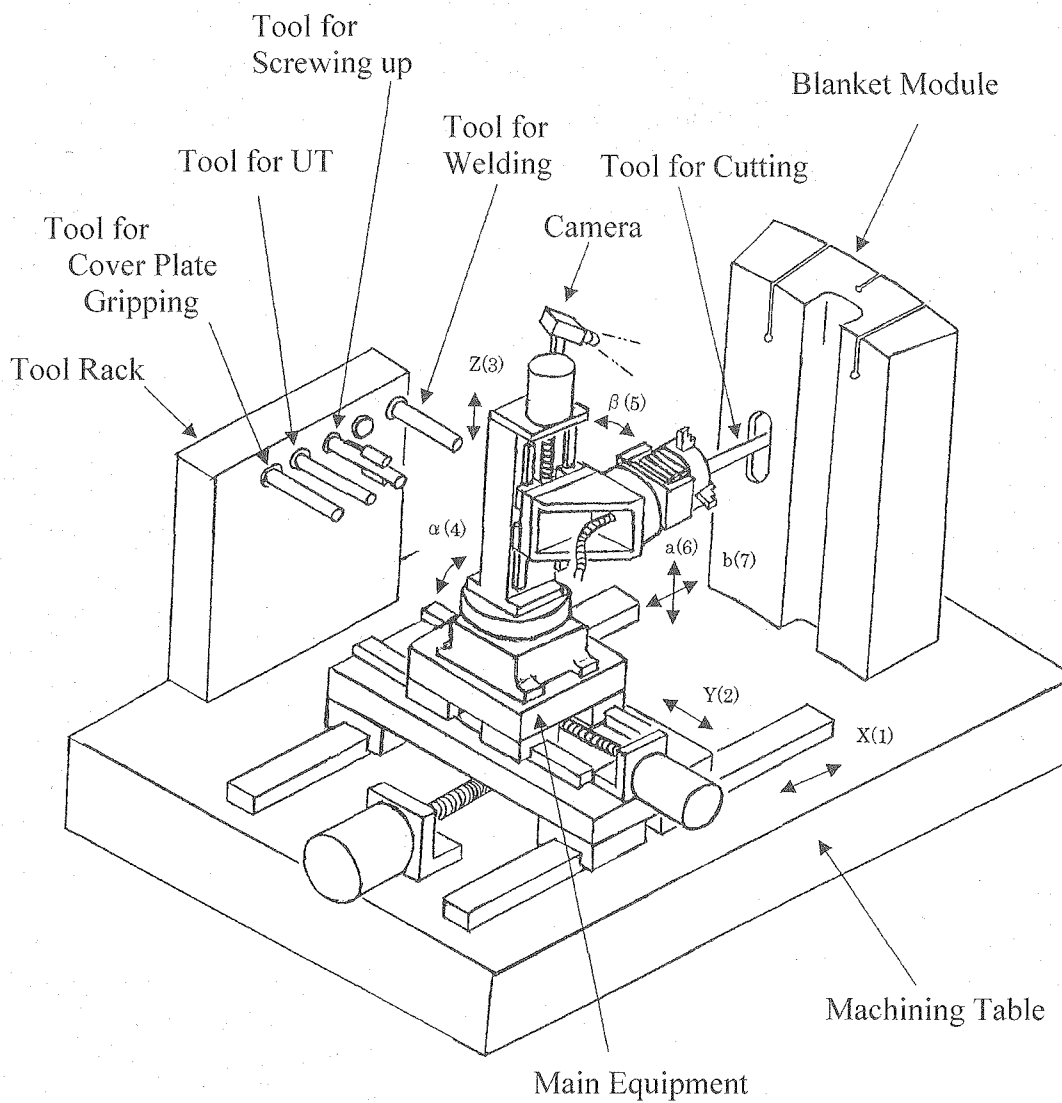
Main Equipment

Fig. 3.4-1 Schematics of Maintenance Equipments for FW Replacement

Fig. 3.4-2 Compliance System

Error of detection < Diagonal length in one pixel

It depends on the magnification rate.
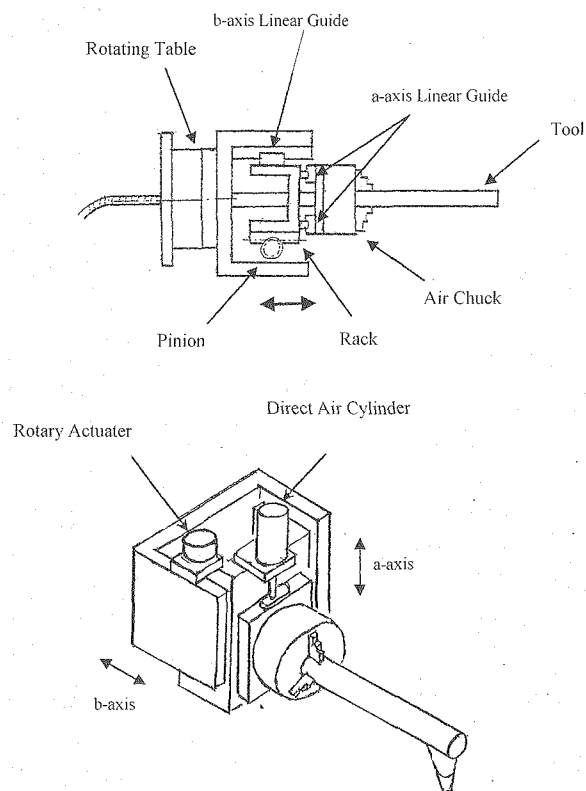
Fig. 3.4 - 3   Optical compliance method and detection error

4. Investigation of Blanket Module Design

In this chapter, the investigation of the FW support leg structure with new two circular type connection based on the technology of Disc-Cutter cutting and YAG Laser beam welding is described. And the structure of Disc-Cutter head and the shield blanket module #10, which are consistent with the new two circular type of FW support leg structure, are also investigated.

4.1 Design of Blanket Module

4.1.1 Design of FW Support Leg
(1) Proof against EM Loads

Fig. 4.1-1 shows a back side view of the two circular connection type of FW support leg structure onto the shield blanket module #10. EM loads on the inboard FW panel in the case of slow vertical displacement event described in ITER Design Description Documents (DDD)* are used for a preliminary stress calculation of the structure. The details are shown in Table 4.1-1. For the halo current in the worst loading case, it was assumed to be 70kA on each FW panel resulting from an assumed FW-normal halo current density of $0.18MA/m^2$. It produced a poloidal shear force of 150kN (F_p) per FW panel, a toroidal and a radial shear force of 31kN (F_t) and 79kN (F_r).

On the rough stress calculation for the two circular type, with new six elements on the FW support leg structure, namely moments (M_r, M_p and M_t) and forces (F_r, F_y a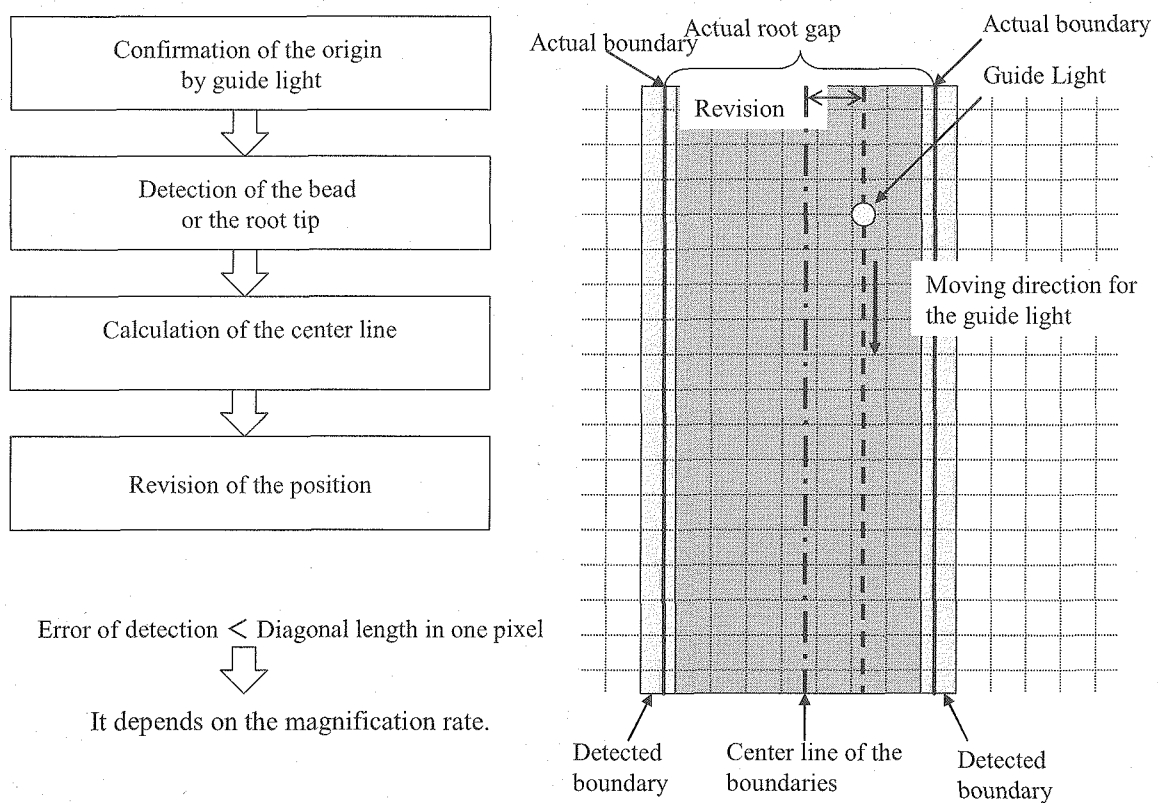nd F_z) recalculated from the above forces on the FW panel, main composition stresses are obtained considering the following conditions and general equations. Schematic of stress distributions on the round pipe structure are illustrated in Fig. 4.1-2.

- FW panel of 1005^Lmm x 345^Wmm.
- Pipe thickness of about 10mm (t) required from YAG Laser welding performance.
- Minimum inner diameter of pipe 80mm (d_i) required from Disc-Cutter cutting performance.
- Coolant pressure of 5MPa (P) required in the IT design condition for cooling.
- Dead weight of FW panel 2kN.
- The composition of stresses $(\sigma_1, \tau_{max})^{1)}$ based on bending stress $(\sigma_{Mp}, \sigma_{Mt})^{2)}$, twist

---

*: G16 DDD 2001, 0.1-06-07 W0.1, P201 Table 2.1.1-2

$$1): \sigma_1 = \frac{\sigma}{2} + \frac{1}{2} \times \sqrt{\sigma^2 + 4 \times \tau^2}$$

$$\tau_{max} = \frac{1}{2} \times \sqrt{\sigma^2 + 4 \times \tau^2}$$

where,   Stresses at a point $: \sigma_{Mt}, \tau_{Mr}, \tau_{Fy}, \sigma_t$

Stresses at another point $: \sigma_{Mp}, \tau_{Mr}, \tau_{Fz}, \sigma_t$

on the assumption that $\sigma = \sum \sigma_k$, $\tau = \sum \tau_k$

$$2): \sigma_{Mt} = M_t \times \frac{J}{I_1} \quad or \quad \sigma_{Mp} = M_p \times \frac{d_o}{2 \times I_2}$$

$$3): \tau = d_o \times \frac{M_r}{4 \times I_1 \ (or \ I_2)}$$

$$4): \tau = \frac{(d_o^2 + d_o \times d_i + d_i^2) \times F}{12 \times I_1 \ (or \ I_2)}$$

$$5): \sigma_t = P \times \frac{d_i}{2 \times t}$$

where, d_o : Outer diameter of Pipe

$I_1 \ (or \ I_2)$: Polar moment of Inertia

J : Distance from axis center to the top

Table 4.1-2 shows the results of the stresses with typical geometrical conditions. From the results, it becomes clear that it is possible to keep the composition stress within the range of 206MPa (allowable stress: 1.5Sm at 150°C) under the following conditions.

Thickness of the pipe	: ≥ 10 mm
Length of the FW support leg structure	: ≤ 200 mm
Height of the FW support leg structure	: ≥ 230 mm
Inner diameter of the pipe	: ≥ 80 mm

While case 7 is in the case of all equal signs in the above inequalities, it becomes 184 MPa with the maximum composition stress in the range. As compared case 7 with 8, for the effect of the thickness it is found that the composition stress reduces about 9% to 169MPa increasing the thickness from 10mm to 11mm. In the case 9 and 10 supposed to be the case of the inner and outer side of FW panel in the blanket module #10 described in section 4.1.3, the composition stresses reduce to 181MPa and 172MPa, respectively. Though the length of the FW support leg has to be changed in accordance with the configuration of each shield module and with the EM loads, almost the lengths of the FW support legs are supposed to be within the range of 200mm. These data in this section will be a good guide to the detail design in the next stage.

Detail calculation will be required to confirm the consistency of the two circular connection type of FW caused by the EM loads and other forces.

(2) Application of the equipments

An applicability of YAG Laser beam welding and that of Disc-cutter cutting to FW support leg with $\Phi 80^{ID}/100^{OD}$ mm connection has been developed considering not only the premise conditions summarized in Table 2.2-1 but also the following requirements.

- The shield block outer line and position of FW insertion holes should be no making alterations, which is a strong requirement from the IT.
- It should be possible to grip and hold the tools during the operation and to access to the cutting/ welding point.
- It should avoid rewelding at the weldment.
- It should be possible to remove the dross after welding and to apply the UT.

A schematic view of Laser tools relating to the welding of FW support leg structure is shown in Fig. 4.1-3. The welding tolls consist of ball rollers for positioning system and Laser beam transmission tools which have collimater lens and a parabolic reflecter. YAG Laser beam which has a 1.06μm wavelength of the light passes through a $\Phi 0.6$mm fiber and spreads in the directions from the edge of the fiber. After turning into the parallel rays by the collimater lens, the rays of light reflected from the parabolic reflecter are concentrated upon a welding focus. The spot diameter will be $\Phi 0.6$mm estimated from the image formation rate 1:1 in this case. N_2 gas is applied for an assist gas passing through a protective tube and all the welding region have to be filled with the gas. Though there is no description of the cooling tools for the parabolic reflecter and the body of tool in the figure, it needs to evaluate the necessity of the cooling in future work. Figure 4.1-4 illustrates a schematic view of FW support leg structure and the welding points. For the welding position, it takes at the distance, 7mm, from the previous joint and keeps a some inclined angle for butt welding, 20° in the figure. Though the welding and cutting thickness based on this concept becomes more than 10.6mm, it is no problem for Laser and Disc-Cutter performance. For the typical structure, there are an oblong groove with 10mm x 20mm that is installed for the purpose of collecting the welding dross which is located just behind the welding point, and a $\Phi 6$mm hole with a view to releasing the welding gas. And also it keeps a working space for the Laser head just rear side of the joint. Figure 4.1-5 shows a schematic view of positioning system for FW support leg welding at first maintenance stage.

Figure 4.1-6 illustrates a back side view of the Disc-Cutter head in progress of the cutting, and Fig. 4.1-7 shows a configuration of the Disc-Cutter head corresponding to a $\phi 80^{ID}$ mm/100 ^{OD} mm size of connection which can withstand the EM loads described above. The Disc-Cutter head shown in the figure mainly consists of a disc knife with a sharp V-shaped tip around $\phi 46$mm, of which axis has an own moving system toward the

outer direction, and two support rollers which hold the reaction force from the disc knife .
On the machine shown in the figure, it is possible to cut up to 11.6mm thickness pipe. A
procedure of FW panel replacement by Disc-Cutter is shown in Fig. 4.1-8. After the back
cover plates severed from the shield block by YAG Laser beam (shown in step 2), the
Disc-Cutter head is installed in the correct cutting position of the connection (step 3 and 4).
After the other one's cutting by Disc-Cutter (step 6), the FW is removed by the remote
handling equipment (step7) .

4.1.2 Design of the back cover plate

An applicability of YAG Laser beam welding and that of Hole-Saw cutting to the back
cover plate have been developed considering the requirements described in section 4.1.1(2).

A schematic view of Laser tools relating to the welding of the back cover plate are
shown in Fig. 4.1-9. The tolls for the back cover plate welding consist of almost same
components as the tools for FW support leg structure except the parabolic reflecter and the
positioning system. Since it needs a movement range for Laser equipment within the
distance, 150mm, from the surface of the back cover plate, it has to keep about $\Phi120$mm x
150mm space void for the remote handling movement space. Figure 4.1-10 illustrates a
configuration of the back cover plate in consideration of welding and cutting by the
remote handling. At the shield block side, there is an circular groove with 10mm x 15mm
cross section installed for the purpose of collecting the welding dross which is located just
behind the welding point. It keeps a 10mm thick wall to withstand the inner pressure
5MPa. For a pitch of the welding points, it takes 3mm at the distance from the previous
joint and keeps a normal shape for I butt welding, taking the investigation described in
chapter 3 into account. For the shape of the back cover plate, there are a groove for
gripping by the remote handling tools at the center of the outer surface, and a step for the
UT probe and for the ball roller for the positioning system around the cover plate edge.
Three ball plungers for keeping the own position instead of the remote handling gripper
during the welding, and a net with fine mesh for collecting the dross are installed on the
inner surface of the cover plate. And also four holes with $\Phi3$mm for releasing the welding
gas are installed between the groove and the mesh. In order to stop at a correct position, a
step is installed around the bottom of the back cover plate, which is shown in the figure.

On the Hole-Saw cutting, a schematic example of a part of the machine applied to the
cover plate cutting in the Hot Cell is shown in Fig. 4.1-11. The machine has a system of
material chips collection with use of compressed air and that of fixing to the shield block
except that of cutting. Since it is an elementary level of the investigation, further
investigation will be needed in order to put a consistent cutting system based on the
Hole-saw machine.

On the removing procedure of the back cover plate, it is shown in Fig.4.1-12. After the cutting by the Hole-Saw, fingers of an end-effector are moved into the gripping groove. Grasping the back cover plate with expanding the fingers, the end-effector carries and puts the plate in place. At the setting, it takes in the opposite procedure. After setting the cover plate to the correct position, the end-effector is housed back in order to avoid standing in the welding way. Therefore, it needs for the cover plate to keep the position with using the ball plunger shown in Fig. 4.1-10 till after the welding.

4.1.3 Design of Shield Blanket Module #10
(1) Overall design

Slits configuration in a special shield block #10 and a skeleton view of the designed shield block structure based on the two circular connection type of FW support leg are shown in Fig. 4.1-13. The shield block of the blanket module #10 is divided vertically into four trapezoid shape blocks which are fabricated individually and assembled together by EB-welding to form the module. There are five of C-shaped slits and two of partials, and three of C-shaped slits are located at the boundary between the blocks. Concept of a poloidal flow is partially adopted in a thin wall block and in a complicated structure besides the main radial flow concept*.

Configuration of structure around FW support leg and back region of FW in the outer shield block are shown in Fig. 4.1-14, and these in the inner one are in Fig. 4.1-15. All the structures relating to the FW panel replacement in the maintenance stage have been taking into account, such as the back cover plate and grooves for cutting and welding. In regards to the access hole from the cover plate to the FW support leg connection, a simple two holes concept with Φ80mm. is introduced in spite of the complex semicircular hole in the race track one. There are no inadequate points and interference among the components to be found in the structure. It is clear to make the structure simplify by means of integrating the inlet and outlet collector of FW into the shield block semi-permanently instead of using the incidental parts in the Race Track type. Accordingly, it is seen that the distance from the front surface of outer block to a weld point of FW beam becomes 129-149mm and that of inner one is 170-190mm. It has a high possibility to keep He production rate below 3 appm at the FW connection point through the optimization of the structure. All the selected methods described in chapter 3 will result in a remarkable improvement in the Hot Cell work for replacing FW panel.

The designed structure of a typical FW with the two circular connection type of the support leg is shown in Fig. 4.1-16. The configuration of the FW support leg connection to the shield block corresponds to the application of Disc-Cutter and YAG Laser beam welding. Inlet and outlet coolant are completely separated by the leak tight boundary in

*: ITER Task report 16-11, "EM Analysis of Modules, Dynamic Analysis of the Key and Module 10 Design Improvement", Chapter V.

order to avoid commingling with each other. Other whole structure in the FW panel are almost same as the FW designed by IT, except the position of two diverging points of coolant with Φ30mm hole.

(2) 3-D Thermal and Stress analyses

3-D thermal and stress analysis of a part of shield block in #10 module, by way of experiment, were carried out using I-DEAS ver11 NX in order to evaluate the soundness. The two models which were used for analyses that had the about 1/40 portion of the shield block, just below the FW insertion hole, are shown in Figs. 4.1-17 and 4.1-18.

1) Model A

a) Thermal analysis

A constant coolant temperature 125°C has been used in all cooling channels. Conditions of heat transfer coefficient for coolant holes and headers were considered based on the turbulence flows in equivalent diameter. The heat transfer coefficients used in the analysis are summarized in Fig. 4.1-19, and adiabatic conditions were applied on other interface surfaces. All material properties such as thermal conductivity for SUS316L(N)-IG were taken from the ITER Material Properties Handbook. On the conditions of the loads onto the shield, 5MPa of a coolant design pressure is applied. And the radial nuclear heating rate distribution $H_{\#10}$ calculated by the next equation (4.1-1) where $H_{\#14}$ has 0.78 MW/m^2 highest nuclear wall load in the outboard shown in the equation 4.1-2 from the ITER Nuclear Analysis Report (2001)*, has been used. In this connection, the range of nuclear heating rate onto module #10 is about 0.35-0.46MW/m^2 estimated from the report.

$$H_{\#10}(w/cc) = \frac{0.46}{0.78} \times H_{\#14} \qquad\qquad (4.1\text{-}1^{**})$$

$$H_{\#14}(w/cc) = 16.964 \times e^{0.1149y} \quad (9cm\langle \quad y \quad \langle 45cm) \qquad (4.1\text{-}2)$$

The resulting temperature distribution is shown in Fig. 4.1-20. Though the maximum temperature of 263°C (ΔT=138 °C) and a couple of more than 250°C heat spots occur at the front surface of front cover plate, those are much below the allowable value of 400°C indicated in the ITER Design Description Documents 2001. On the backward region from the front headers, the maximum temperature rises up to no more than 154°C (ΔT=29°C) at the location of the bottom surface of the shield, and almost all other heat spots' temperature at the internal part of the shield block are below 143°C (ΔT=18°C). Therefore, it is clear from the analyses that it is cooled very much in the shield block.

b) Stress analysis

Two load conditions have been taken into account for the analyses; the thermal loads calculated above section and a coolant design pressure 5MPa in all cooling channels. The

---

*: NAG-201-01-06-17-FDR, Fig. 4.2-19.

**: NAG-201-01-06-17-FDR, Fig. 4.1-3.

resulting intensity of shearing stress distribution caused by thermal loads is shown in Fig. 4.1-21. While the maximum shearing stress intensity of 209MPa occurs at the location of the front corner of edge for FW support beam insertion hole, almost all other maximum stress intensity on the front cover plate are below 120MPa and those at the internal part of the shield block are below 168MPa. Figure 4.1-22 shows an intensity of shearing stress distribution caused by 5MPa coolant pressure. The maximum shearing stress intensity of 32MPa in the model occurs at the location of the base of the front cover plate, and the shearing stress at a center of the front cover plate is below 22MPa.

Table 4.1-3 summarizes the stress in representative points of the shield block. For the stress conversion, the total intensity of Tresca stress at point B for example becomes 304MPa through the next equation; [thermal shearing stress 120MPa + shearing stress caused by coolant pressure 32MPa] x 2. While the maximum Tresca stress intensity of 418MPa occurs at point E, almost all other stress intensity in the shield block have been within the range of the allowable stress 3Sm.

2) Model B

a) Thermal analysis

The heat transfer coefficients used in the analysis are summarized in Fig. 4.1-23, and all other conditions used are same as Model A.

The resulting temperature distributions are shown in Fig. 4.1-24. The maximum temperature of 249°C ($\Delta T=124$ °C) occurs at the edge of the front cover plate corner. In the backward region from the front headers, the maximum temperature is no more than 160°C ($\Delta T=35$°C) at the location of the bottom surface of the shield, and it is seen that it is cooled very much.

b) Stress analysis

The resulting intensity of shearing stress caused by thermal loads is shown in Fig. 4.1-25. While the maximum shearing stress intensity of 227MPa occurs at the location of the corner of the front cover plate, almost all other maximum stress intensity on the front cover plate are below 120MPa and those at the internal part of the shield block are below 72.8MPa.

Table 4.1-4 summarizes the stress in representative points of the shield block. For the stress caused by coolant pressure in the table, they are calculated with using a formula of bending stress in the Mechanical Engineering Handbook in Japan. Almost all Tresca stress intensity in the shield block are within the range of the allowable stress 3Sm except the stress 454MPa at the location of the corner of the front cover plate.

(3) Summary

Almost all Tresca stress intensity in the shield block are within the range of the allowable stress 3Sm except the local two points; Tresca stress intensity of 418MPa at the location of the front corner of the edge for FW support beam insertion hole and that of 454MPa at the location of the corner of the front cover plate. If it necessary to reduce the over stresses at the points, the structural modifications namely the decrease of the wall thickness and the increase of the coolant velocity need to be examined. Further detail study and calculation will be required to confirm the soundness of the shield block caused by the thermal load, the coolant pressure with flow distribution.

In conclusion, the consistent structural concept for the shield blanket module #10 satisfying the requirements mentioned previously has been obtained through this study. Finally, in any case described above, it needs to be noted that the feasibility confirmation by R&D is required.

4.2 Design of Disc-Cutter Head

We have investigated the design of $\Phi 80^{ID}$ mm $/100^{OD}$ mm cutting type of Disc-Cutter miniaturizing the 100A - Sch.40 ($\Phi 102.3^{ID}$ mm x 6.0^t mm) cutting type which had been developed in FER design in Japan, since both inner diameters were very close.

The results of the investigation in the design relating to a specification of the disc knife and that of running gear are described in this section.

4.2.1 Premise conditions
(1) Object of the cutting

A new Disc-Cutter has to satisfy the following premise conditions.

Configuration	: Hollow pipe with $\Phi 80^{ID}$ mm.
Thickness	: 10mm or more.
Materials	: Austenitic Stainless Steel (SUS316L)

(2) Results from past R&D

The following results have been obtained from the 100A-Sch. SUS304 cutting test.

- A specification of the disc knife

Diameter	: $\Phi 58$ mm
Knife angle at the first tip	: 30°
Materials	: OT106S (JIS G4404:SKD12 steel)
Surface treatment	: Nitrosulphurizing

Hardness   : H_{RC} 55-56

- A specification of the disc knife axis and the body

     Materials   : SKD11 steel (JIS G4404)

- A proposed specification of the running gear

     Pressing load   : 14710 N

     Revs of principal axis   : 60 rpm

(3) Mechanical properties of SKD11 steel

The mechanical properties of SKD11 steel used in the body of the Disc-Cutter are shown in the followings (Data from Fuji Die Co., LTD.). Since both 0.2% proof stress and tensile strength in this material are almost same level, 1/3 x tensile strength is chosen as a design stress.

         Tensile strength   : 2260 MPa

         Design stress   : 753 MPa   (=2260/3)

         Allowable bending stress : 753 MPa

         Allowable shear stress   : 376.5 MPa (=753/2)

         Elastic coefficient   : 206000 MPa

4.2.2 Evaluation of the strength

(1) The disc knife and the pressing load

When the Disc-Cutter head is scaled down by the ratio of inner diameter ($\Phi 80mm / \Phi 102.3mm$), a diameter of new disc knife comes to 46 mm, 56 mm x 80/102.3. Figure 4.2-1 shows the configuration of the disc knife designed in this study.

A pressure load F on the disc knife at the touching surface, of which schematic concept is illustrated in Fig. 4.2-2, is defined as a next equation.

$$F = \frac{P}{2 \cdot S_1 \cdot \tan(\theta_1 / 2) + 2 \cdot S_2 \cdot \tan(\theta_2 / 2)} \qquad (4.2 \text{-} 1)$$

where, F (MPa)   : Pressure load at the touching surface

          P (N)   : Pressing load from the principal axis of the disc knife

          θ_1 (°)   : A first escape angle at the tip of the disc knife (30°)

          θ_2 (°)   : A second escape angle at the tip of the disc knife (13°)

          S_1 (mm^2)   : Area of the section cut by the 1st escape angle

                             of the disc knife

          S_2 (mm^2)   : Area of the section cut by the 2nd escape angle

The typical conditions of the pressure load obtained from the 100A-Sch. SUS304 past cutting test are shown in the followings.

- F= 170 MPa   with P = 14710 N, 60 rpm and about 1 minute of
                cutting time
- F= 90 MPa   with P = 7649 N, 100 rpm and about 3 minutes of
                cutting time

Taking account of a reduction of stiffness in the principal axis with the miniaturizing, it needs to select the lower value. Therefore, P=11278N calculated from F=90 MPa using the equation (4.2-1) is selected for the pressing load, and the following evaluations are carried out with it.

(2) Strength of the axis of disc knife

Figure 4.2-3 (a) shows a schematic drawing of a cutter head which consists of the disc knife and the principal axis with Φ15mm. The axis is fixed one end to a block at an edge of a cotter in the moving system rigidly and the other end to a sliding system by bolt which has a function not to make a deflection angle.

A calculation model of the axis with both sides fixed is shown in Fig. 4.2-3 (b). For the calculation region, the right half of the model corresponds to the actual one shown in Fig. 4.2-3 (a) . Symbols of q and l used in the figure are shown as the followings.

$$q = \frac{P}{l} = \frac{11278}{58} = 194.4 \qquad (N / mm)$$

where, $q\,(N / mm)$: An uniformly distributed load

      $P\,(N)$: Pressing load from the principal axis
                       of the disc knife (P=11278N.)

      $l\,(mm)$: Length of the uniformly distributed load (l=58mm)

On a calculation of bending stress, since a maximum bending moment $M_{\max}$ is produced at the beam with right hand end fixed, the maximum bending stress $\sigma_{b\max}$ is obtained from the following equations.

$$\sigma_{b\max} = \frac{M}{Z} = \frac{q \cdot l^2}{3} \cdot \frac{32}{\pi \cdot d^3} \qquad\qquad (4.2-2)$$

$$= \frac{194.4 \times 58^2}{3} \cdot \frac{32}{\pi \cdot 15^3} = 658.0 \quad (MPa) \quad (< 753\,MPa : Allowable\ bending\ stress)$$

$$\left(M_{\max} = \frac{q \cdot l^2}{3}, \quad Z = \frac{\pi \cdot d^3}{32} \right)$$

where, $\sigma_{b\max}\,(MPa)$: Maximum bending stress

      $M_{\max}\,(N \cdot mm)$: Maximum bending moment

      $Z\,(mm^3)$: Section modulus

It is possible to withstand the bending moment since the maximum bending stress is about 13% less than the allowable bending stress. When the pressure load F=170 MPa is applied

in this case, it is clear to say that it is difficult to withstand the bending moment because the maximum bending stress becomes 1259MPa much higher than the allowable bending stress (753MPa).

On a calculation of shearing stress, since a maximum shearing force Q_{max} is produced at the beam with right hand end fixed too, the maximum stress τ_{max} is obtained from the following equations.

$$\tau_{max} = \frac{4}{3} \cdot \frac{Q}{A} \qquad\qquad (4.2-3)$$

$$= \frac{4}{3} \cdot \frac{194.4 \times 58}{\pi \times (15/2)^2} = 85.1 \quad (MPa) \qquad (<376.5MPa \text{ Allowable stress})$$

$$\left(Q_{max} = q \cdot l \right)$$

where, $\tau_{max} (MPa)$: Maximum shearing stress

$Q_{max} (N)$: Maximum shearing force

$A \ (mm^2)$: Cross-sectional area

It is possible to withstand the shearing force, since the maximum shearing stress is about 77% less than the allowable shearing stress.

On a calculation of deflection, for your reference, since it can be considered that the maximum deflection of the axis will be produced at the sliding system fixed by bolt, the maximum deflection δ_{max} is obtained from the following equations.

$$\delta_{max} = \frac{q \cdot (2l)^4}{384 \cdot E \cdot I} \qquad\qquad (4.2-4)$$

$$= \frac{194.4 \times (2 \times 58)^4}{384 \times 206000 \times 2485.0} = 0.179 \qquad (mm)$$

$$\left(I = \frac{\pi \cdot d^4}{64} \right)$$

where, $\delta_{max} \ (mm)$: Maximum deflection

$I \ (mm^4)$: Moment of inertia

$E \ (MPa)$: Young's modulus

(3) Strength of the roller axis against the reaction force

Figure 4.2-4 shows the force of two dimensional vector made of the pressing load to the disk knife. The pressing loads to the rollers are obtained from the following equation.

$$P_r = P_l = \frac{P}{2} \cdot \sin\theta$$

$$= \frac{11278}{2} \cdot \sin(40°) = 3624.7 \quad (N)$$

Figure 4.2-5 (a) shows a configuration of a principal axis of the roller. Fixing situations of the axis are similar to the disc knife. The right side edge is fixed to the Disc-Cutter head by bolt rigidly, and the left side one is also bolted to a support body which has a structure without making any deflection angle.

A calculation model of the roller axis which has a beam with both sides fixed is shown in Fig. 4.2-5 (b). The right half of the model corresponds to the actual one shown in Fig. 4.2-5 (a). Symbols of q and l are shown as the followings.

$$q = \frac{P_r}{l} = \frac{3624.7}{69} = 52.5 \quad (N/mm)$$

where, $q\,(N/mm)$: An uniformly distributed load

$P_r\,(N)$: Pressing load from the principal axis of the wall

$l\,(mm)$: Length of the uniformly distributed load (l=69mm)

On a calculation of bending stress, since a maximum bending moment M_{max} is produced at the beam with right hand end fixed, the maximum bending stress $\sigma_{b\,max}$ is obtained from the equation (4.2-2).

$$\sigma_{b\,max} = \frac{M}{Z} = \frac{q \cdot l^2}{3} \cdot \frac{32}{\pi \cdot d^3} = 309.3 \quad (MPa) \qquad (< 753\text{MPa} : \text{Allowable stress})$$

where, $d\,(mm)$: Diameter of the principal axis (d=14mm)

Since the maximum bending stress is about 59% less than the allowable bending stress, it is possible to withstand the bending moment. In the case of F=170 MPa, it is possible to withstand the bending moment too because the maximum bending stress becomes 592.0MPa (<753MPa).

On a calculation of shearing stress, since a maximum shearing force Q_{max} is produced at the beam with right hand end fixed too, the maximum stress τ_{max} is obtained from the equation (4.2-3).

$$\tau_{max} = \frac{4}{3} \cdot \frac{Q}{A} = \frac{4}{3} \cdot \frac{52.5 \times 69}{\pi \times (14/2)^2} = 31.4 \quad (MPa) \qquad (< 376.5 \text{ MPa})$$

There is no problem for the shearing stress on the principal axis.

On a calculation of deflection, for your reference, since it can be considered that the maximum deflection of the axis will be produced at the sliding system fixed by bolt, the maximum deflection δ_{max} is obtained from the equation (4.2-4).

$$\delta_{max} = \frac{q \cdot (2l)^4}{384 \cdot E \cdot I} = \frac{52.5 \times (2 \times 69)^4}{384 \times 206000 \times 1885.7} = 0.128 \quad (mm)$$

(4) Strength of the cotter at moving system

Figure 4.2-6(a) shows a configuration of the cotter in the moving system. The cotter can be considered as a cantilever model where a concentrated load is applied on the free end of the beam with a length l. A calculation model of the cotter is shown in the figure (b).

On a calculation of bending stress, since a maximum bending moment $\dot{M}_{max}$ is produced at the beam with left end fixed, the maximum bending stress $\sigma_{b\,max}$ is obtained from the following equations.

$$\sigma_{b\,max} = \frac{M}{Z} = P \cdot l \cdot \frac{6}{b \cdot h^2}$$

$$= 11278 \cdot 47 \frac{6}{17 \times 16^2} = 730.8 \quad (MPa) \quad (<753\text{MPa})$$

$$\left(M_{max} = P \cdot l, Z = \frac{b \cdot h^2}{6} \right)$$

where, $P\,(N)$: Pressing load $(P = 11278N)$

$l\,(mm)$: Length of the beam to the forced point $(l = 47mm)$

$b, h\,(mm)$: Dimension of the beam cross section $(b = 17mm, h = 16mm)$

While the maximum bending stress is about 3% less than the allowable bending stress, it is possible to withstand the bending moment. In the case of F=170 MPa, it is difficult to withstand the bending moment because the maximum bending stress becomes 1398.1MPa (>753MPa).

On a calculation of shearing stress, the maximum stress τ_{max} is obtained from the following equation.

$$\tau_{max} = \frac{3}{2} \cdot \frac{Q}{A} = \frac{3}{2} \cdot \frac{11278}{17 \times 16} = 62.2 \quad (MPa) \quad (<376.5\text{ MPa})$$

where, $Q_{max}\,(N)$: Maximum shearing force $(Q_{max} = P = 11278N)$

$A\,(mm^2)$: Cross-sectional area $(A = b \times h)$

It is possible to withstand the shearing force.

On a calculation of deflection, for your reference, since it can be considered that the maximum deflection of the axis will be produced at the sliding system fixed by bolt, the maximum deflection δ_{max} is obtained from the following equation.

$$\delta_{max} = \frac{P \cdot l^3}{3 \cdot E \cdot I} = \frac{11278 \times 47^3}{3 \times 206000 \times 5802.7} = 0.327 \quad (mm)$$

$$\left(I = \frac{b \cdot h^3}{12} \right)$$

where, $I\,(mm^4)$: Moment of inertia

$E\,(MPa)$: Young's modulus

4.2.3 New Disc-Cutter head

Figure 4.1-7 shows a configuration of the new designed Disc-Cutter head applied to the $\Phi 80^{ID}/100^{OD}$ mm pipe cutting. It is possible to reduce the stress on the principal axes under the allowable stress by means of keeping the pressing load lower, and to obtain the consistent structure of Disc-Cutter head in design, while it takes more time to cut off the pipe. It has a capacity to cut off not only the 10mm thick pipe normally but also up to a maximum thickness of 11.6mm.

The following results relating to the specification of the disc knife and that of running gear have been obtained.

- The specification of the disc knife
    Diameter   : $\Phi 46$ mm
    Knife angle at the first tip   : 30°
    Materials   : OT106S (JIS SKD12)
    Surface treatment   : Nitrosulphurizing
    Hardness   : H_{RC} 55-56
- The specification of the disc knife axis and the body
    Materials   : SKD11 steel
- The specification of the running gear
    Pressing load   : 11278 N
    Revs of principal axis   : 100 rpm

Table 4.1-1 Maximum EM Loads on the Inboard Module (DDD2001)

		Shield block	FW*	
Module 2				Fp=150kN/FW Mt(Fr)=29kNm/FW
I_{halo}**	kA	280	70	
EM force F_r	MN	+/- 0.32	+/- 0.079	
EM force F_p	MN	1.1	0.15	
EM force F_{tor}	MN	0.21	0.031	Ihalo =280kA FW panel Shield block
Torque M_{tor}	MNm	0.36***	0.029	
Module 1				Fp=140kN/FW Mt(Fr)=27kNm/FW
I_{halo} **	kA	274	69	
EM force F_r	MN	+0.39/-0.19	+0.098/-0.047	
EM force F_p	MN	1.0	0.14	
EM force F_{tor}	MN	0.21	0.030	FW panel
Torque M_{tor}	MNm	0.33***	0.027	Electrical straps Ihalo=270kA Shield block

* Number of FW panels is 4 per module
** FW-normal halo current density of 0.18 MA/m^2 is assumed.
*** M_{tor}(module) = F_p(module)*l_{rad}/2 + 4*M_{tor}(FW), where l_{rad} = 0.45 m.

Table 4.1-2 Conditions of Stress Calculation and Results

UNIT : MPa

Case	Configuration					Results of Stress[1),2)]		
	FW Support Beam		Round Pipe Structure			Bending Stress	Composition Stress (Maximum point)	
	Length	Height	ID	Thickness	OD	MPa	$\sigma1$	τmax
1	200	220	80	9	98	192	217	109
2			100	9	108	181	211	106
3		220	80	10	100	174	198	99
4	200		90	10	110	169	195	98
5			80	11	102	160	181	91
6				9	98	177	202	102
7				10	100	161	184	92
8		230	80	11	102	147	169	85
9	190			10	100	158	181	91
10	160					149	172	86

1): Due to EM loads and Inner Pressure (5MPa)
2): SUS316LNIG 1.5Sm at 150°C=206 MPa

Table 4.1-3 Stress Evaluations for Model A

Evaluated points shown in Fig.4.1-21 (1/2)		A	B	C	D	E
Temp. (°C)		237	140	240	166	263
Occurring shearing stress (MPa)	Thermal loads	111	120	97	94	209
	Inner pressure	7	32	14	2	6
	Total	118	152	111	96	215
Conversion to Tresca Stress (MPa)		236	304	222	192	430
Allowable Stress (MPa)	Sm	127	137	127	135	124
	3Sm	381	411	381	405	372

Table 4.1-4   Stress Evaluations for Model B

Evaluated points shown in Fig.4.1-25(1/3)		A	B	C	D
Temp. (°C)		249	201	188	203
Occurring shearing stress (MPa)	Thermal loads	167	177	120	227
	Inner pressure*	<10	<10	60	60
	Total	177	187	180	287
Conversion to Tresca Stress (MPa)		354	374	360	574
Allowable Stress (MPa)	Sm	126	132	133	131
	3Sm	378	396	399	393

*: Using the formula of bending stress in the Mechanical Engineering Handbook in Japan
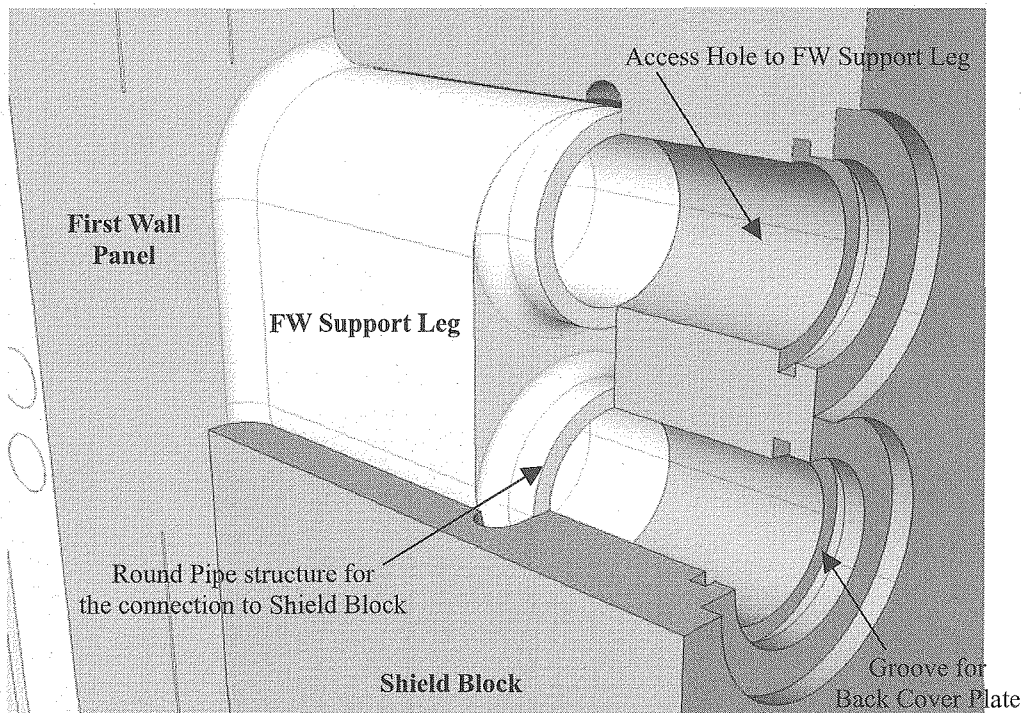
Fig. 4.1-1   Back side view of Two Circular type of
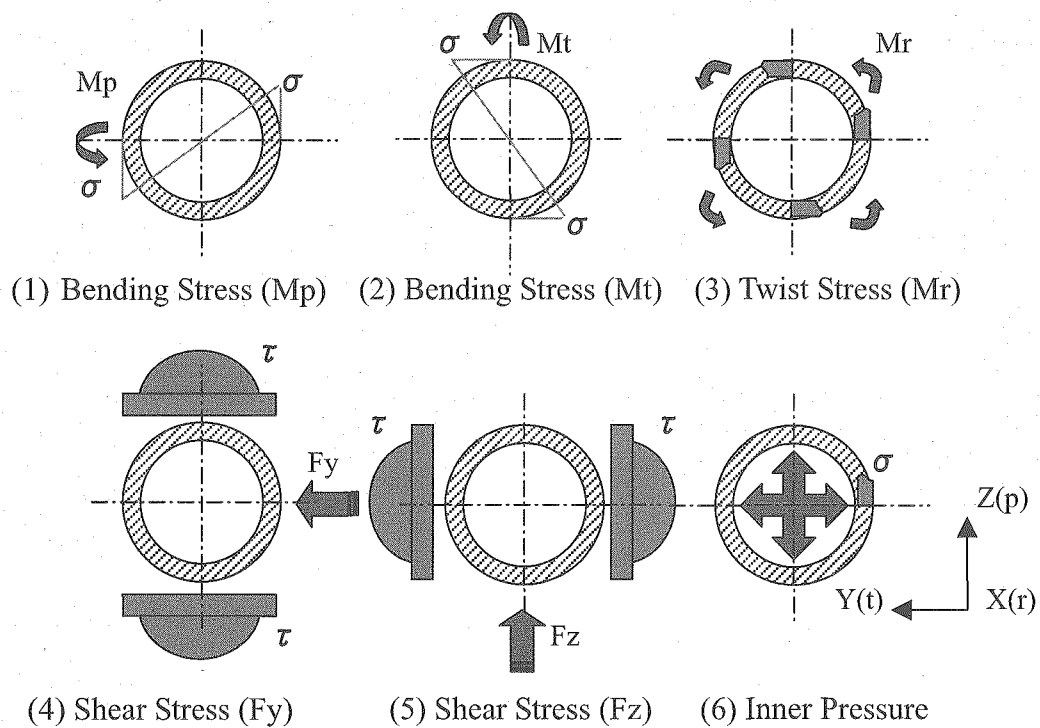FW Support Leg structure

(1) Bending Stress (Mp)   (2) Bending Stress (Mt)   (3) Twist Stress (Mr)

(4) Shear Stress (Fy)   (5) Shear Stress (Fz)   (6) Inner Pressure

Fig. 4.1-2   Schematic of Stress Distributions on Round Pipe structure
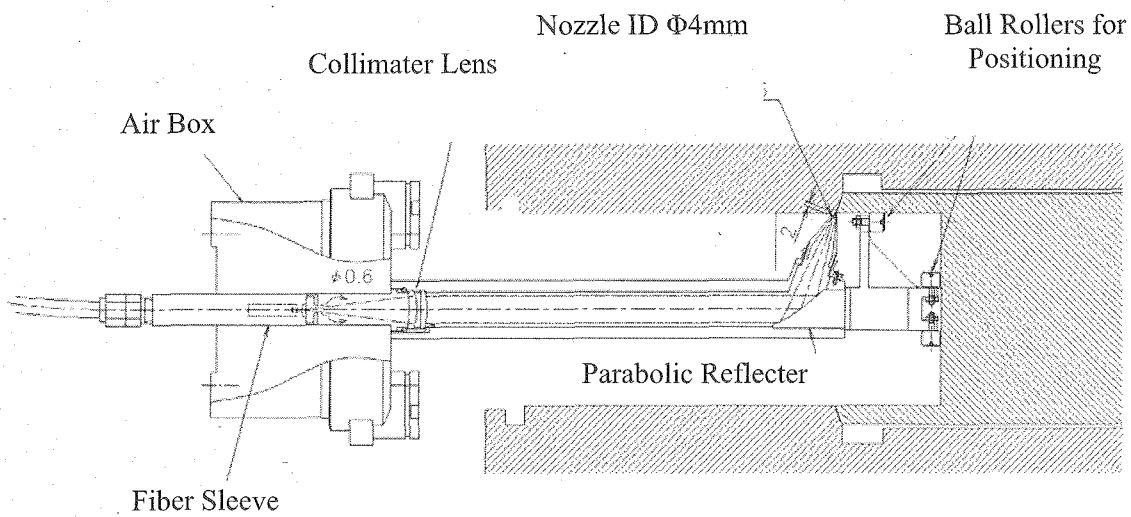due to EM Loads, dead weight and an inner pressure

Air Box

Collimater Lens

Nozzle ID Φ4mm

Ball Rollers for
Positioning

Φ0.6

Parabolic Reflecter

Fiber Sleeve

Fig. 4.1-3   Welding Tools for FW Support Leg

30mm 20mm

Welding point at 1st maintenance stage

Weldment at the initial assembly

Welding point at 2nd maintenance stage

7 7

UT Probe

Hole for releasing
the gas

Φ6mm

Space for dross caused
by YAG Laser beam welding
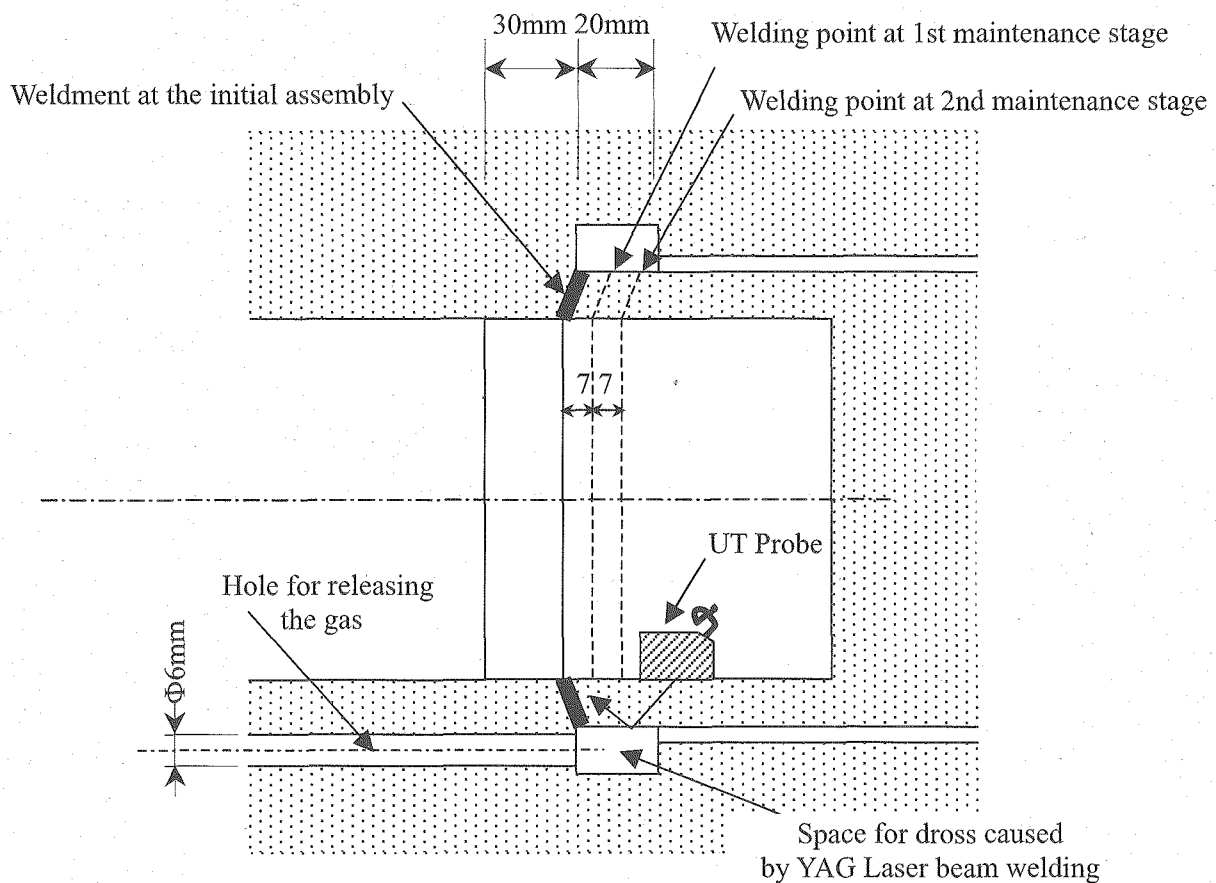
Fig. 4.1-4   Structure of the FW Support Leg connection (Two Circular Type)
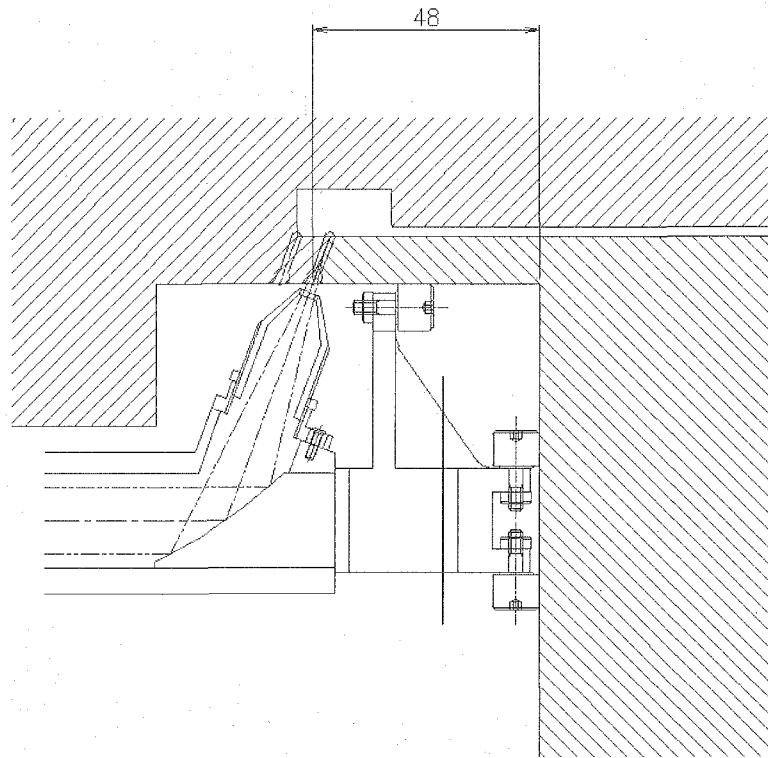
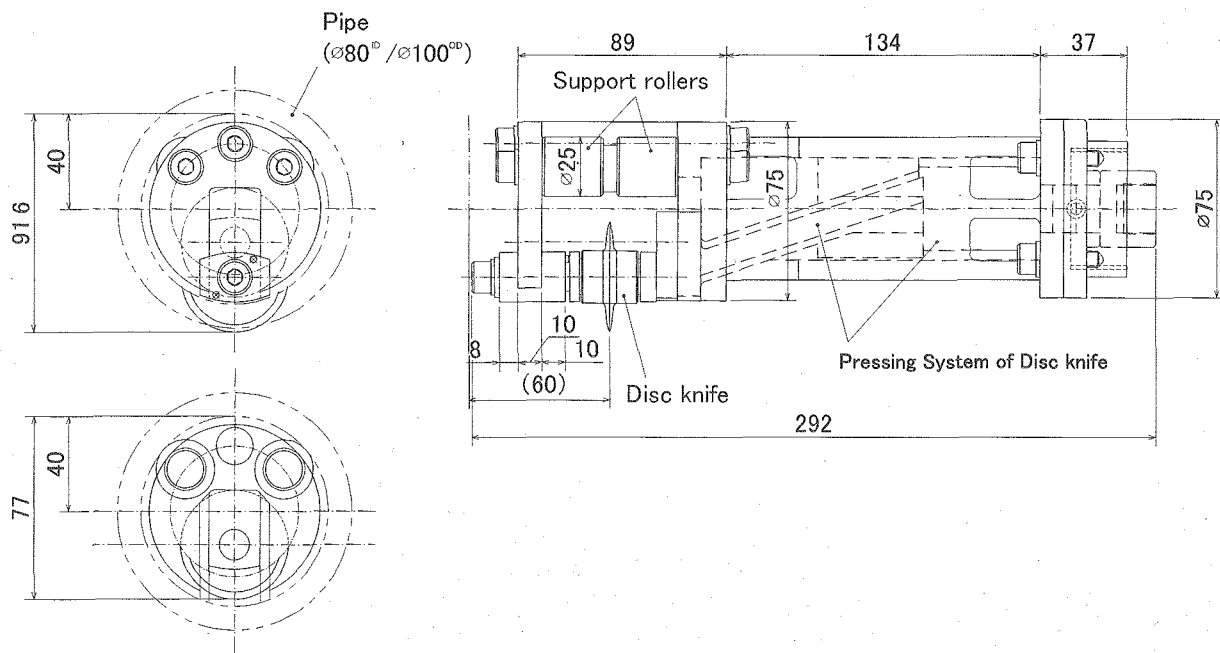Fig. 4.1-5　Schematics of Positioning System for FW Support beam Welding at 1st term
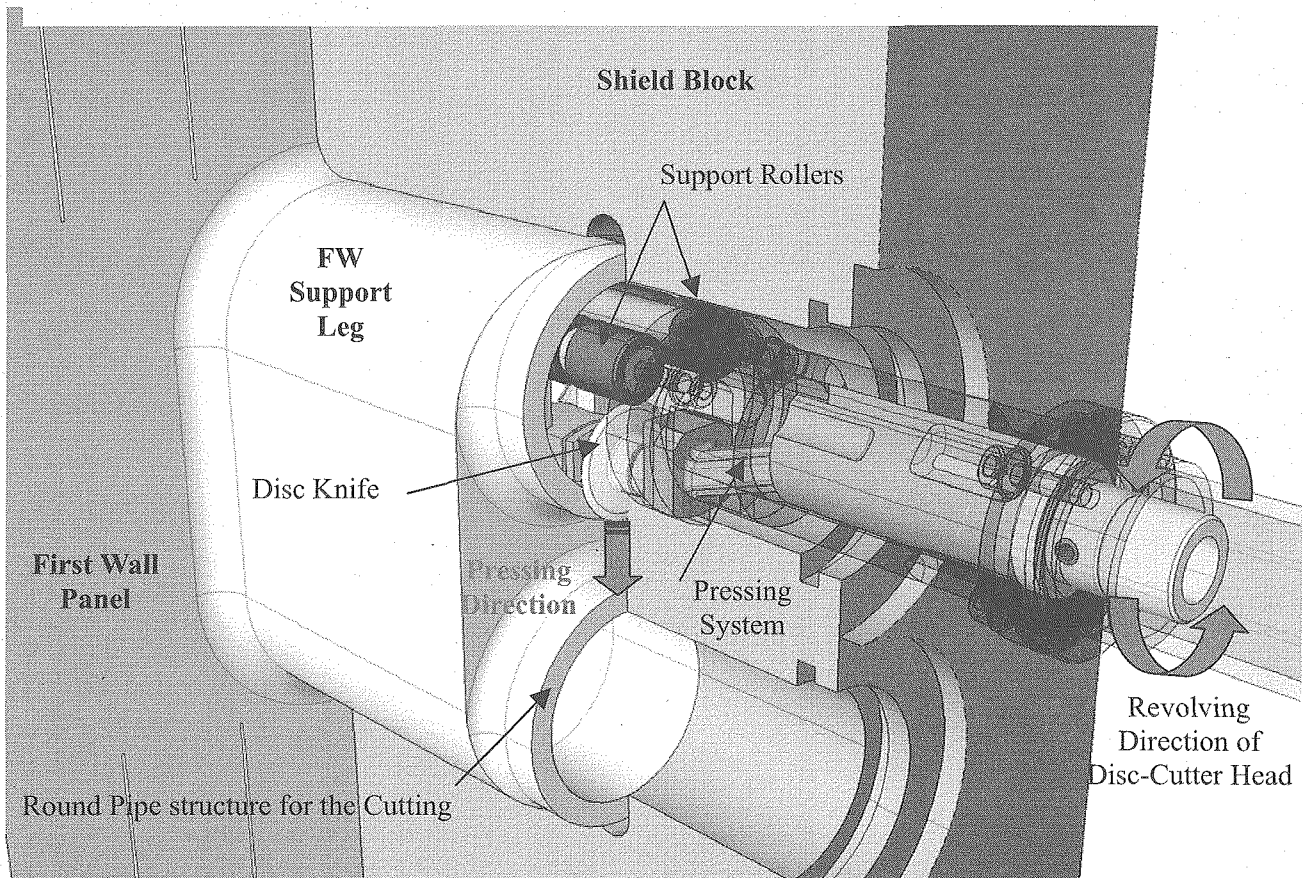
Fig. 4.1-6　Back side view of FW Support Leg structure
in progress of the cutting by Disc-Cutter

Before Cutting

Fig. 4.1-7 Configuration of Disc-Cutter Head just after cutting
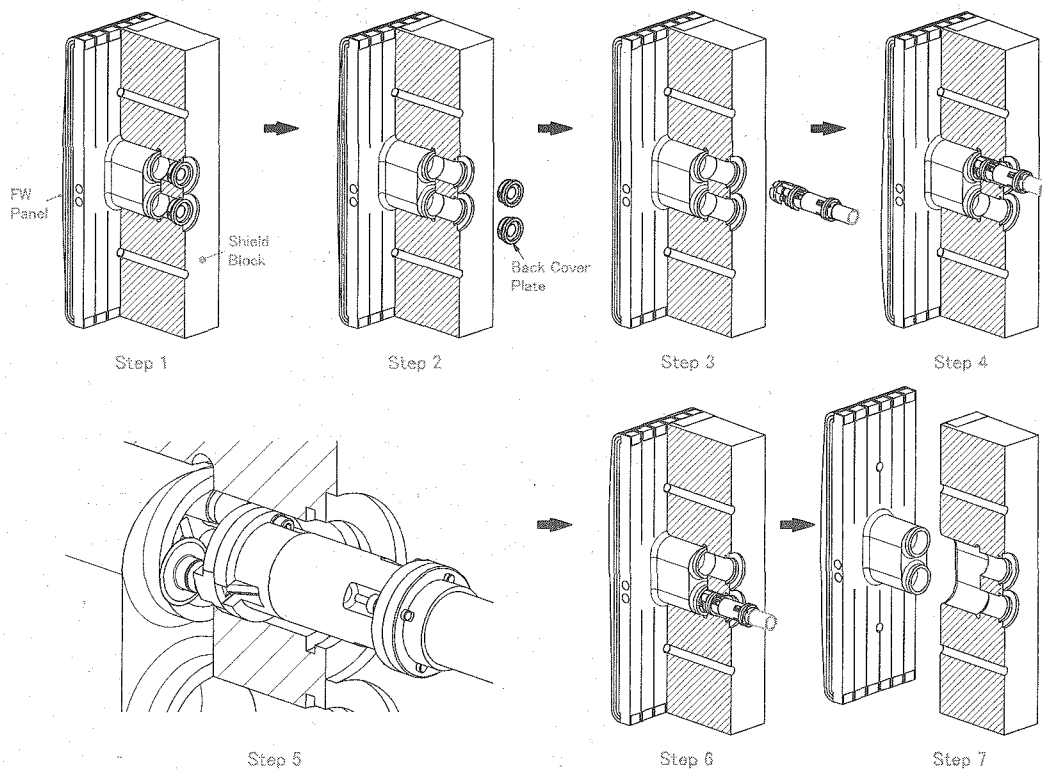(Maximum cutting thickness ≤ 11.6mm)

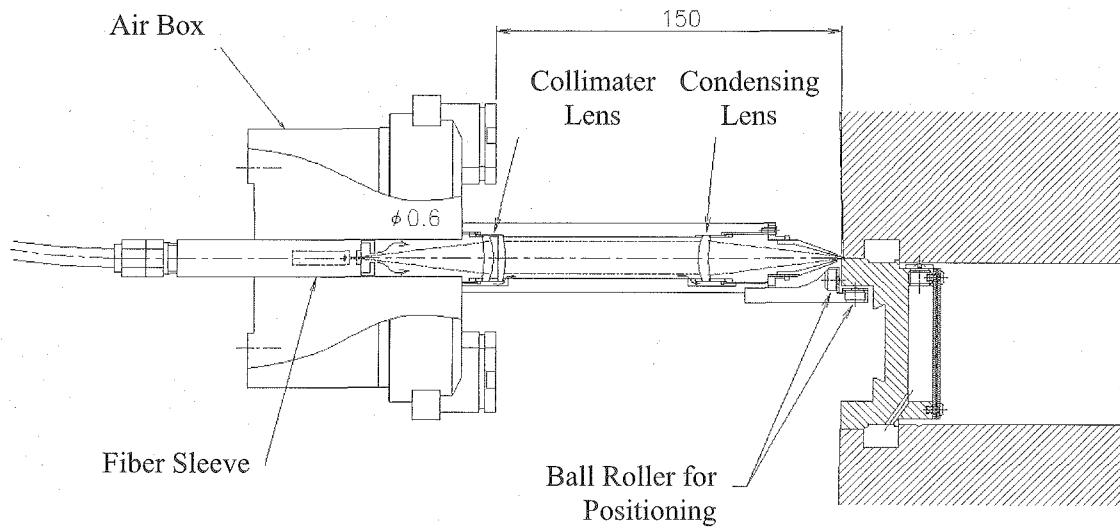Fig. 4.1-8 Replacement procedure of FW Panel by Disc-Cutter

Air Box

Collimater Lens Condensing Lens

150

φ0.6

Fiber Sleeve

Ball Roller for Positioning

Fig. 4.1-9   Welding Tools for Cover Plate

Weld joints at Initial Assembly stage, 1st and 2nd term according to the order from the inner-side

Groove for Dross

Step

45

34

25 ±0.5

10

3

3

UT Probe

10

10~20

Gripper of End-Effector

Mesh

70

Groove for Gripper

Access Hole

Cover Plate

Hole for letting the gas escape

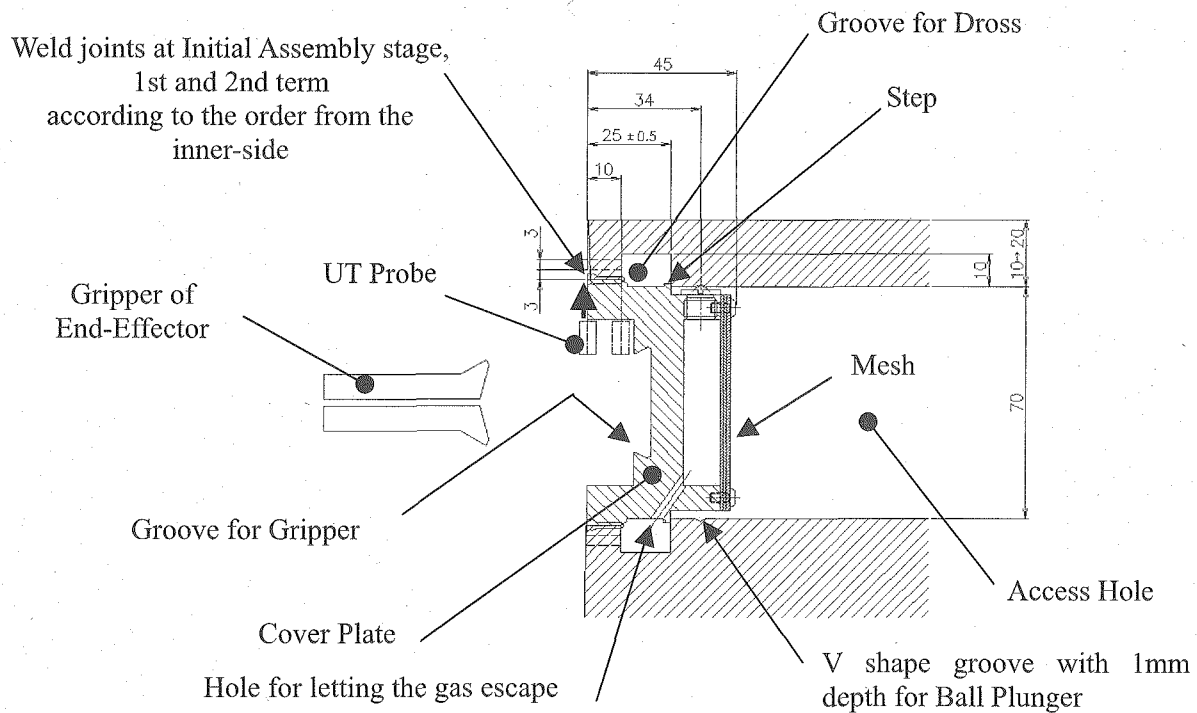V shape groove with 1mm depth for Ball Plunger

Fig. 4.1-10   Configuration of Back Cover Plate in consideration of welding by remote handling
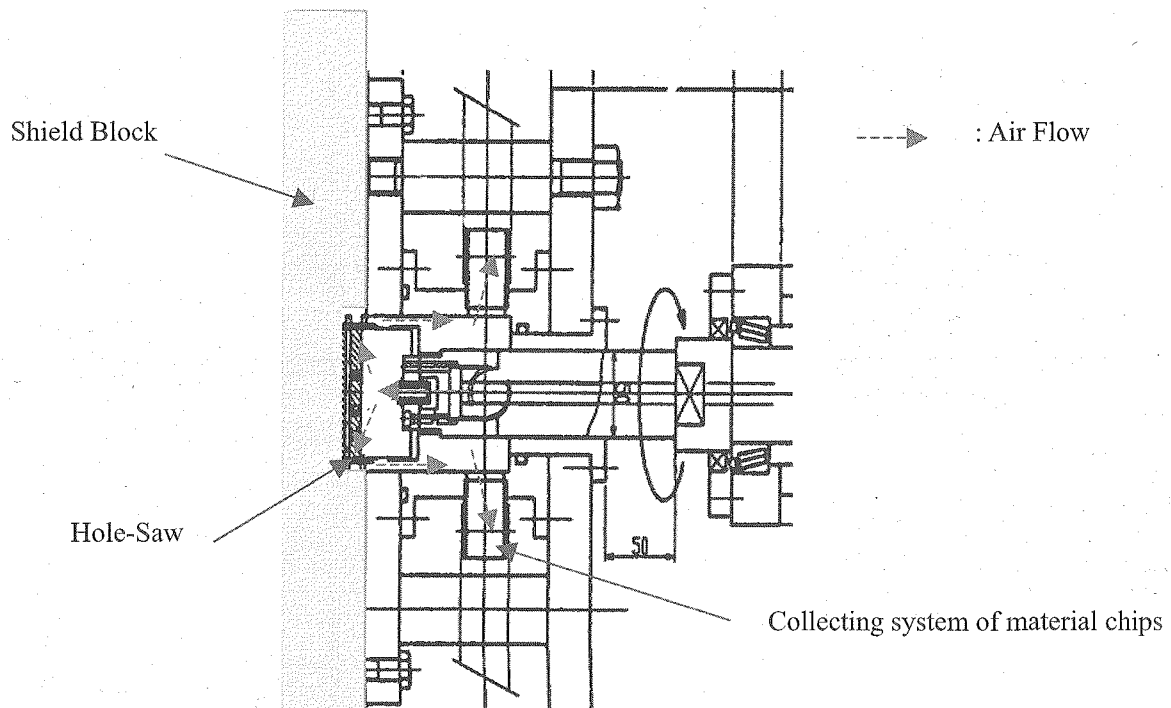
Fig. 4.1-11 Schematic of Hole-Saw machine applied to the shield block in Hot Cell
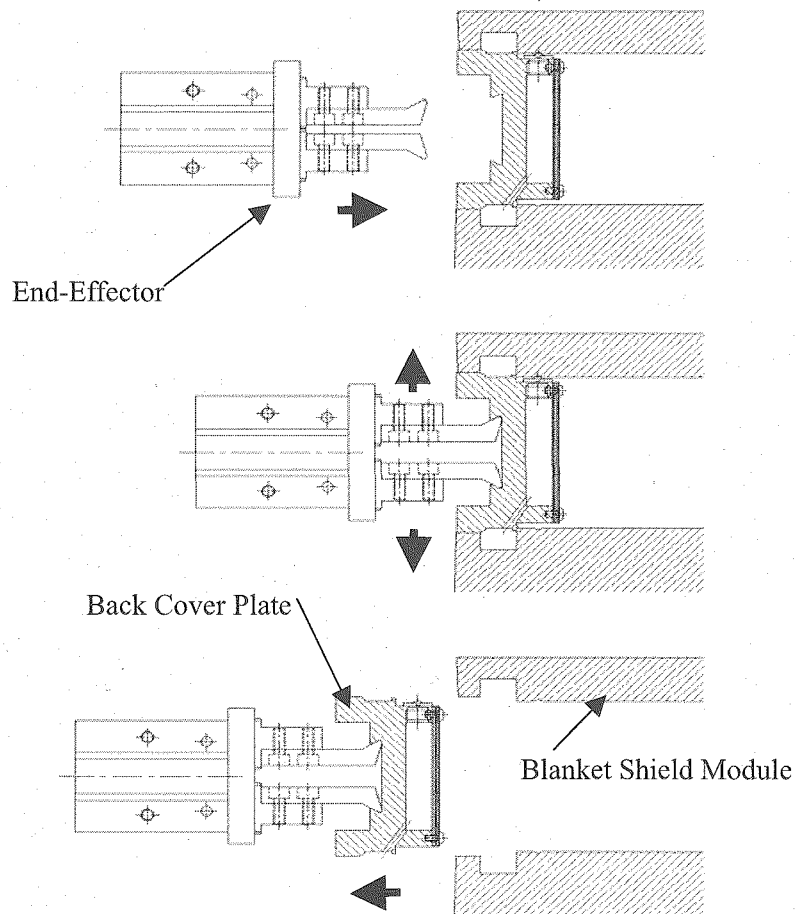

Fig. 4.1-12 Procedure for removing Back Cover Plate from Shield Block by End-Effector
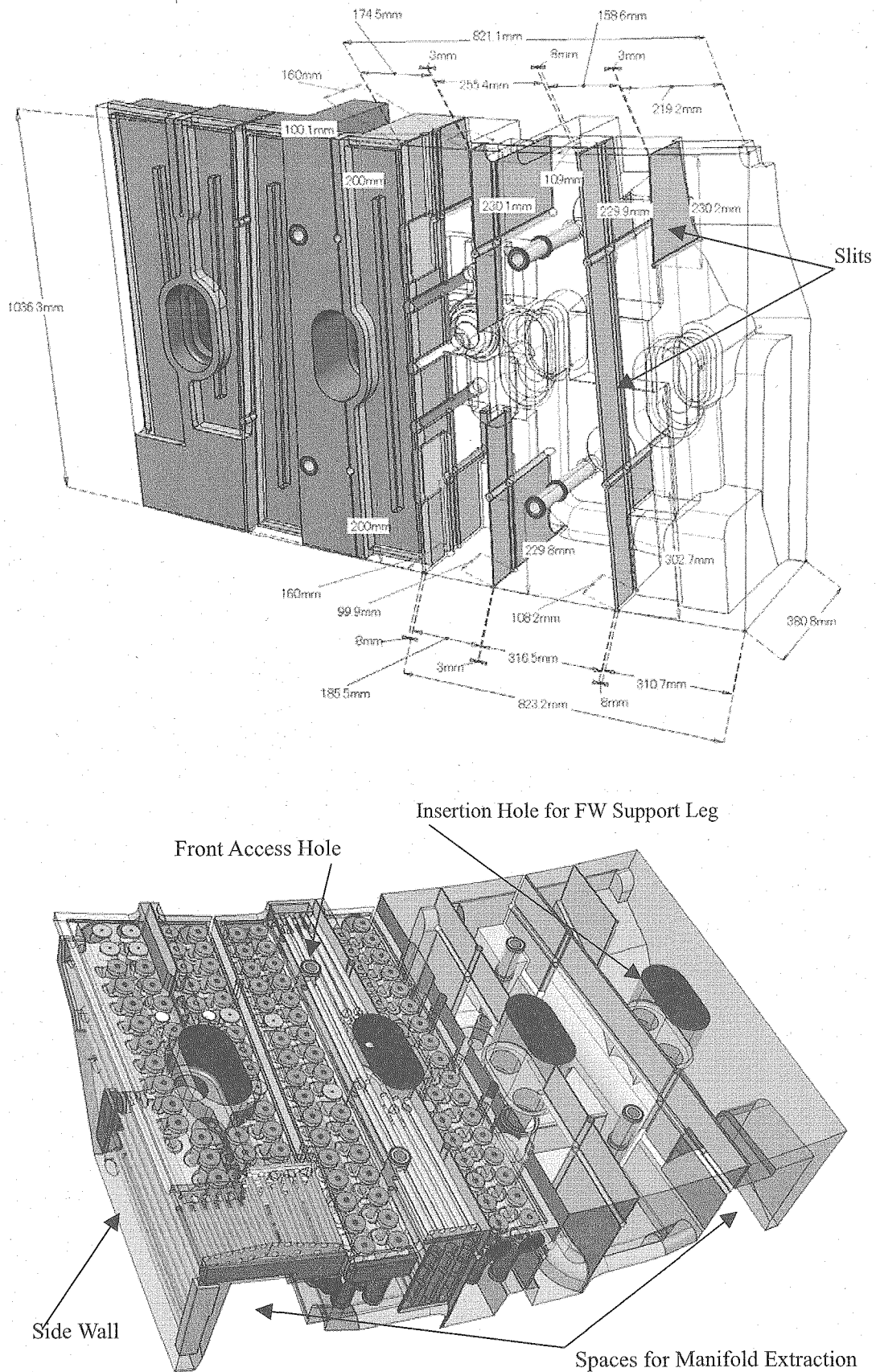
Fig. 4.1-13 Slits configuration and skeleton view of shield block #10
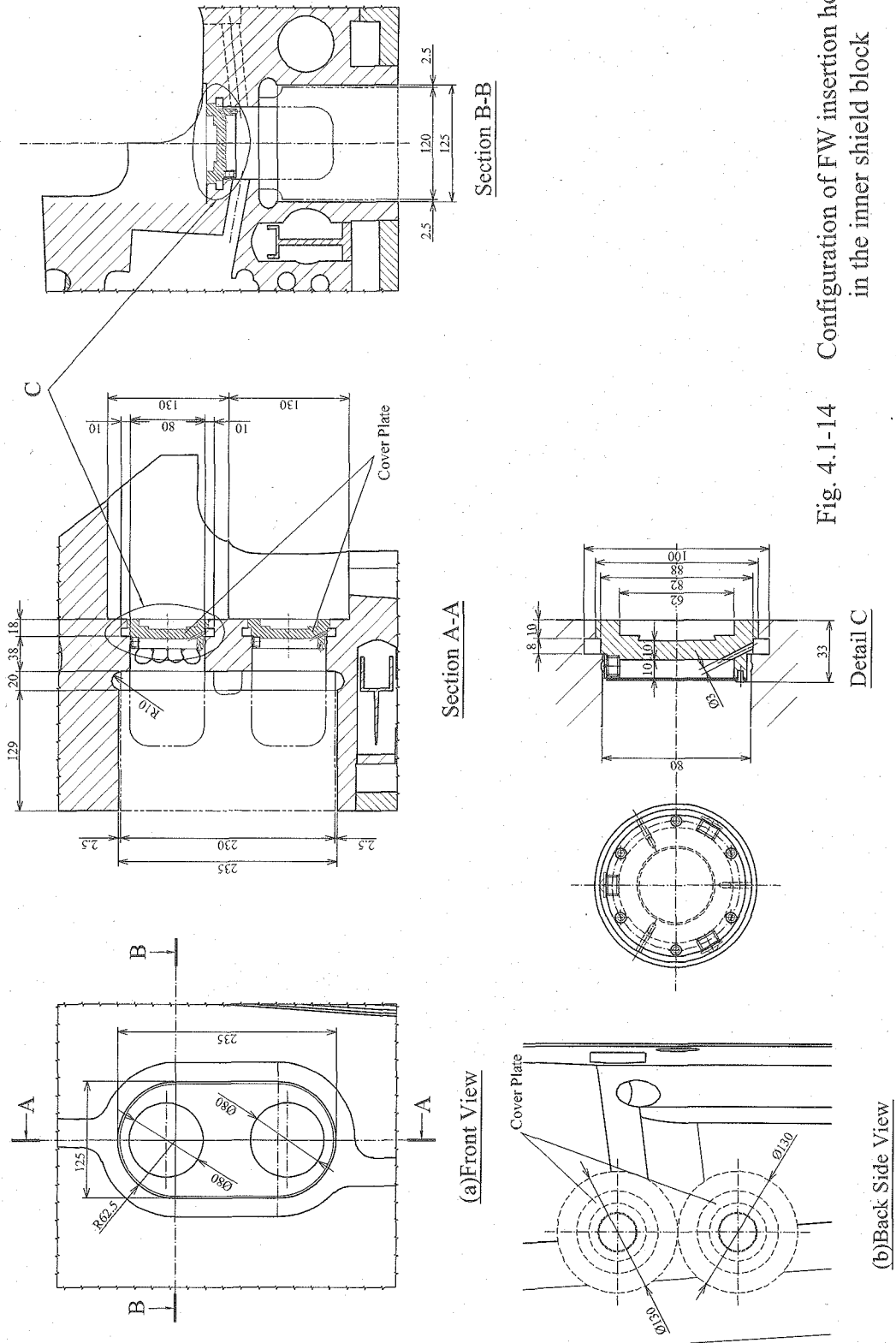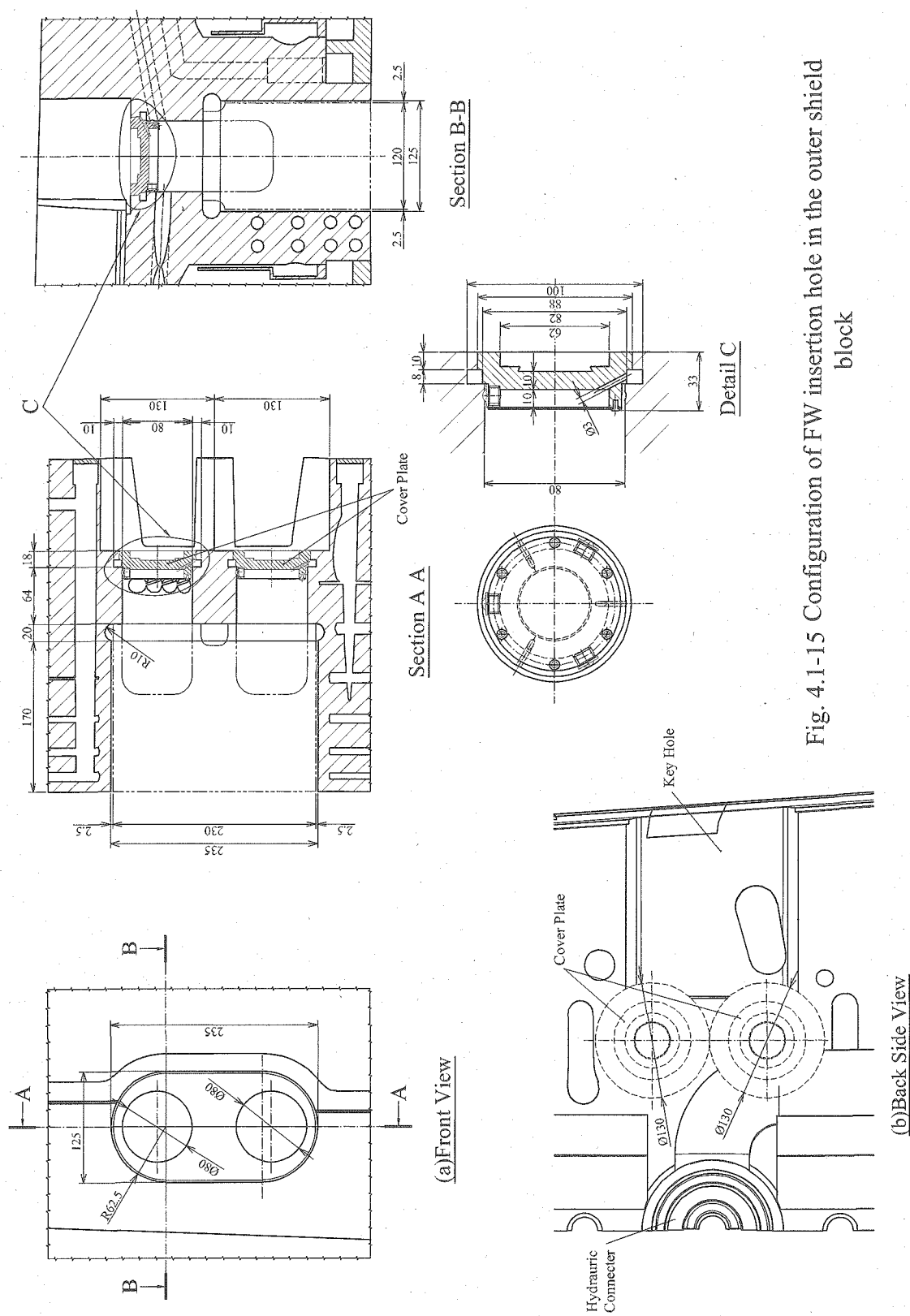with Two Circular type of FW Support Leg

Fig. 4.1-14 Configuration of FW insertion hole in the inner shield block

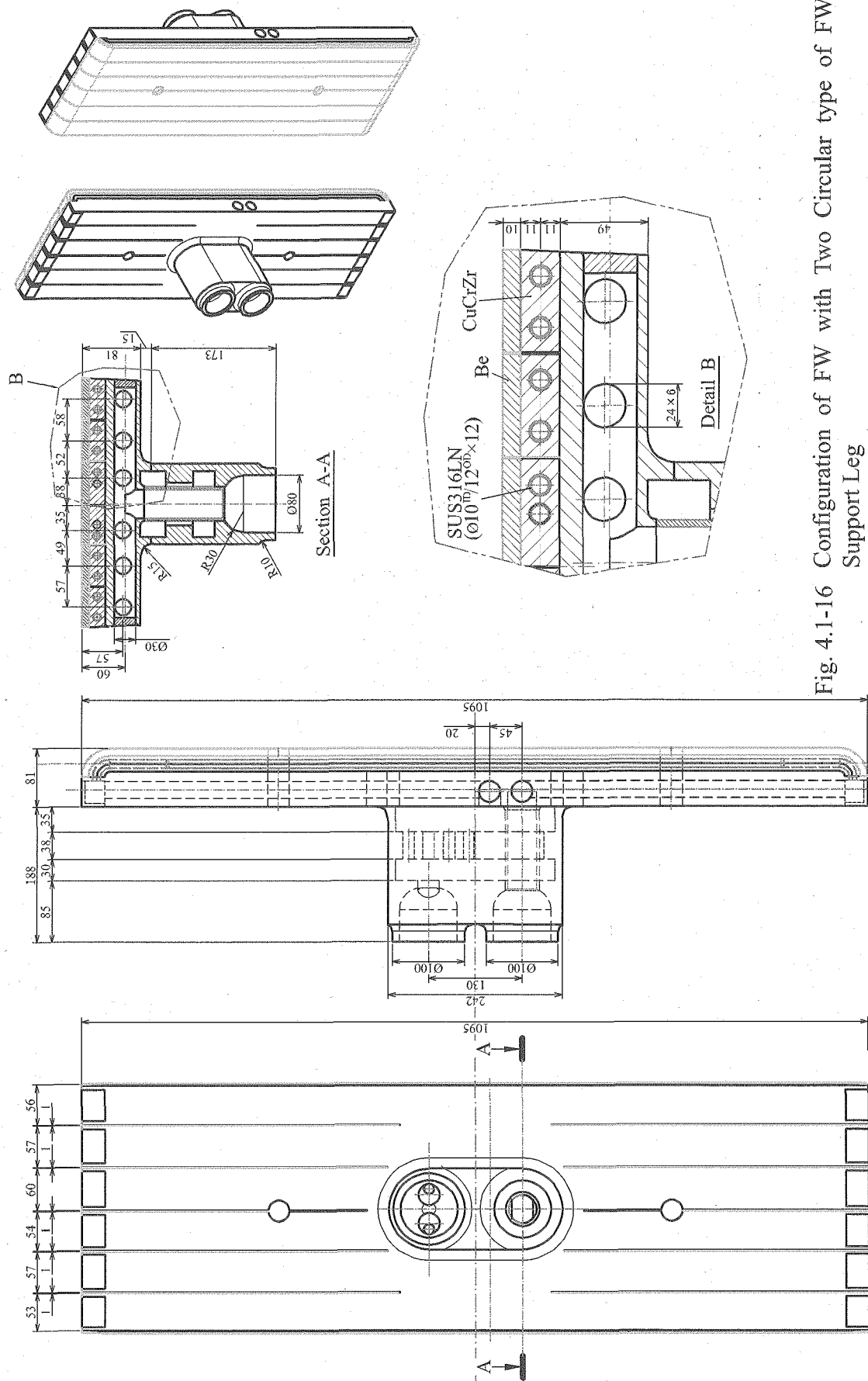Fig. 4.1-15 Configuration of FW insertion hole in the outer shield block

Section B-B

Section A A

Detail C

(a)Front View

(b)Back Side View

Cover Plate

Key Hole

Hydraulic Connecter

Fig. 4.1-16 Configuration of FW with Two Circular type of FW Support Leg

Poloidal Main Hole (60Φ)

Front Header

Front Cover Plate

Back Side

Poloidal Holes (14Φ x 13)

FW Side

Radial Holes (45Φ)
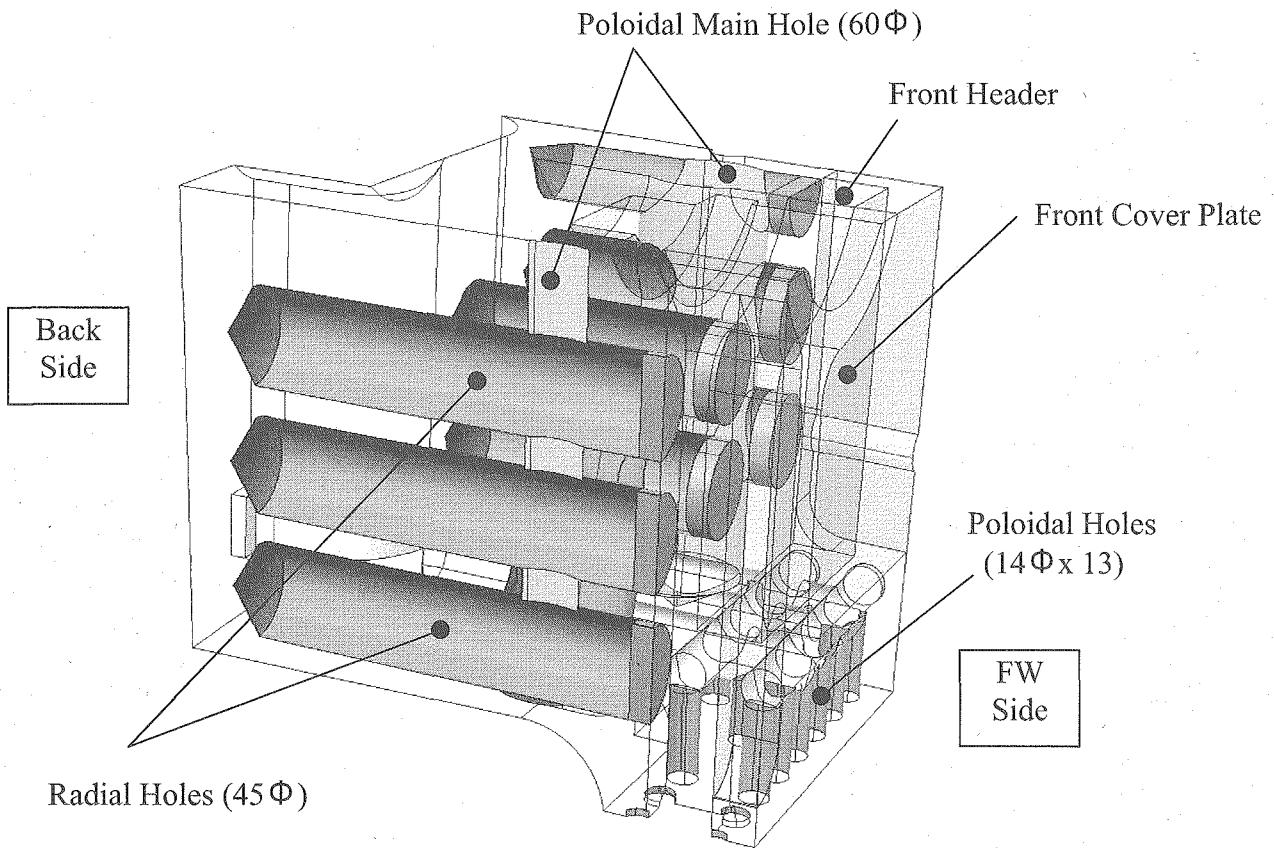
(1) Based Model by 3D CAD Drawing
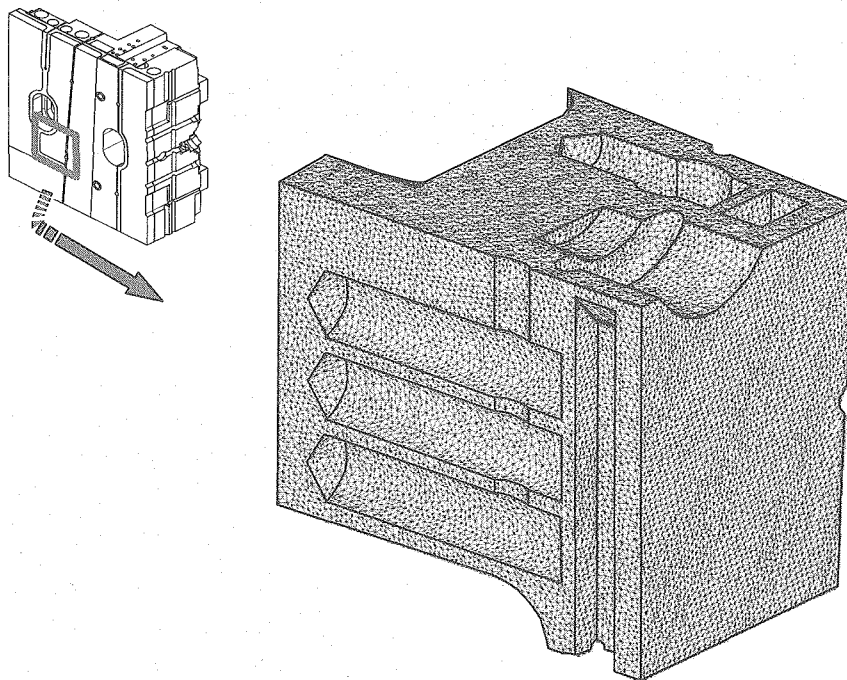
(2) The 3D Meshes for Calculation Model

Fig. 4.1-17   3D Thermal Calculation Model in the outer shield block in #10 Module (Model A)

Poloidal Holes (20 Φ x 8)

Side Wall

Back Side

FW Side

Front Cover Plate

Radial Holes (45 Φ)

Poloidal Main Hole (60 Φ)
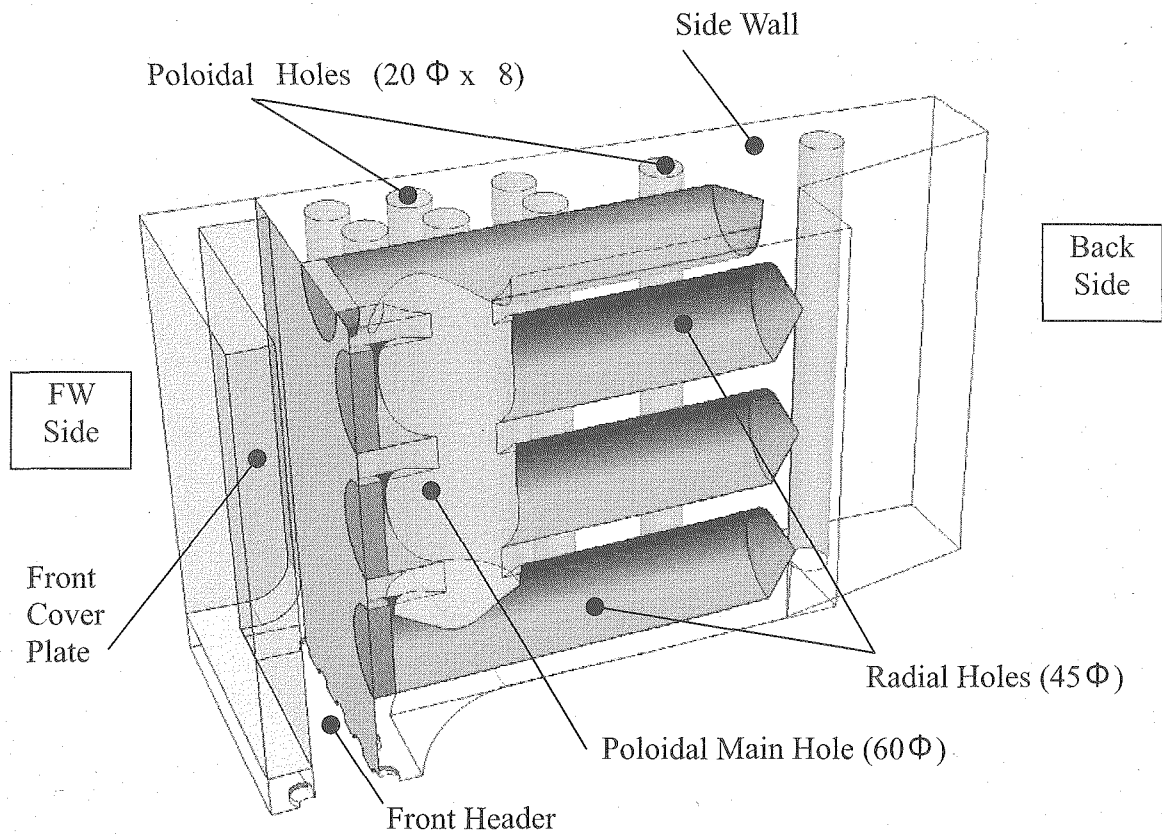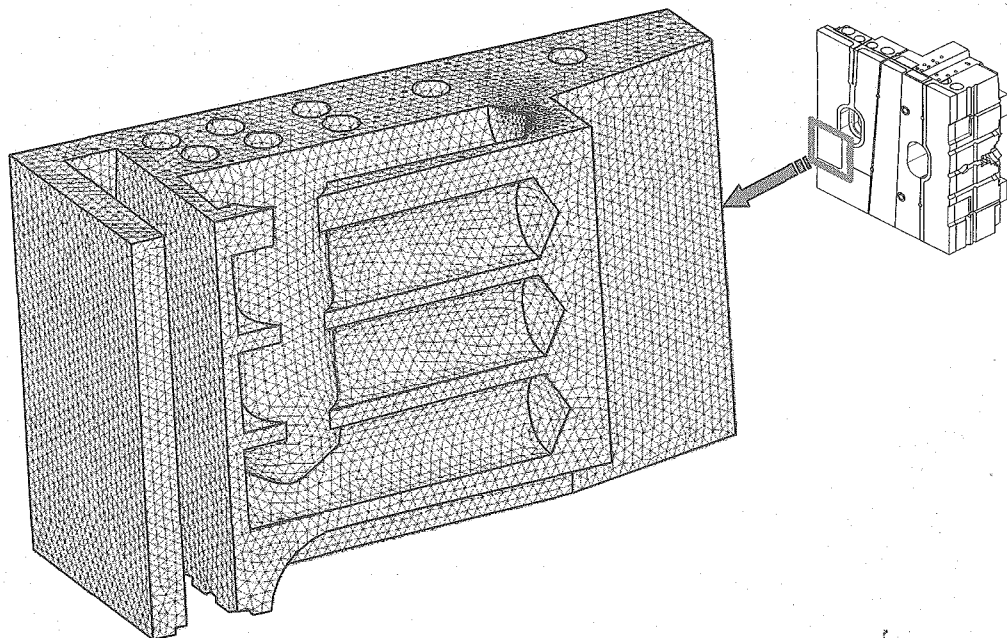
Front Header

(1) Based Model by 3D CAD Drawing

(2) The 3D Meshes for Calculation Model

Fig. 4.1-18   3D Thermal Calculation Model in the outer shield
block in #10 Module (Model B)

Front Header (L)
1780 x 3 Surfaces (See Fig. A1-2-1)

Poloidal Main Holes (Upper)
1370 x 2 Holes

Radial Holes
5840 x 5 Holes

Front Header (Upper R)
2260 x 4 Surfaces

Radial Holes
5550 x 3 Holes

Front Header
(Lower R)
800 x 5 Surfaces

Connection Holes
7110 x 4 Holes

Connection Holes
4000 x 2 Holes

Poloidal Holes
7310 x 13 Holes

Connection Holes
7750 x 3 Holes

Back Side Header
1000 x 8 Surfaces

Poloidal Main Holes (Lower)
2380 x 2 Holes

UNIT: W/m2k
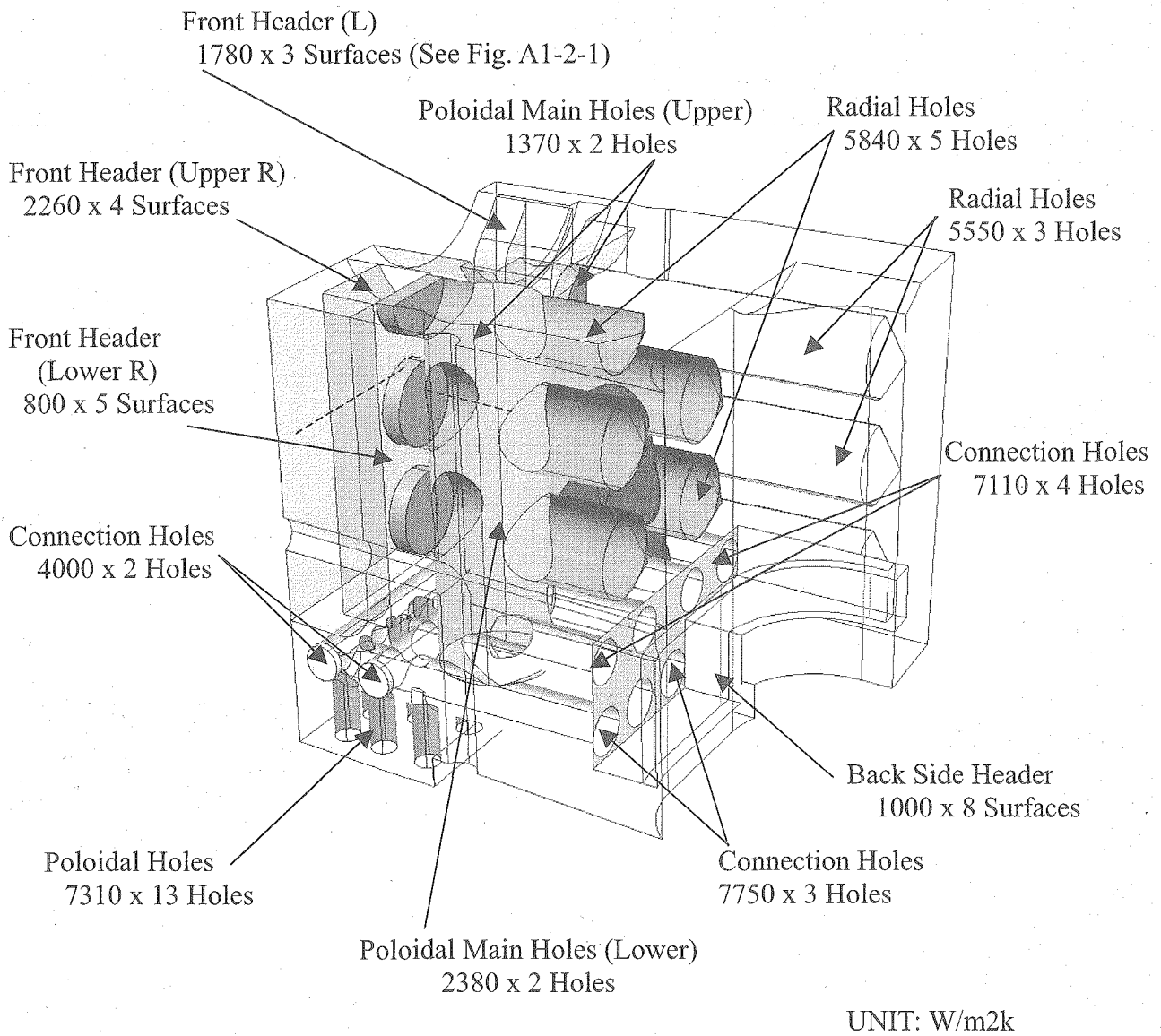
Fig. 4.1-19   Interface Conditions of Heat Transfer Coefficient in Model A.

(1) Front View

(2) Back Side View
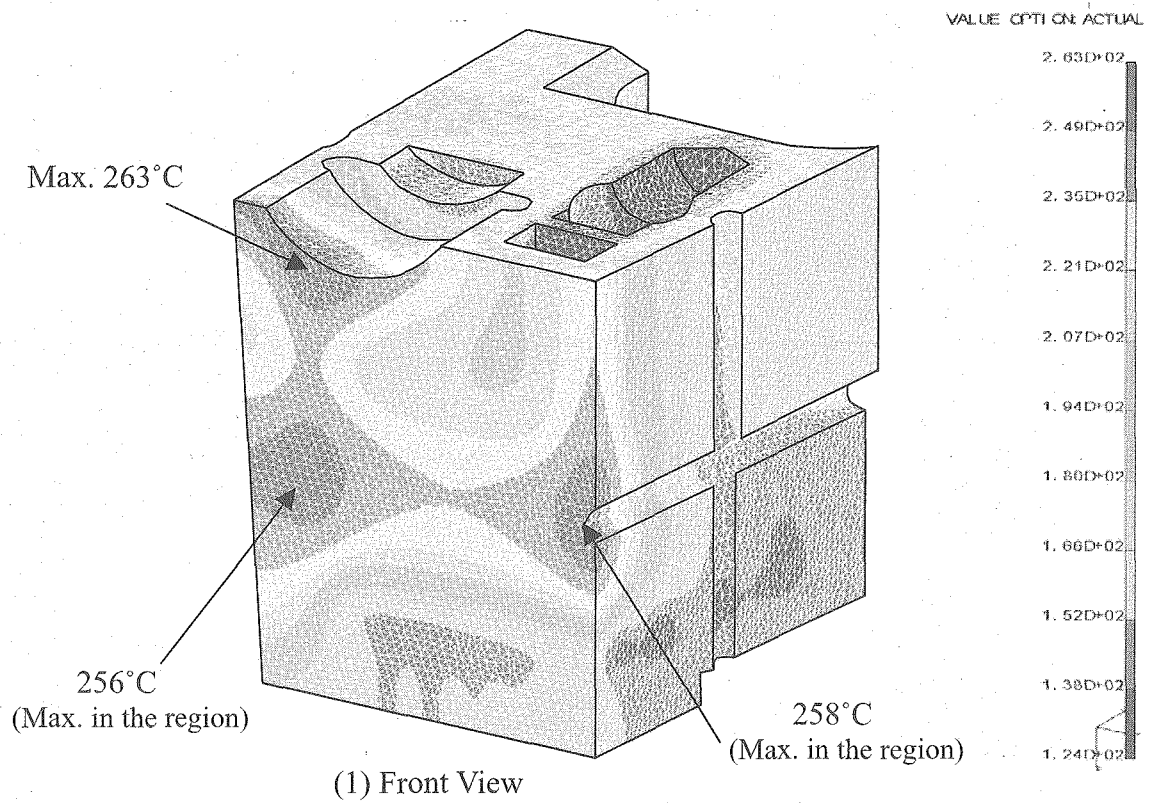
Fig. 4.1-20 (1/2) Temperature Distribution in the outer shield block
in #10 Module (Model A)

Max 263°C

VALUE OPTION: ACTUAL

2.63D+02
2.49D+02
2.35D+02
2.21D+02
2.07D+02
1.94D+02
1.80D+02
1.66D+02
1.52D+02
1.38D+02
1.24D+02

(3) Top Side View

Bottom Surface
154°C (Max. in the region)

E OPTION: ACTUAL

2.63D+02
2.49D+02
2.35D+02
2.21D+02
2.07D+02
1.94D+02
1.80D+02
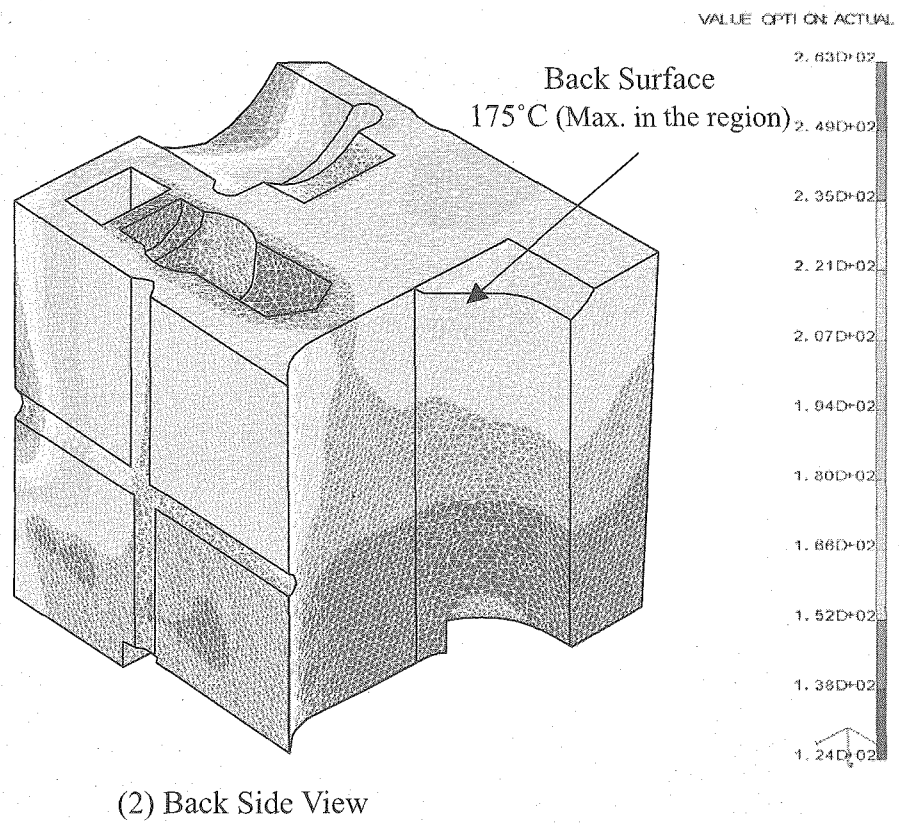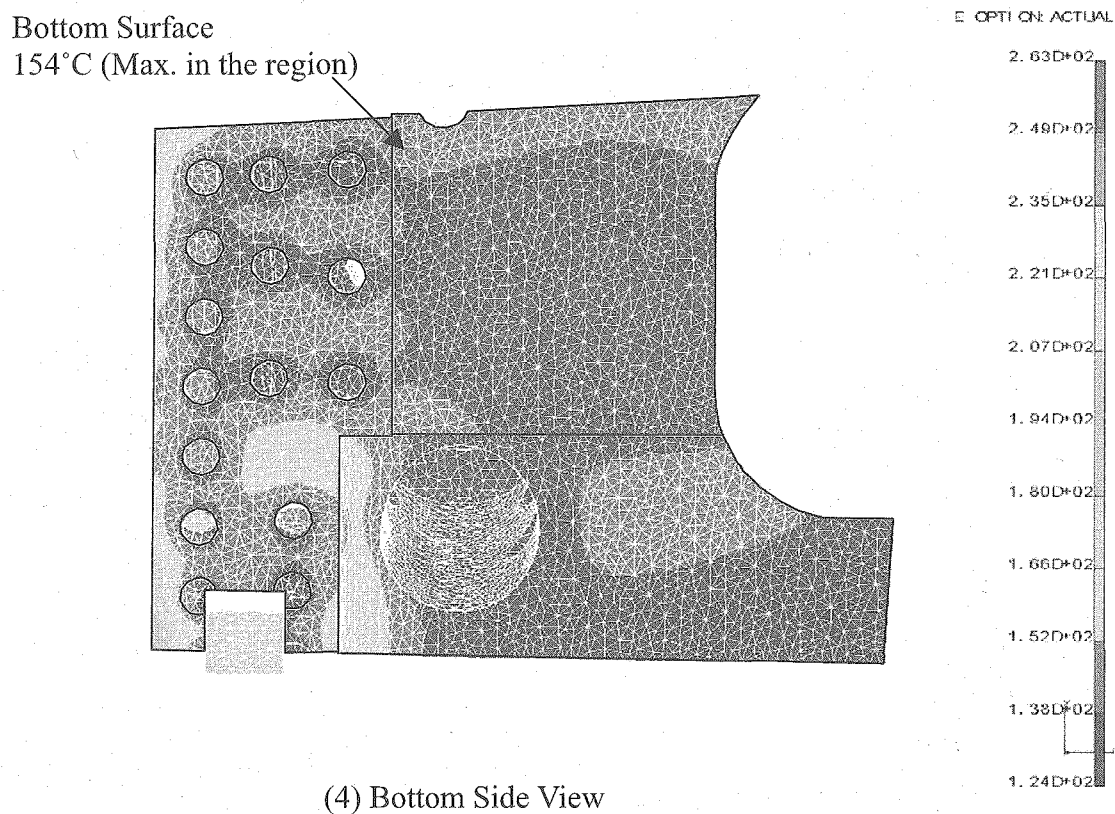1.66D+02
1.52D+02
1.38D+02
1.24D+02

(4) Bottom Side View

Fig. 4.1-20 (2/2) Temperature Distribution in the outer shield block
in #10 Module (Model A)

(1) Front View

(2) Front View without Front Cover Plate

Fig. 4.1-21 (1/2)　　Intensity of Shearing Stress on the Front Side of shield
in #10 Module produced by Thermal Loads

Point X
163MPa
(Max. in the
region)

VALUE OPTION ACTUAL

1.63D+08
1.47D+08
1.30D+08
1.14D+08
9.77D+07
8.15D+07
6.52D+07
4.89D+07
3.27D+07
1.64D+07
1.35D+05

(3)   Bottom Side View without Front Cover Plate

163MPa
(Max. in the
region)

PTION ACTUAL

1.63D+08
1.47D+08
1.30D+08
1.14D+08
9.77D+07
8.15D+07
6.52D+07
4.89D+07
3.27D+07
1.64D+07
1.35D+05

(4)   Horizontal cross section at X point
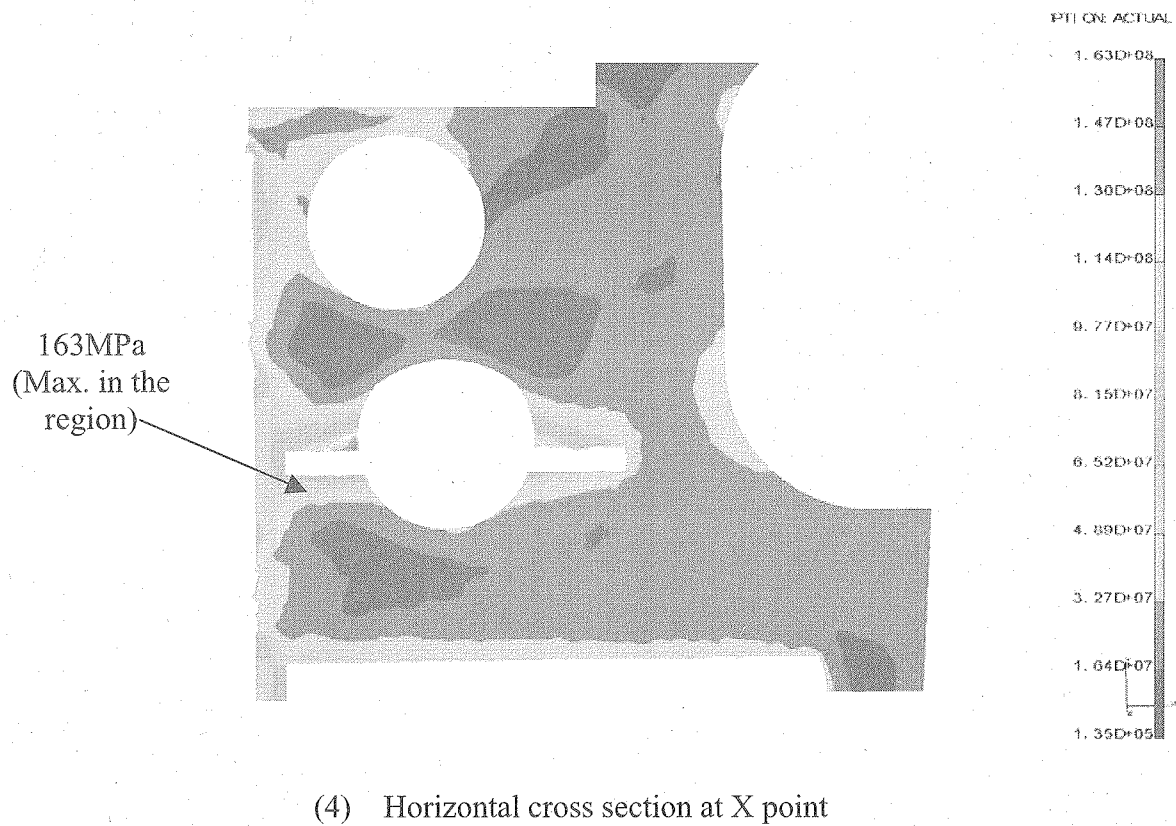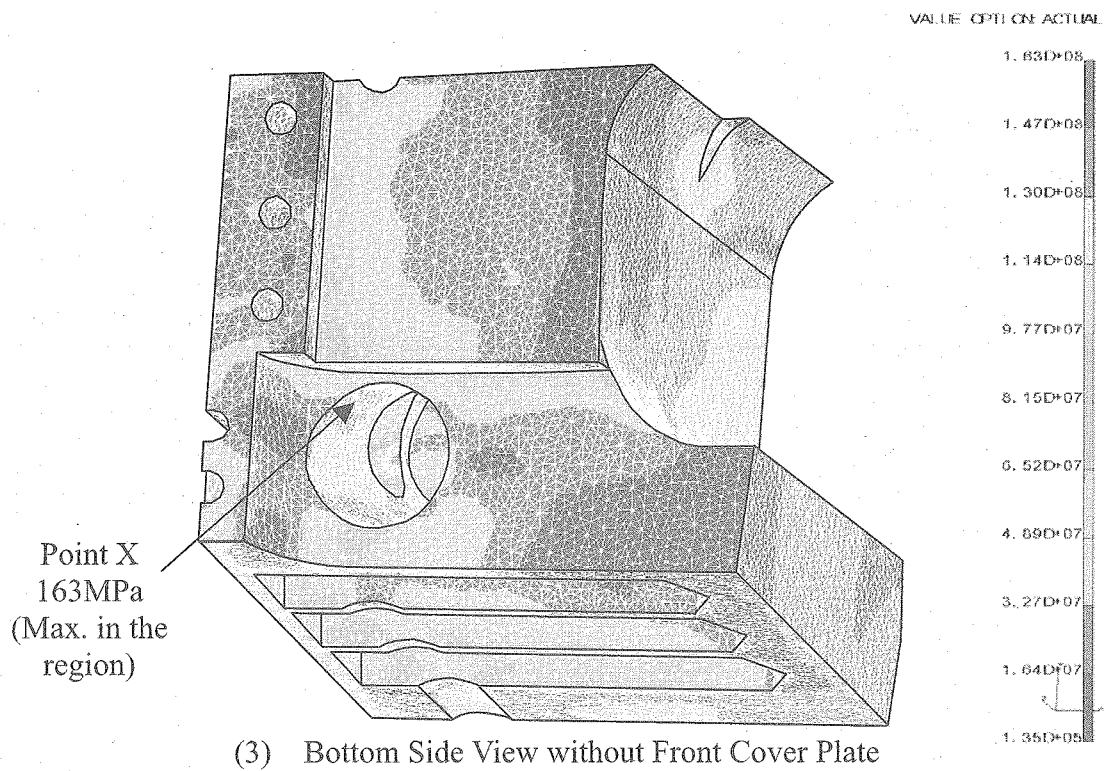
Fig. 4.1-21 (2/2)   Intensity of Shearing Stress on the Front Side of shield
in #10 Module produced by Thermal Loads
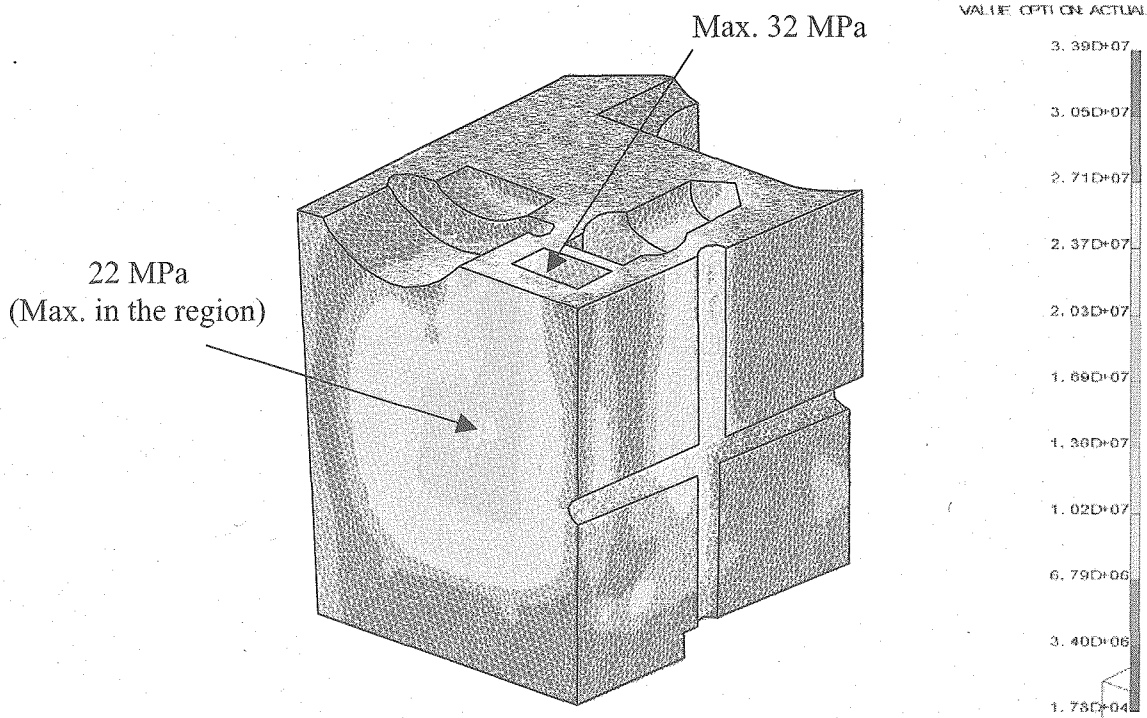
Fig. 4.1-22   Intensity of Shearing Stress on the Front Side of shield
in #10 Module produced by Coolant Pressure

UNIT: W/m2k
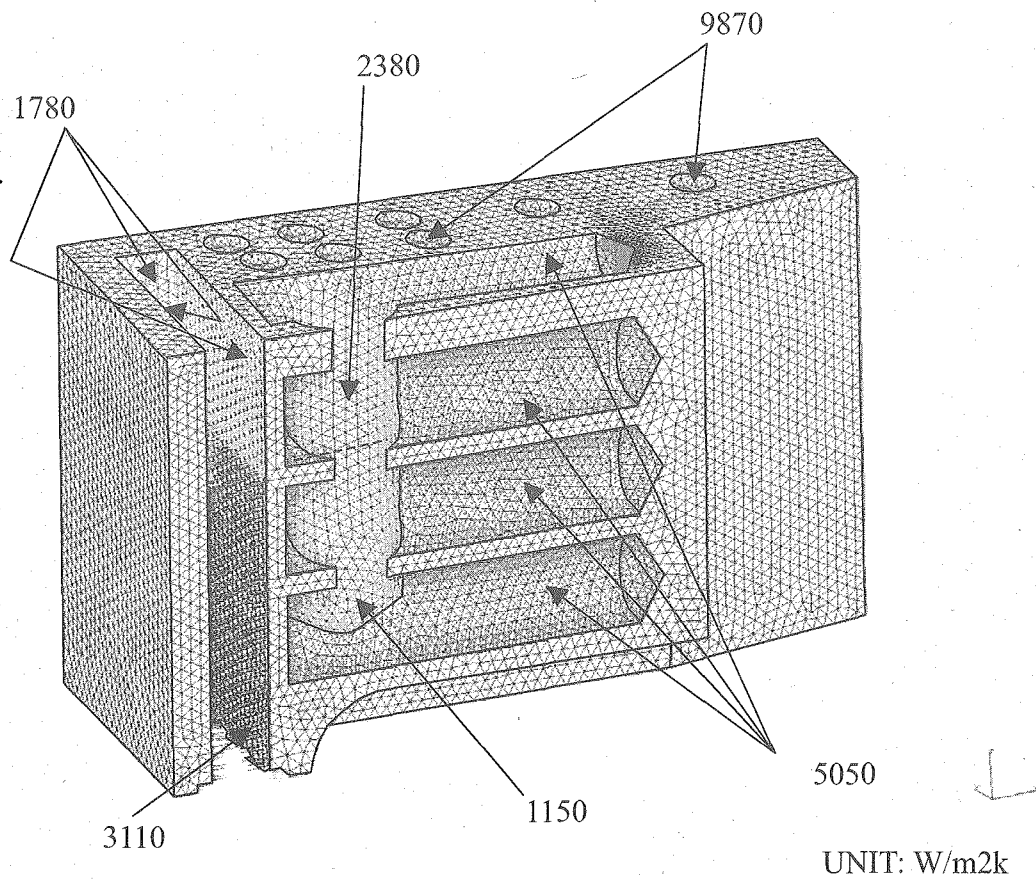
Fig. 4.1-23   Interface Conditions of Heat Transfer Coefficient
in Model B (Coolant Temperature : 125°C)
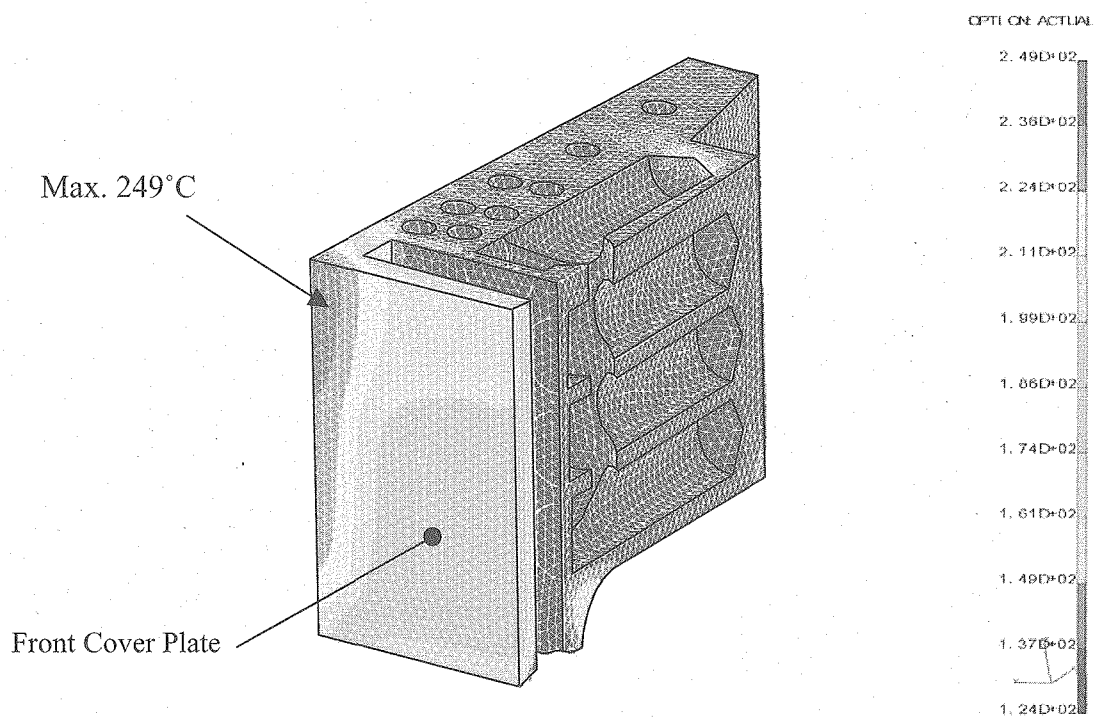
(1) Front View from Inner Side
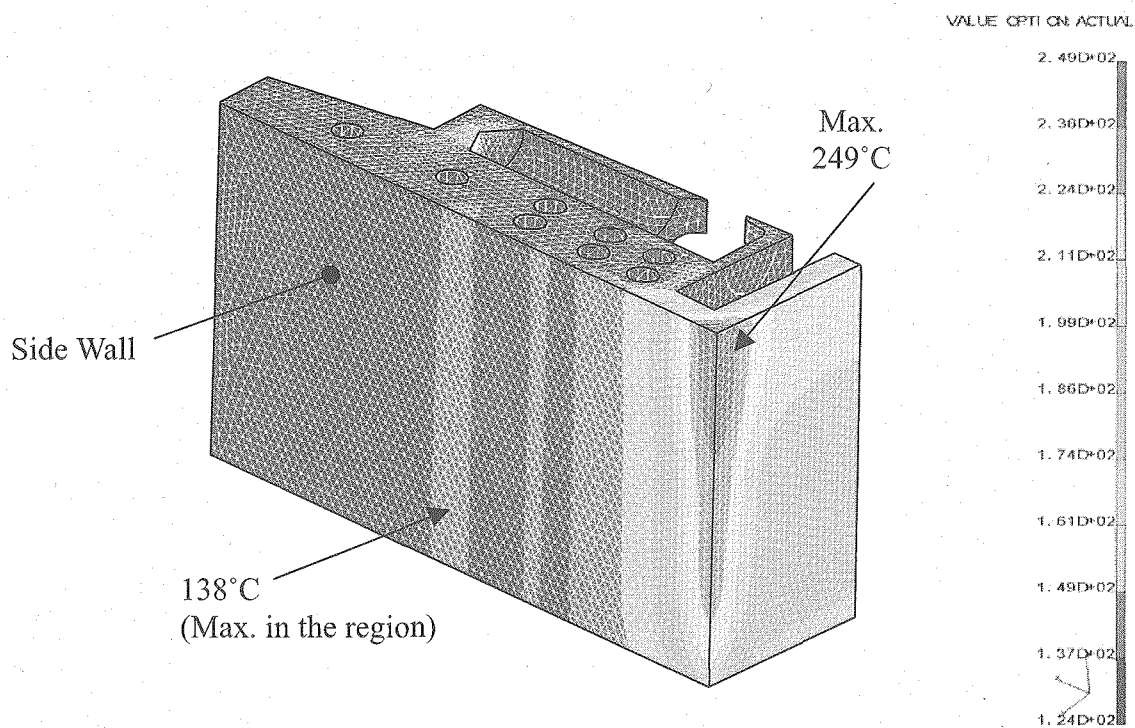
(2) Front View from Side Wall Side

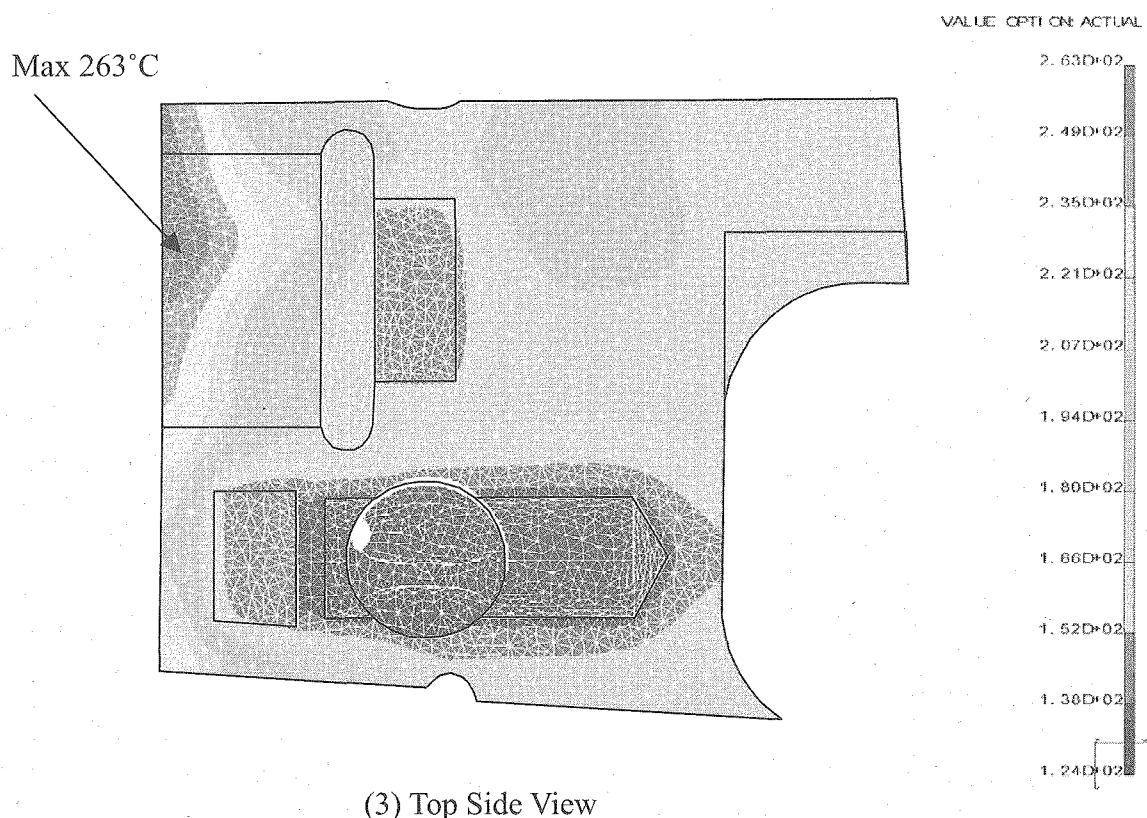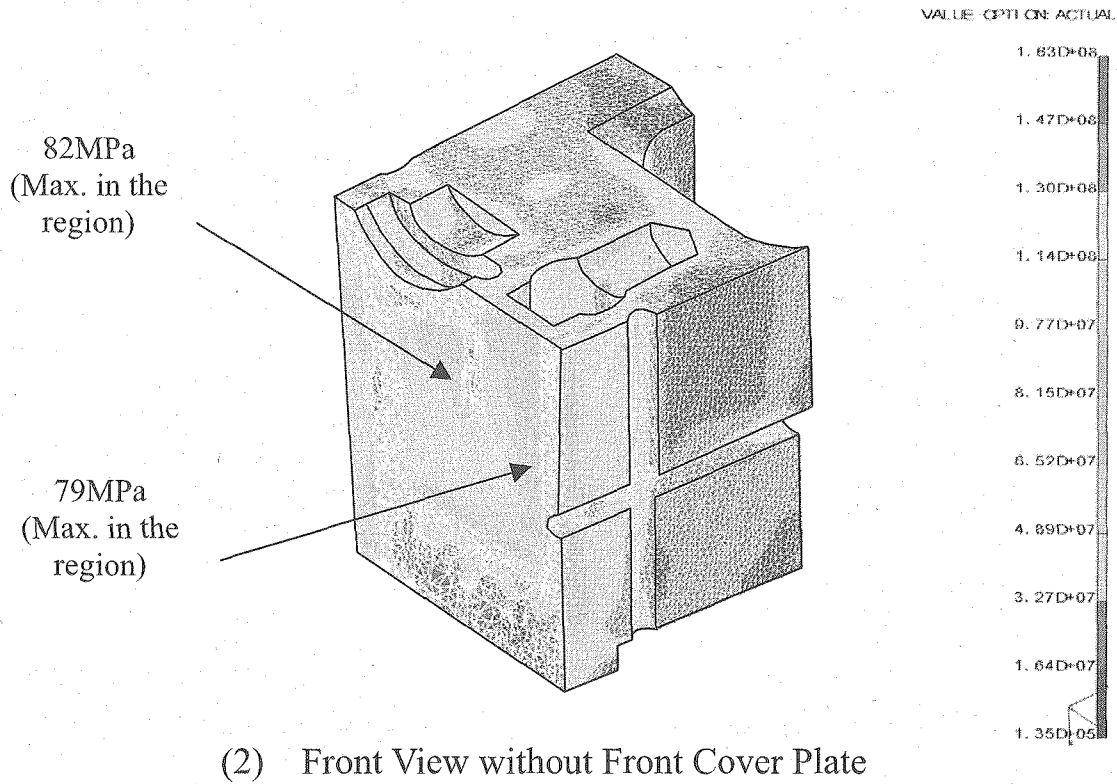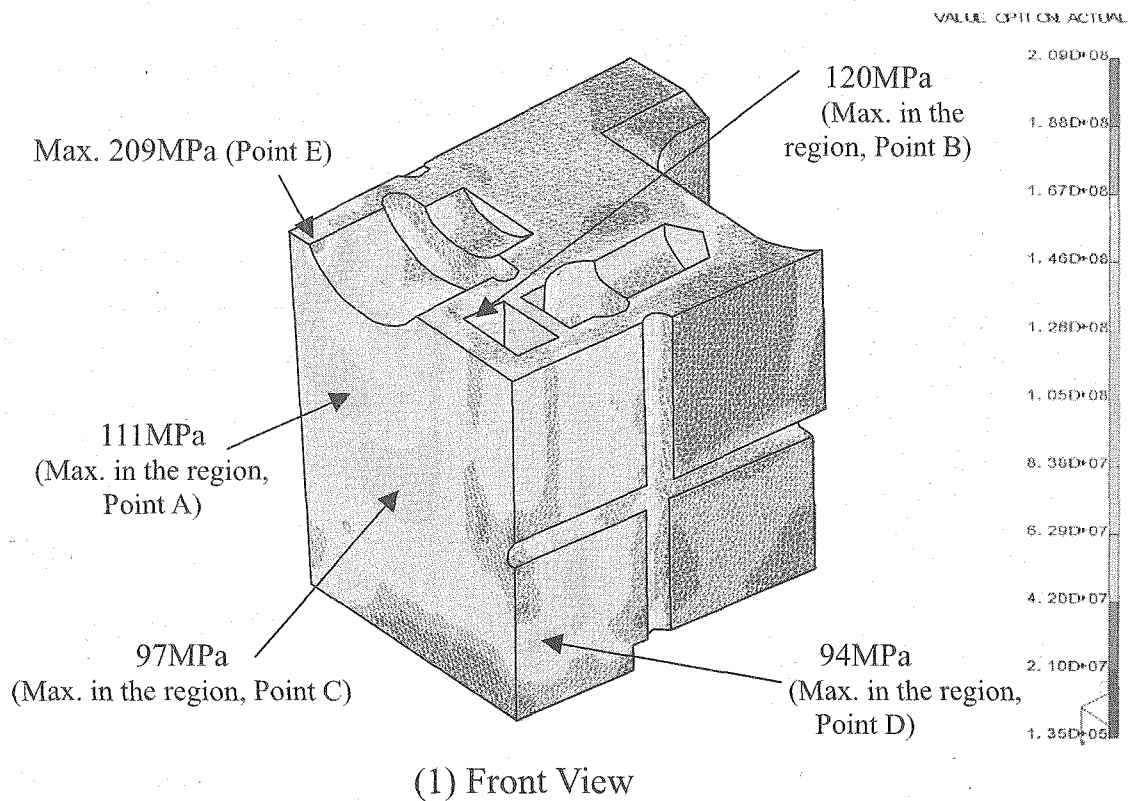Fig. 4.1-24 (1/2)　Temperature Distribution in the outer shield block
in #10 Module (Model B)

(3) Bottom View from Inner Side
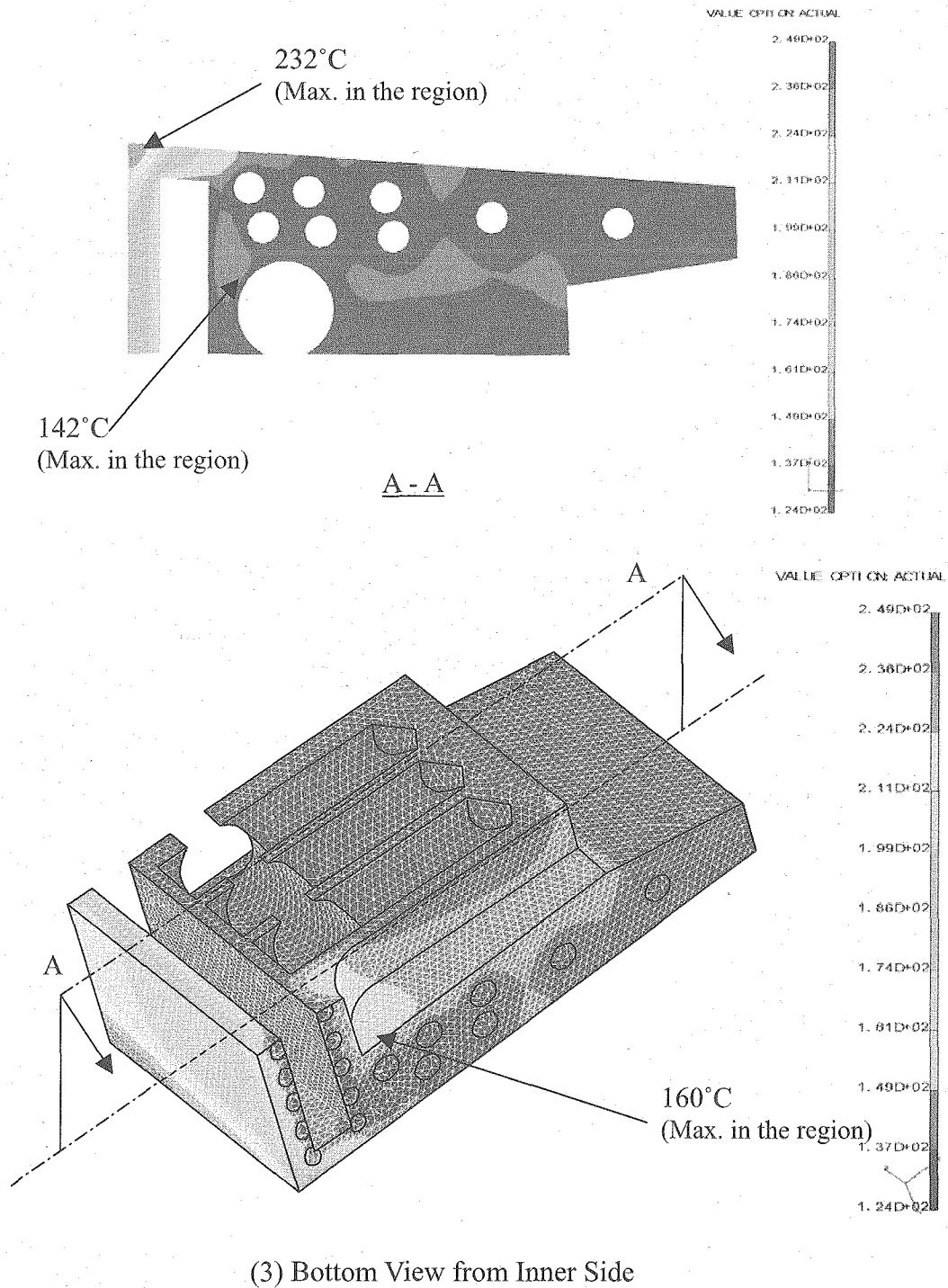
Fig. 4.1-24 (2/2)   Temperature Distribution in the outer shield block
in #10 Module (Model B)

VALUE OPTI ON: ACTUAL

2. 27D+08

2. 04D+08

1. 82D+08

1. 59D+08

1. 37D+08

1. 14D+08

9. 14D+07

6. 87D+07

4. 61D+07

2. 35D+07

8. 71D+05

167MPa
(Max. in the region, Point A)

Front Cover Plate

177MPa
(Max. in the region,
Point B)

Max. 227MPa
(Point D)
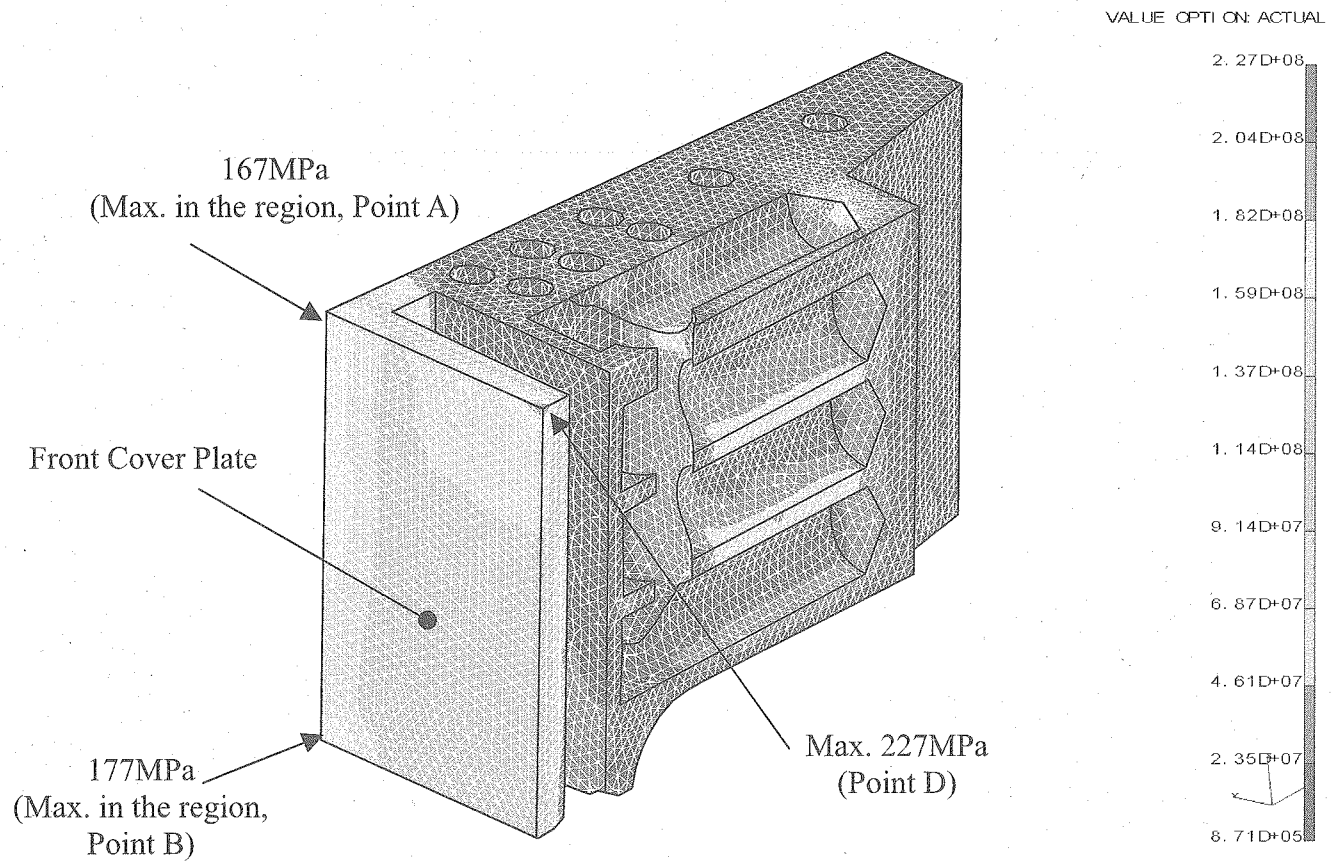
(1) Front View of Whole Model

Fig. 4.1-25 (1/3)   Intensity of Shearing Stress in #10 Module
produced by Thermal Loads

72.8MPa
(Max. in the region)

A-A

(2) Front View without Front Cover Plate
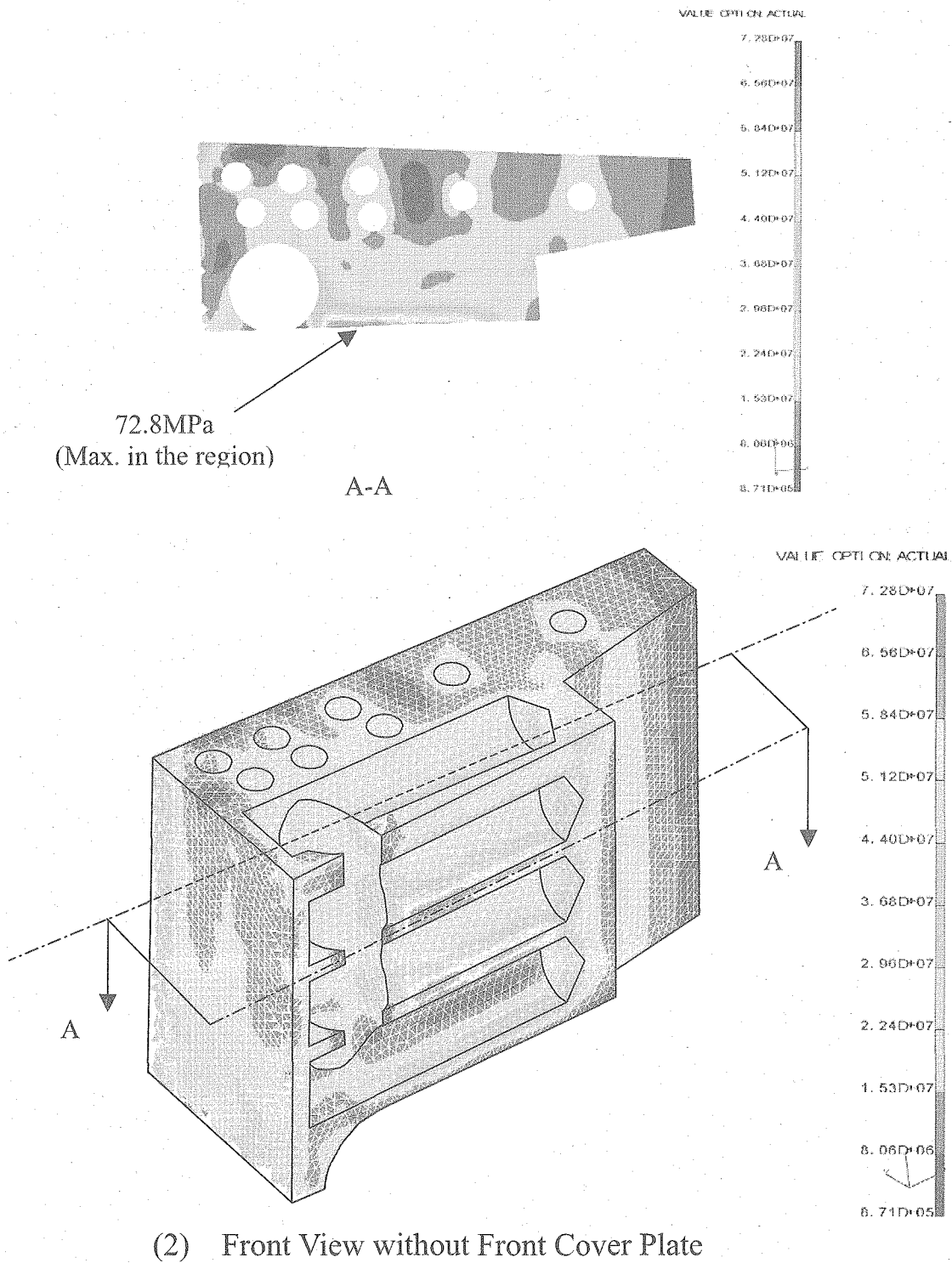
Fig. 4.1-25 (2/3) Intensity of Shearing Stress in #10 Module
produced by Thermal Loads

71MPa (Max. in the region)

(3) Top View without Front Cover Plate
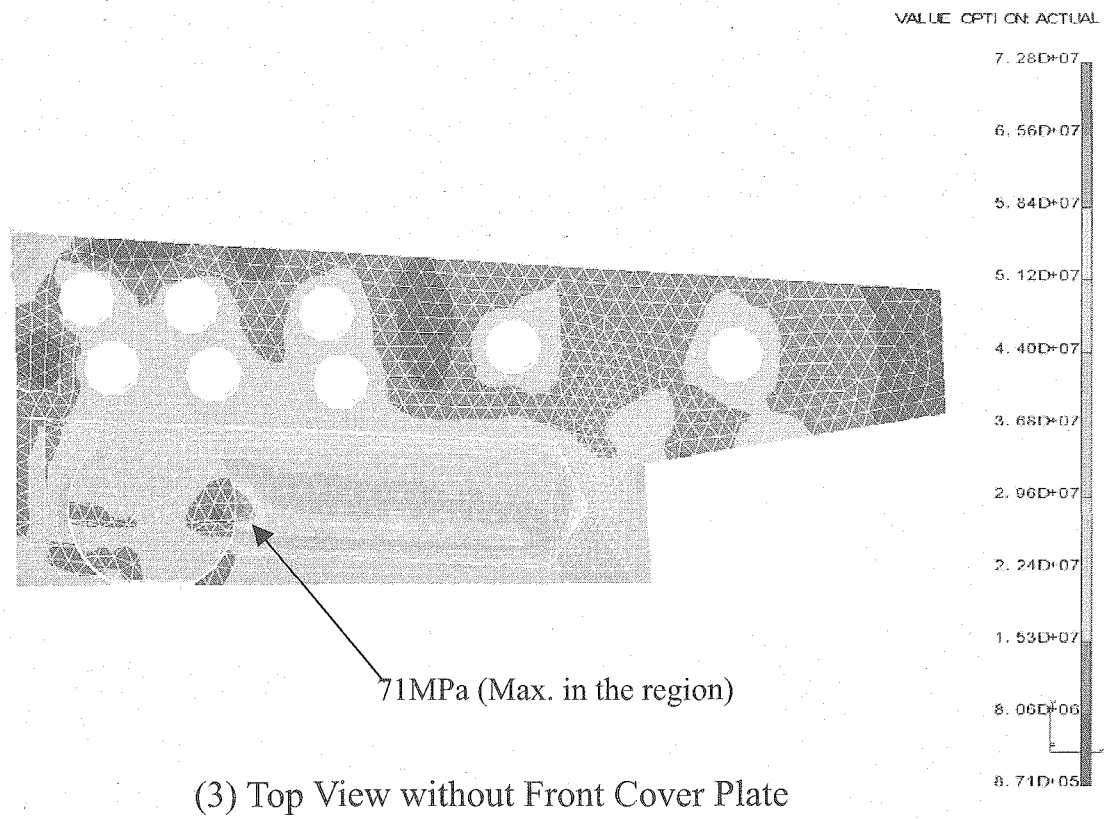
Fig. 4.1-25 (3/3)   Intensity of Shearing Stress in #10 Module
produced by Thermal Loads
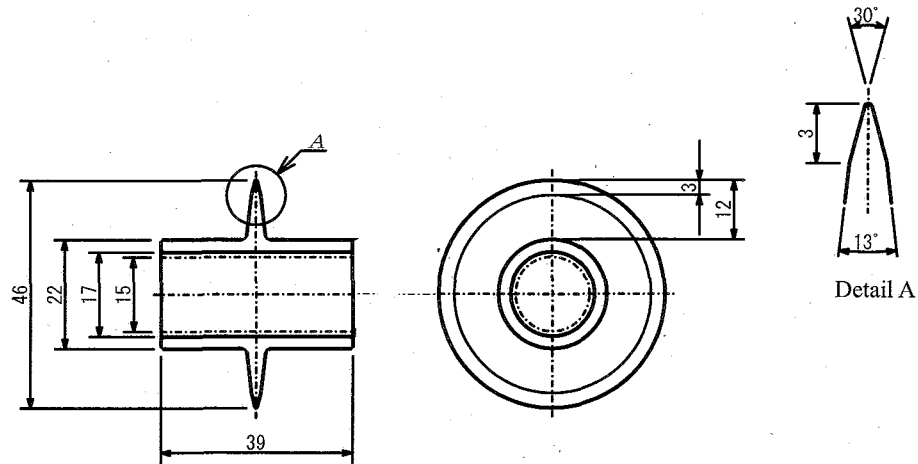
Fig. 4.2-1   Configuration of the disc knife for $\Phi 80^{ID}/\Phi 100^{OD}$ mm pipe cutting
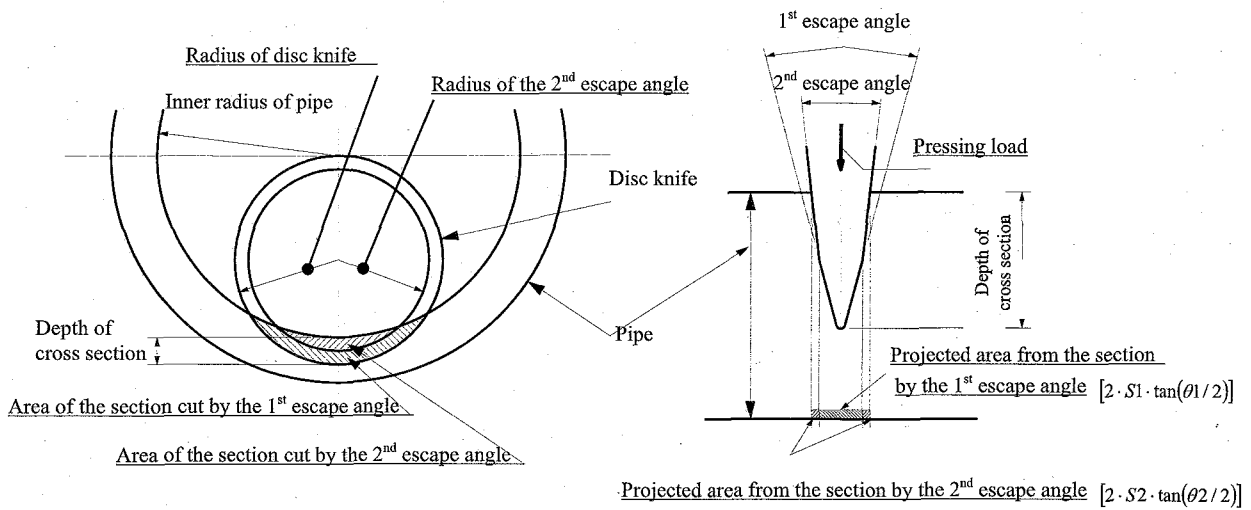
Fig. 4.2-2   Definition of the technical names for the disc knife

(a)   (b)
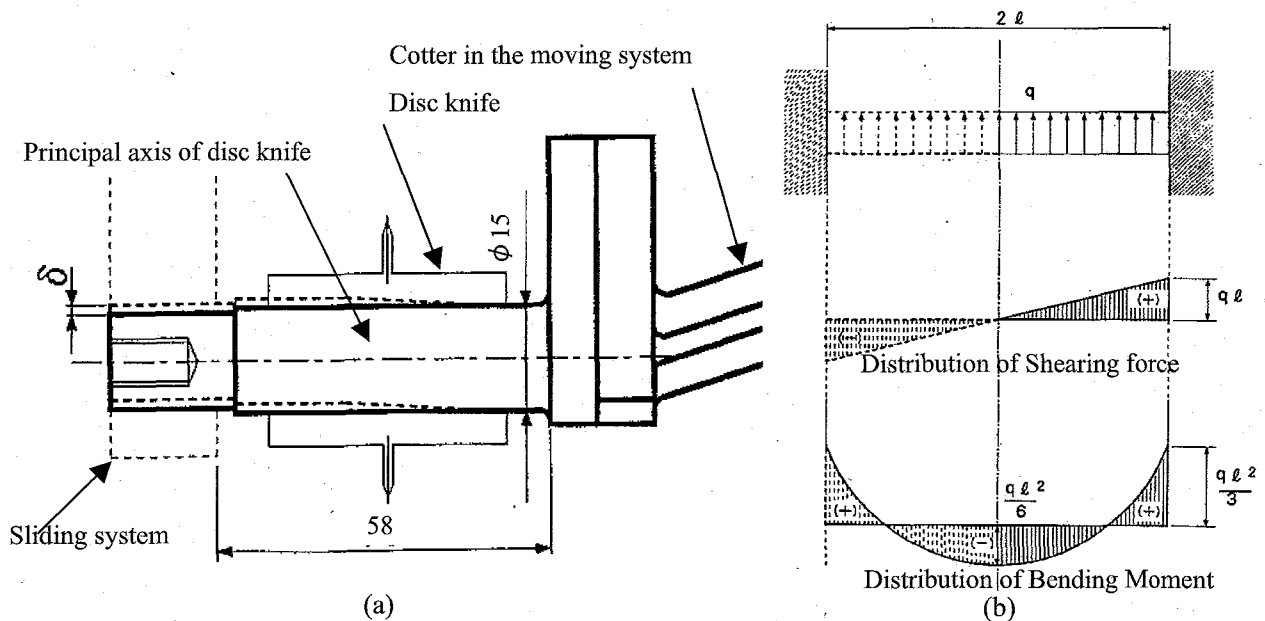
Fig. 4.2-3   Configuration of the axis of the disc knife and the calculation model $(l = 58mm)$
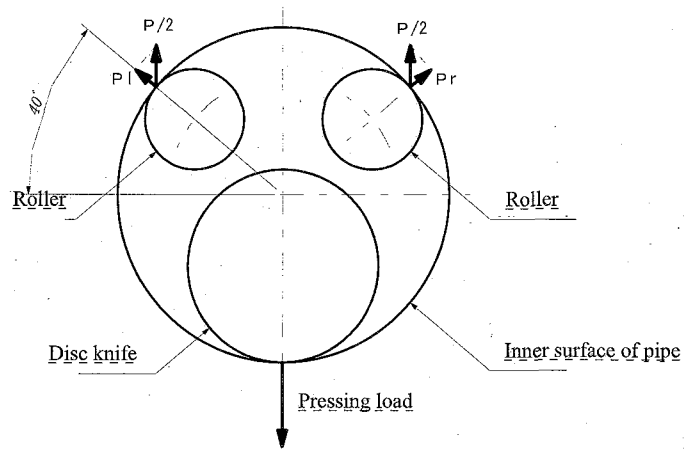
Fig. 4.2-4　Force of the vector made of the pressing load

(a)

Distribution of Shearing force

Distribution of Bending Moment

(b)
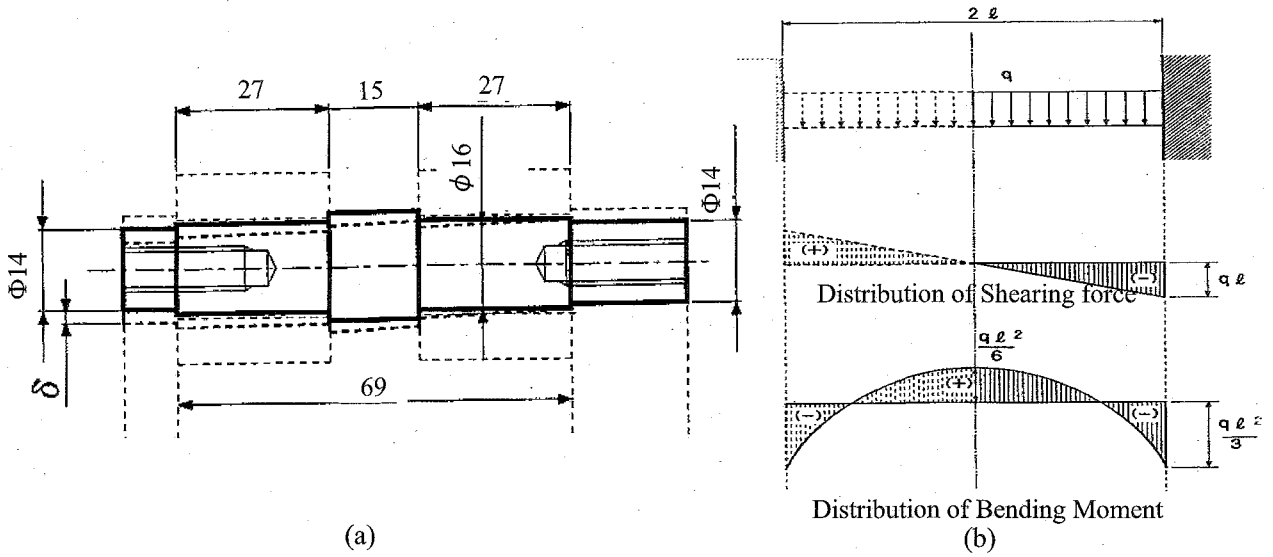
Fig. 4.2-5　Configuration of the roller axis and the calculation model ($l = 69mm$)

(a)

Distribution of Shearing force

Distribution of Bending Moment

(b)
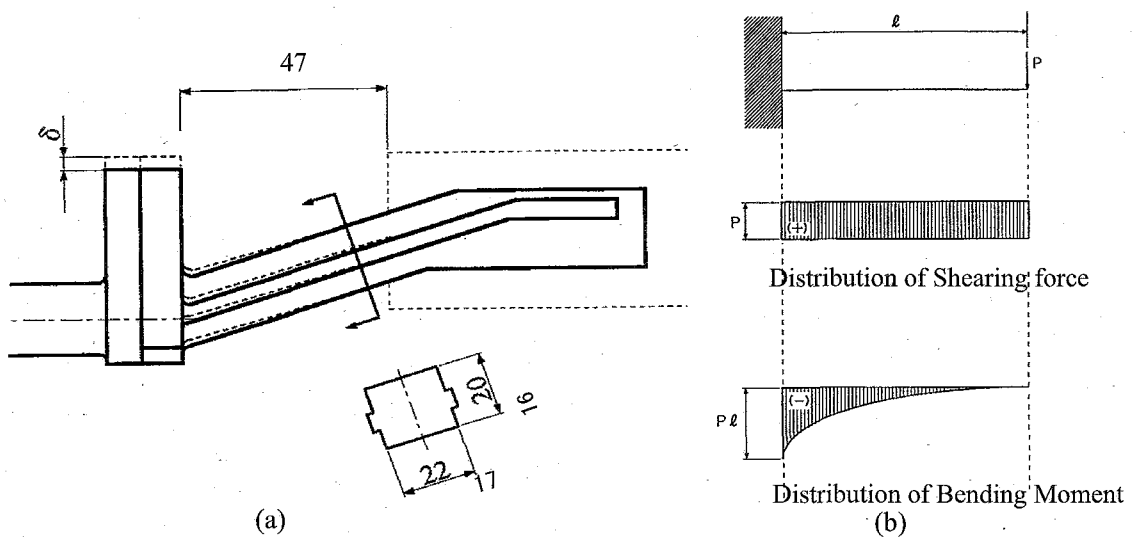
Fig. 4.2-6　Configuration of the cotter in the moving system and the calculation model　($l = 47mm$)

5. Conclusions

The concepts of the FW support leg and the shield block #10 based on the suitable replacement methods in the Hot Cell have been investigated. The preliminary design study of the cutting machine, what we call Disc-Cutter, has been performed to confirm the structural feasibility.

The following conclusions are drawn from the studies.

(1) In the selection of the replacement methods for the FW support leg , Disc-Cutter cutting machine and YAG Laser beam welding one with more than 5 kW Laser rated power have been selected out of a number of candidate methods in consideration of the advantages in the Hot Cell and of the high accessibility to the connection through the narrow cavity in the shield block. The Disc-Cutter machine designed in the study is corresponding to a $\phi 80^{ID}/100^{OD}$ mm size of pipe which can withstand the EM force.

(2) In the selection of the methods for the header cover plate in the back of the shield block, Hole-Saw cutting and YAG Laser beam welding machine have been selected out of a number of candidate methods.

(3) For the design of shield blanket module #10, consistent structure to satisfy the requirements from the remote handling equipments are proposed, such as

- the new simple structure concept of FW support beam, namely two circular connection type, based on Disc-Cutter cutting and YAG Laser beam welding,
- that of the header cover plate in the back of the shield block, based on Hole-Saw cutting and YAG Laser beam welding.

The two circular connection support has enough structural integrity for all load combinations and the stresses are within the allowable limit.

Acknowledgement

The authors wish to express sincere appreciation to Drs. Toshihide Tsunematsu, Ryuji Yoshino and Masahiro Mori for their continuous encouragement. Also, authors wish to express special gratitude to Drs. Kimihiro Ioki and Filippo Elio of ITER JCT for their guidance of the design items. The authors acknowledge the tremendous contributions by Toshiba Co. and Kawasaki Plant Systems, Ltd. to accomplish this work.

References

[1] Technical basis for the ITER-FEAT outline design, ITER EDA Documentation Series, 19, IAEA, VIENNA (2000).

[2] ITER Technical Basis, ITER EDA Documentation Series, 24, IAEA, VIENNA (2002).

[3] ITER-FEAT outline design report, ITER EDA Documentation Series, 18, IAEA, VIENNA (2001), P95.

[4] S.Yoshizawa, S.Kakudate, etc., "Feasibility study of Inside Automatic Welding System of Cooling Pipe of Divertors for FER", Fusion Technology (1994), pp.1415-1418

[5] M.Kawasaki, etc., "Development of Inside Disc-Cutter for Remote Cutting of Reactor Vessel Pipe", FAPIG No.113, July (1986), pp. 51-55

国際単位系 （SI）

表1．SI 基本単位

基本量	SI 基本単位 名称	記号
長　　　　さ	メートル	m
質　　　　量	キログラム	kg
時　　　　間	秒	s
電　　　　流	アンペア	A
熱力学温度	ケルビン	K
物　質　量	モル	mol
光　　　　度	カンデラ	cd

表2．基本単位を用いて表されるSI組立単位の例

組立量	SI 基本単位 名称	記号
面　　　　　積	平方メートル	m²
体　　　　　積	立法メートル	m³
速さ，速度	メートル毎秒	m/s
加　速　度	メートル毎秒毎秒	m/s²
波　　数	毎メートル	m⁻1
密度（質量密度）	キログラム毎立法メートル	kg/m³
質量体積（比体積）	立法メートル毎キログラム	m³/kg
電　流　密　度	アンペア毎平方メートル	A/m²
磁界の強さ	アンペア毎メートル	A/m
（物質量の）濃度	モル毎立方メートル	mol/m³
輝　　　　　度	カンデラ毎平方メートル	cd/m²
屈　　折　　率	（数　の）　1	1

表5．SI 接頭語

乗数	接頭語	記号	乗数	接頭語	記号
10²⁴	ヨタ	Y	10⁻1	デシ	d
10²1	ゼタ	Z	10⁻²	センチ	c
10¹⁸	エクサ	E	10⁻³	ミリ	m
10¹⁵	ペタ	P	10⁻⁶	マイクロ	μ
10¹²	テラ	T	10⁻⁹	ナノ	n
10⁹	ギガ	G	10⁻¹²	ピコ	p
10⁶	メガ	M	10⁻¹⁵	フェムト	f
10³	キロ	k	10⁻¹⁸	アト	a
10²	ヘクト	h	10⁻²1	ゼプト	z
10¹	デカ	da	10⁻²⁴	ヨクト	y

表3．固有の名称とその独自の記号で表されるSI組立単位

組立量	SI 組立単位 名称	記号	他のSI単位による表し方	SI基本単位による表し方
平　　面　　角	ラジアン [(a)]	rad		$m \cdot m^{-1}=1$ [(b)]
立　　体　　角	ステラジアン [(a)]	sr [(c)]		$m^2 \cdot m^{-2}=1$ [(b)]
周　波　数	ヘルツ	Hz		s⁻¹
力	ニュートン	N		$m \cdot kg \cdot s^{-2}$
圧力，応力	パスカル	Pa	N/m²	$m^{-1} \cdot kg \cdot s^{-2}$
エネルギー，仕事，熱量	ジュール	J	N・m	$m^2 \cdot kg \cdot s^{-2}$
工率，放射束	ワット	W	J/s	$m^2 \cdot kg \cdot s^{-3}$
電荷，電気量	クーロン	C		s・A
電位差（電圧），起電力	ボルト	V	W/A	$m^2 \cdot kg \cdot s^{-3} \cdot A^{-1}$
静　電　容　量	ファラド	F	C/V	$m^{-2} \cdot kg^{-1} \cdot s^4 \cdot A^2$
電　気　抵　抗	オーム	Ω	V/A	$m^2 \cdot kg \cdot s^{-3} \cdot A^{-2}$
コンダクタンス	ジーメンス	S	A/V	$m^{-2} \cdot kg^{-1} \cdot s^3 \cdot A^2$
磁　　　　束	ウェーバ	Wb	V・s	$m^2 \cdot kg \cdot s^{-2} \cdot A^{-1}$
磁　束　密　度	テスラ	T	Wb/m²	$kg \cdot s^{-2} \cdot A^{-1}$
インダクタンス	ヘンリー	H	Wb/A	$m^2 \cdot kg \cdot s^{-2} \cdot A^{-2}$
セルシウス温度	セルシウス度 [(d)]	℃		K
光　　　　束	ルーメン	lm	cd・sr [(c)]	$m^2 \cdot m^{-2} \cdot cd=cd$
照　　　　度	ルクス	lx	lm/m²	$m^2 \cdot m^{-4} \cdot cd=m^{-2} \cdot cd$
（放射性核種の）放射能	ベクレル	Bq		s⁻¹
吸収線量，質量エネルギー分与，カーマ	グレイ	Gy	J/kg	$m^2 \cdot s^{-2}$
線量当量，周辺線量当量，方向性線量当量，個人線量当量，組織線量当	シーベルト	Sv	J/kg	$m^2 \cdot s^{-2}$

(a)ラジアン及びステラジアンの使用は、同じ次元であっても異なった性質をもった量を区別するときの組立単位の表し方として利点がある。組立単位を形作るときのいくつかの用例は表4に示されている。
(b)実際には、使用する時には記号rad及びsrが用いられるが、習慣として組立単位としての記号 "1" は明示されない。
(c)測光学では、ステラジアンの名称と記号srを単位の表し方の中にそのまま維持している。
(d)この単位は、例としてミリセルシウス度m℃のようにSI接頭語を伴って用いても良い。

表6．国際単位系と併用されるが国際単位系に属さない単位

名称	記号	SI 単位による値
分	min	1 min=60s
時	h	1h=60 min=3600 s
日	d	1 d=24 h=86400 s
度	°	1°=(π/180) rad
分	’	1'=(1/60)°=(π/10800) rad
秒	”	1"=(1/60)'=(π/648000) rad
リットル	l、L	1l=1 dm³=10⁻³m³
トン	t	1t=10³ kg
ネーパ	Np	1Np=1
ベル	B	1B=(1/2)ln10(Np)

表7．国際単位系と併用されこれに属さない単位でSI単位で表される数値が実験的に得られるもの

名称	記号	SI 単位であらわされる数値
電子ボルト	eV	1eV=1.60217733(49)×10⁻¹⁹J
統一原子質量単位	u	1u=1.6605402(10)×10⁻²⁷kg
天　文　単　位	ua	1ua=1.49597870691(30)×10¹¹m

表8．国際単位系に属さないが国際単位系と併用されるその他の単位

名称	記号	SI 単位であらわされる数値
海　　里		1海里=1852m
ノ　ッ　ト		1ノット=1海里毎時=(1852/3600)m/s
ア　ー　ル	a	1a=1 dam²=10²m²
ヘクタール	ha	1ha=1 hm²=10⁴m²
バ　ー　ル	bar	1bar=0.1MPa=100kPa=1000hPa=10⁵Pa
オングストローム	Å	1 Å=0.1nm=10⁻¹⁰m
バ　ー　ン	b	1 b=100fm²=10⁻²⁸m²

表4．単位の中に固有の名称とその独自の記号を含むSI組立単位の例

組立量	SI 組立単位 名称	記号	SI 基本単位による表し方
粘　　　　度	パスカル秒	Pa・s	$m^{-1} \cdot kg \cdot s^{-1}$
力のモーメント	ニュートンメートル	N・m	$m^2 \cdot kg \cdot s^{-2}$
表　面　張　力	ニュートン毎メートル	N/m	$kg \cdot s^{-2}$
角　速　度	ラジアン毎秒	rad/s	$m \cdot m^{-1} \cdot s^{-1}=s^{-1}$
角　加　速　度	ラジアン毎平方秒	rad/s²	$m \cdot m^{-1} \cdot s^{-2}=s^{-2}$
熱流密度，放射照度	ワット毎平方メートル	W/m²	$kg \cdot s^{-3}$
熱容量，エントロピー	ジュール毎ケルビン	J/K	$m^2 \cdot kg \cdot s^{-2} \cdot K^{-1}$
質量熱容量（比熱容量），質量エントロピー	ジュール毎キログラム毎ケルビン	J/(kg・K)	$m^2 \cdot s^{-2} \cdot K^{-1}$
質量エネルギー（比エネルギー）	ジュール毎キログラム	J/kg	$m^2 \cdot s^{-2} \cdot K^{-1}$
熱　伝　導　率	ワット毎メートル毎ケルビン	W/(m・K)	$m \cdot kg \cdot s^{-3} \cdot K^{-1}$
体積エネルギー	ジュール毎立方メートル	J/m³	$m^{-1} \cdot kg \cdot s^{-2}$
電界の強さ	ボルト毎メートル	V/m	$m \cdot kg \cdot s^{-3} \cdot A^{-1}$
体　積　電　荷	クーロン毎立方メートル	C/m³	$m^{-3} \cdot s \cdot A$
電　気　変　位	クーロン毎平方メートル	C/m²	$m^{-2} \cdot s \cdot A$
誘　電　率	ファラド毎メートル	F/m	$m^{-3} \cdot kg^{-1} \cdot s^4 \cdot A^2$
透　磁　率	ヘンリー毎メートル	H/m	$m \cdot kg \cdot s^{-2} \cdot A^{-2}$
モルエネルギー	ジュール毎モル	J/mol	$m^2 \cdot kg \cdot s^{-2} \cdot mol^{-1}$
モルエントロピー，モル熱容量	ジュール毎モル毎ケルビン	J/(mol・K)	$m^2 \cdot kg \cdot s^{-2} \cdot K^{-1} \cdot mol^{-1}$
照射線量（X線及びγ線）	クーロン毎キログラム	C/kg	$kg^{-1} \cdot s \cdot A$
吸　収　線　量　率	グレイ毎秒	Gy/s	$m^2 \cdot s^{-3}$
放　射　強　度	ワット毎ステラジアン	W/sr	$m^4 \cdot m^{-2} \cdot kg \cdot s^{-3}=m^2 \cdot kg \cdot s^{-3}$
放　射　輝　度	ワット毎平方メートル毎ステラジアン	W/(m²・sr)	$m^2 \cdot m^{-2} \cdot kg \cdot s^{-3}=kg \cdot s^{-3}$

表9．固有の名称を含むCGS組立単位

名称	記号	SI 単位であらわされる数値
エ　ル　グ	erg	1 erg=10⁻⁷ J
ダ　イ　ン	dyn	1 dyn=10⁻⁵N
ポ　ア　ズ	P	1 P=1 dyn・s/cm²=0.1Pa・s
ストークス	St	1 St =1cm²/s=10⁻⁴m²/s
ガ　ウ　ス	G	1 G ^10⁻⁴T
エルステッド	Oe	1 Oe ^(1000/4π)A/m
マクスウェル	Mx	1 Mx ^10⁻⁸Wb
ス　チ　ル　ブ	sb	1 sb =1cd/cm²=10⁴cd/m²
ホ　ト	ph	1 ph=10⁴lx
ガ　ル	Gal	1 Gal =1cm/s²=10⁻²m/s²

表10．国際単位に属さないその他の単位の例

名称	記号	SI 単位であらわされる数値
キュリー	Ci	1 Ci=3.7×10¹⁰Bq
レントゲン	R	1 R = 2.58×10⁻⁴C/kg
ラ　ド	rad	1 rad=1cGy=10⁻²Gy
レ　ム	rem	1 rem=1 cSv=10⁻²Sv
X　線　単　位		1X unit=1.002×10⁻⁴nm
ガ　ン　マ	γ	1γ= 1nT=10⁻⁹T
ジャンスキー	Jy	1 Jy=10⁻²⁶W・m⁻²・Hz⁻¹
フェルミ		1 fermi=1 fm=10⁻¹⁵m
メートル系カラット		1 metric carat = 200 mg = 2×10⁻⁴kg
ト　ル	Torr	1 Torr = (101 325/760) Pa
標準大気圧	atm	1 atm = 101 325 Pa
カ　ロ　リ　ー	cal	
ミ　ク　ロ　ン	μ	1 μ =1μm=10⁻⁶m